Improved Shallow Depth Patches for Concrete Structures

Final Report to the Michigan Department of Transportation

by

Ronald S. Harichandran
Professor and Chairperson

and

Golrokh Nossoni
Graduate Student

Department of Civil and Environmental Engineering
Michigan State University
East Lansing, MI 48824-1226

Tel: (517) 355-5107
Fax: (517) 432-1827
E-Mail: harichan@egr.msu.edu
Web: www.egr.msu.edu/cee/~harichan

February 2008

Technical Report Documentation Page

1. Report No. Research Report RC-1502	2. Government Accession No.	3. MDOT Project Manager : Steve Kahl
4. Title and Subtitle: Improved Shallow Depth Patches for Concrete Structures		5. Report Date: February 2008
7. Author(s): Ronald Harichandran & Golrokh Nossoni		6. Performing Org. Code
9. Performing Organization Name and Address Department of Civil and Environmental Engineering Michigan State University East Lansing, MI 48824-1226		8. Performing Org. Report No.
12. Sponsoring Agency Name and Address Michigan Department of Transportation Construction and Technology Division P.O. Box 30049 Lansing, MI 48909		10. Work Unit No. (TRAIS)
		11. Contract Number: 2002-0532
		11(a). Authorization Number: 7R1
15. Supplementary Notes		13. Type of Report & Period Covered Research Report, 10/01 to 10/07
		14. Sponsoring Agency Code

16. Abstract:

MDOT currently performs shallow depth repairs to bridge superstructures using polymer mortar patch materials. The lifetime of these patches is typically 2-5 years. The research reported herein evaluates the use of a new dual patch system that uses a polymer mortar patch and a fiber reinforced polymer (FRP) overlay that is expected to significantly lengthen the lifetime of patch repairs.

Finite element models are initially used to study the behavior of different patch materials as well as the new dual system under shrinkage, mechanical and corrosion induced loads. Both 2-D and 3-D models were used in the evaluation with four different patch materials and five different FRP materials. Based on the results of this study, the strongest and weakest patch materials were used with a single FRP material in experimental studies.

Experimental studies were performed on small beam specimens fabricated with cavities that were patched. The specimens were subjected to freeze-thaw and wet-dry cycles followed by cyclic flexural fatigue loading and a pull-out test to assess the durability of the patches with and without an FRP overlay. A different set of specimens were subjected to accelerated corrosion testing to evaluate the durability of the patch repairs to withstand the expansion caused by corrosion.

Both the numerical and experimental studies confirm that repairs using the proposed dual system consisting of a polymer mortar patch with an FRP overlay perform significantly better than repairs that use only a mortar patch. It is expected that repairs using the proposed dual system will last about 15 years and provide significant cost savings to MDOT.

17. Key Words: patching, shallow, bridge repair, mortar, FRP.		18. Distribution Statement No restrictions. This document is available to the public through the Michigan Department of Transportation.	
19. Security Classification (report) Unclassified	20. Security Classification (Page) Unclassified	21. No of Pages 160	22. Price

Acknowledgements

Table of Contents

List of Figures

List of Tables

Chapter 1

Introduction

1.1 Background

Cracking and full or partial delamination of shallow depth surface patches used to repair damaged concrete bridge elements from the concrete substrate is generally unavoidable. The cracking and delamination is due to many factors such as truck impact corrosion, and the shrinkage exhibited by rapid cure patches. Since shrinkage is restrained, the patch materials cracks at an early age causing delamination of the patch from the concrete substrate within a year or two of application. The tensile strength, modulus of elasticity of the repair material at an early age, and structural characteristics govern the effect of restrained shrinkage (Yuan et al., 2003). Restrained shrinkage results in the development of various stresses, and failure modes due to shrinkage include vertical cracking due to direct tension and delamination due to interfacial stresses. As mentioned earlier, there are other factors such as corrosion that can also contribute to the rapid degradation of the patch materials. The choice of an optimum repair material should be based on the best compromise of required properties, and may also be influenced by the availability of materials and technical experience, and other constraints such as the application technique and construction environment.

Most standards and specifications for repair material are based on limited quantitative knowledge of the structural interaction between the concrete substrate and repair patch during the service life of a structure. They do not take into account, in any significant quantitative manner, the mismatch in basic properties such as elastic modulus, shrinkage and creep on the long-term in-service performance of the repair. Emphasis for repair material selection is usually placed on short-term properties such as strength (compressive, tensile, bond) and early age shrinkage. A critical evaluation of the recommendations of repair standards and material specifications reveals significant limitations and contradictions (Mangat et al., 2000)

Most of the research done on the patch repairs has focused on improving the compatibility between the concrete substrate and the patching material to prevent cracking. The development of a durable repair mortar, using a criterion of minimum cracking coupled with

1

impermeable or dense internal structure, has led to a number of superior new generation products, utilizing various admixtures. However finding reliable criteria for the required parameters is difficult. The problem is further compounded by lack of standardization of specifications addressing measurement and tolerable limits of free shrinkage strain, a parameter sensitive to specimen geometry, ambient temperature and relative humidity, curing conditions, and the degree of shrinkage compensation in the form of initial expansion. Decter and Keeley (1997) presented the various standards that exist worldwide for measurement of drying shrinkage.

Despite these advances even with patching materials that are highly compatible with concrete, the repair typically lasts only for a few years. To minimize this problem and improve the performance and durability of shallow depth surface patches on concrete substrates, the use of an FRP overlay as a secondary reinforcement is investigated in this study. The additional reinforcement should hold the patching material in place and prevent its premature failure.

1.2 Problem and Proposed Solution

The poor performance of shallow depth surface patches applied by MDOT to concrete structures is most likely due to two reasons. The rapid cure patches, typically consisting of latex modified concrete, demonstrate extensive cracking due to high shrinkage during curing and subsequent aging. As a result of the restraint provided by the substrate at the interface, and periphery, drying shrinkage cannot occur freely. This leads to the development of various stress components, the interaction of which can lead to premature degradation of the patch (Baluch et al., 2002). After cracking, the problem is further exacerbated if the repaired structure is subjected to an aggressive environment, where cracks provide free access for intrusion of chloride ions and diffusion of carbon dioxide.

In order to have longer and better lifetime performance it is necessary for the repair to retain its integrity and display few or no cracks. Thus, the performance criterion should be that of a minimum, or crack-free, repair layer (Baluch et al., 2002). Theoretically, it should be possible to develop improved patching materials that bond well to concrete, are shrinkage resistant, have coefficients of thermal expansion that are compatible with that of concrete, and are resistant to environmental damage. However, the development of such materials will involve costly research, product development and field-testing before these materials are likely to be adopted by

2

MDOT. On the other hand, the use of fiber-reinforced polymer (FRP) fabrics applied in a "band-aid" fashion over traditional patching materials that are currently used, has a very strong potential to provide highly durable patches (see Figure 1-1).

(a) Damaged concrete   (b) Repaired with filler only   (c) Filler and FRP repair
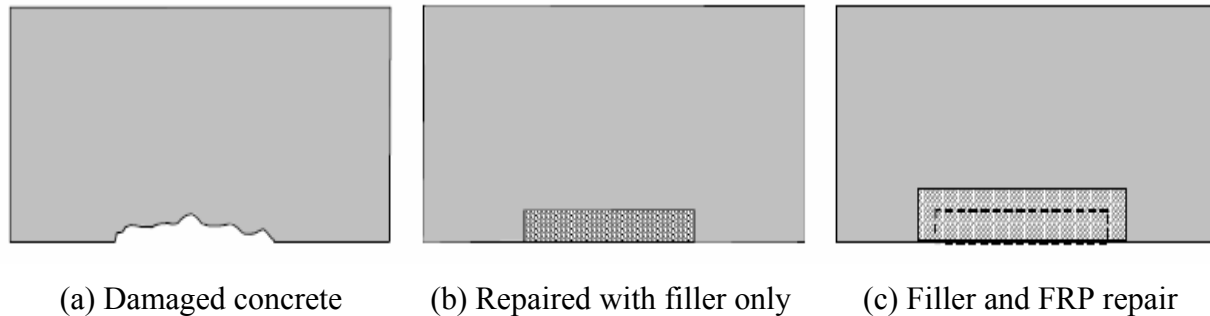
Figure 1-1: Concept of improved dual filler-and-FRP shallow depth patches

The FRP fabric will serve as:

- temporary formwork to hold the filler material place after initial application, thereby providing construction cost savings;

- a physical barrier that retards the ingress of chlorides and moisture into the filler material; and

- secondary reinforcement to hold the filler material in place if it should debond from the concrete due to shrinkage and environmental effects.

In order to obtain the desired performance under field conditions, the complex conditions leading to the buildup of stress in the repair zone need to be understood (Baluch et al., 2002; Mangat et al., 2000). The role of different parameters has to be identified to allow the identification of suitable materials and procedures for repair (Mangat et al., 2000). Thus, a quantitative assessment of the compatibility of basic properties such as elastic modulus, shrinkage and creep on the long-term service life of the repair is needed. Unfortunately, most repair material selection is based on short-term response and most standards and recommendations are based only on limited quantitative knowledge of structural interaction between the concrete substrate and the repair patch throughout its service life (Mangat et al., 2000).

In the research reported herein, two and three-dimensional finite element analyses as well as laboratory testing was employed. Finite element (FE) models were used to develop suitable

3

FRP fabric configurations (FRP type, length, width, fiber orientation, etc.) for bottom surface subjected to thermal and shrinkage strains, corrosion of the reinforcing bars, as well as traffic-induced loads. Based on results from the FE analysis, specimens were prepared for laboratory testing of repaired specimens under freeze-thaw, wet-dry, and accelerated corrosion environments. Samples exposed to freeze-thaw and wet-dry conditioning was subsequently subjected to fatigue loading to evaluate the durability of the repair under simulated traffic loading.

1.3 Research Objectives

The main objective of the proposed research is to improve the performance and durability of shallow depth surface patches on concrete structures that are exposed to aggressive freeze-thaw, wet-dry and high chloride environments. This is achieved by developing and characterizing a new repair concept consisting of a dual filler-and-FRP overlay.

1. *Literature review*: To identify the mechanisms that lead to failures in shallow-depth patch repairs, identify and select a pool of potential patching materials, and evaluate numerical approaches that have been successfully used to evaluate the performance of shallow-depth patch repairs.

2. *Numerical Simulation*: To develop finite element models to predict the behavior of concrete patch repairs with and without FRP overlays and use them to conduct parametric studies to investigate the effects of damage geometry and selection of patching materials.

3. *Experimental Characterization*: To investigate the durability and performance of the dual filler-and-FRP overlay repair system in comparison with repairs based on filler materials only.

4. *Guidelines and Recommendations*: To develop specifications for the selection of the appropriate repair procedure, surface preparation, repair material and placement, and maintenance considerations based on damage type, location, and environmental and mechanical demand.

5. *Cost/Benefit Analysis*: To perform a life-cycle economic analysis that takes into account the cost and durability of the proposed improved patching technique and compares this to the life-cycle cost of a filler-only repair.

4

The application of the FRP overlay hides the filler material and hence cracking and debonding of the filler from the concrete substrate will not be visible to inspectors. However, it is not important to know the condition of the filler within the FRP overlay since patching is done essentially for cosmetic reasons and not intended to provide structural strength. The FRP overlay will be designed to hold the filler material in place even if it is loose and cracked. Complete failure of a patch will be preceded by peeling of the FRP which can be detected visually. Recommendations regarding a simple "tap test" to ascertain the condition of the filler will be provided as part of the research. Evaluation of more involved nondestructive evolution techniques is beyond the scope of this project.

Chapter 2
Literature Review

2.1 Introduction

A literature review was conducted to identify candidate repair materials based on their performance in practice and their compatibility with concrete. The materials under consideration were taken from MDOT's Qualified Product List (QPL) and approved materials from other State DOTs. A review was also conducted on: the numerical approaches that have been used for evaluating the behavior of repair material for concrete structures, the type of the damage in the patch material, and maintenance techniques.

2.2 Repair Material

To achieve a lasting repair, it is essential that properties of the repair material and substrate be properly matched to the concrete structure as given in Table 2-1. A variety of materials are available for repair purposes, they can be classified into two primary groups: cementitious mortars (CM), and polymer modified cementitious mortars (PCM).

Table 2-1: Properties Governing Compatibility of Concrete and Patch Material (Emberson and May, 1990)

Property	Relationship of Repair Materials (R) to Concrete (C)
Elastic Modulus	Cosmetic (R<C), Structural (R>C)
Poisson's Ratio	Depends on the modulus and type of the repair
Coefficient of Thermal Expansion	R ~ C
Adhesion in Tension and Shear	R >C
Curing and Long Term Shrinkage	R < C
Strain Capacity	R > C
Creep and Relaxation	Depends on whether creep causes desirable or undesirable effects
Fatigue Performance	R>C

2.2.1 PCM and CM

Polymer cement mortar is a modified mortar in which part (10 to 15% by weight) of the cement binder is replaced by a synthetic organic polymer. Modification of mortar with a polymer latex (colloidal dispersion of polymer particles in water) results in greatly improved properties, at a reasonable cost. Therefore, a great variety of latexes are now available for use in polymer cement concrete products and mortars. The most common latexes are based on poly methyl methacrylate (also called acrylic latex), poly vinyl acetate, vinyl chloride copolymers, poly vinylidene chloride, styrene-butadiene copolymer, nitrile rubber and natural rubber. Each polymer produces characteristic physical properties. The acrylic latex provides a very good water-resistant bond between the modifying polymer and concrete components, whereas use of latexes of styrene-based polymers results in a high compressive strength. Table 2-2 categorizes generic repair product types (Emberson and May, 1990).

Table 2-2: Generic System for Concrete Patch Repair (Emberson and May, 1990).

Cementitious Mortars	Polymer-Modified Cementitious Mortar
Portland Cement (PC)	Styrene Butadiene Rubber
High Alumina Cement (HAC)	Vinyl Acetate
PC/HAC Mixture	Magnesium Phosphate
Expansion Production Grouts	Acrylic

Curing of latex PCM is different from that of conventional mortar, because the polymer forms a film on the surface of the product, retaining some of the internal moisture needed for continuous cement hydration. Because of the film-forming feature, the curing time for latex products is generally shorter.

Generally, PCM made with polymer latex exhibits better bonding to steel reinforcement and to old concrete, good ductility, resistance to penetration of water and aqueous salt solutions because of lower permeability, and resistance to freeze-thaw damage. Its flexural strength and toughness are usually higher than those of unmodified concrete. The modulus of elasticity may or may not be higher than that of unmodified mortar, depending on the polymer latex used. For example, the more rubbery the polymer, the lower the modulus. Generally, as the polymer forms

a low modulus phase with the polymer cement concrete, the creep is higher than that of plain concrete and decreases with the type of polymer latex used in the following order: polyacrylate; styrene-butadiene copolymer; polyvinylidene chloride; unmodified cement (Blaga and Beaudoin, 1985).

The drying shrinkage of PCM is generally lower than that of conventional concrete. The amount of shrinkage depends on the water-to-cement ratio, cement content, polymer content and curing conditions. PCM is more susceptible to higher temperatures than ordinary cement concrete. For example, creep increases with temperature to a greater extent than in ordinary cement concrete, whereas flexural strength, flexural modulus and modulus of elasticity decrease. These effects are greater in materials made with elastomeric latex (e.g., styrene-butadiene rubber) than in those made with thermoplastic polymers (e.g., acrylic). Typically, at about 45°C, PCM made with thermoplastic latex retains only approximately 50 percent of its flexural strength and modulus of elasticity.

Because of lower shrinkage, good resistance to permeation by various liquids such as water and salt solutions, and good bonding properties to old concrete, PCM is particularly suitable for thin (even less than 1-inch) floor toppings, concrete bridge deck overlays, anti-corrosive overlays, concrete repairs, and patching (Blaga and Beaudoin, 1985)

2.2.2 Selection Criteria

The material properties that most influence the selection of patch repair materials include shrinkage strain, bond strength, modulus of elasticity, and tensile and shear strength (REMR Technical Note, 1994). The long-term performance of the patch materials is the key consideration while comparing different alternatives. There are numerous material factors that affecting the long-term performance of the patch, as illustrated in Figure 2-1.

Other criteria that should be considered in comparing material alternatives are the cost for the repair, non-monetary factors such as geometric restriction, construction duration, and environmental impact of the repair process, the agency's experience with the use of the rehabilitation techniques involved, traffic, and worker safety during construction (Fuller and Peterson, 1995).
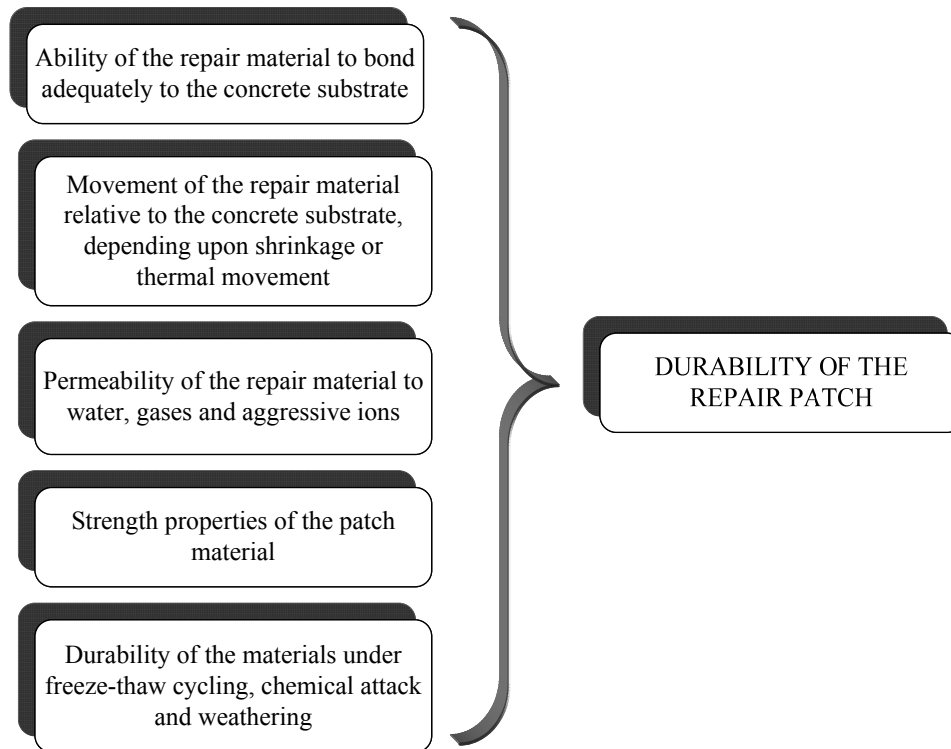
Figure 2-1: Material factors contributing to the long-term performance of the patch (Rizzo and Sobleman, 1989a)

A critical factor that dictates the durability of the repair in a concrete structure is the dimension of the repair related to the existing concrete substrate such as the depth of the repair and type of the application. Patches are typically referred to as 'shallow' for depth less than 1-inch and 'deep' for 1 to 3 inch for overhead, vertical, or horizontal application. This research focuses on the behavior of shallow depth patches.

Factors that affect the durability of shallow depth patches are:

1. Placement method– hand applied, form and pour, form and pump and shot applied.
2. Environmental exposure–weather, chemicals, de-icing salts, and abrasion.
3. Load exposure–compressive, tensile and shear load.
4. Patch geometry–thickness, width, and length.
5. Interaction with patch materials and substrate–bond, strength gain with time, shrinkage, resistance to cracking. (Kelley, 1996).

The choice of an optimum repair material may also be influenced by the availability of materials, the cost of construction, and the schedule and need for future rehabilitation schedule.

Traditionally, the selection of the best possible patch material is based on the material properties supplied by the manufacturers. However, many times the manufacturer's data sheet provides only partial information and some important properties (e.g., elastic modulus, shear strength, bond strength, etc.) are not provided. Furthermore little information is typically given about long-term behavior or field performance.

Appendix A summarizes the materials identified from MDOT's and some other states's Qualified Product List (QPL), and they are classified based on their application and states. There are four vertical and overhead patching materials approved by MDOT. These four repair materials are Sika Top 126 Plus (Sika corp.), HB2 (ThoRoc Ind), Emoco R350-CI (Master Builder Tech), and John M 90(John M). These materials were chosen because of manufacture tested bond strength and inclusion of corrosion inhibitors (Staton, 2001). However M-DOT reports that these materials have problems with adhesion and also the potential for shrinkage cracking that can contribute to future degradation.

Table 2-3 summarizes the mechanical and physical properties of these four repair materials based on the manufacturer's data sheet. It should be noted that all four materials are classified as polymer-modified mortars. As Table 2-3 illustrates, the manufacturer's data sheet gives only partial information about the mechanical and physical properties of these repair materials. Missing material property information limits the analytical studies that can be performed. Therefore, the finite element model developed in Task 2 is limited to two materials from MDOT's list and two more materials used in other states. These materials were selected based on the manufacturer's technical data sheet and the type of application. Missing properties for the repair materials were obtained by contacting the product manufactures.

2.3 Damage Type

Thorough knowledge of the mechanical and physical characteristics of the available products, the existing substrate, and the type of damage in the concrete substrate is needed before a suitable repair material can be chosen. Deterioration of the patch over time is due to; (1) load-induced damage, and (2) environmental-induced damage. Premature failure of the patch

materials is usually due to (1) construction related causes, (2) design related causes, and (3) restrained shrinkage.

Table 2-3: MDOT Repair Materials

	Sika Top 126 Plus	Emoco R350 CI	HB2	John M90
Compressive Strength (psi) (ASTM C109)	5500	5000	5800	4160
Flexural Strength (psi) (ASTM C348)	1600	900	1000	–
Tensile Strength (psi) (ASTM C496)	–	600	590	510
Elastic Modulus (psi) (ASTM C469)	–	2.0×10^6	2.0×10^6	2.44×10^6
Drying Shrinkage (μs)	–	1410	350	–
Slant Shear Bond Strength (psi) (ASTM C882)	–	1500	2700	–

–   Not reported in material data sheet

2.3.1 Cause of Damage and Deterioration

Certain type of damage in concrete structures cannot be prevented over time, and that can occur in the concrete structure or the repaired part. This damage is not avoidable because it is due to mechanical load or environmental load such as corrosion. However the damage and deterioration due to these effects could be decreased by knowing the cause of damage in the concrete or repair element and choosing a more compatible and stronger patch, thereby increasing the lifetime of the patch.

2.3.1.1 Mechanical-Load Induced Damage

This class of damage includes the distress primarily caused by overloading or fatigue of the structure due to the passage of the vehicular loading (mechanical load) or other effects like impact. This load-induced damage mostly occurs at the bottom of girders and slabs of the bridges, and typically causes some tension cracking and spalling of the concrete cover. Tension cracks can accelerate further environmental damage.

2.3.1.2 Environmental-Load Induced Damage

Durability in general is the ability of the concrete and patch to withstand weathering action, chemical attack, abrasion and other service conditions (ACI, 1990). Concrete bridges in Michigan are exposed mostly to thermal cycles; freeze-thaw cycles, wet-drying cycles, acidic gasses (carbonation), and deicing solutions that later two environmental exposures induce corrosion in the steel.

Thermal Distortion

Most Michigan bridges are exposed to un-even solar heating. Having a temperature difference on an element induces additional stresses on the beams and slabs of bridges and results in thermal cracking. The coefficient of thermal expansion of the concrete and degree of restraint affect the amount of thermal distortion related distress. Thermal cracks become worse when the component are frozen winter.

Freeze-Thaw Deterioration

Freeze-thaw deterioration is a function of porosity, moisture saturation, aggregate quality, and also on the number of freeze-thaw cycles (Emmons, 1994). Dry concrete that has a very small amount of moisture will not be damaged even by a large number of freeze-thaw cycles. The concrete moister content will change with the humidity of the environmental. According to Michigan weather statics if only the daily average temperature and fluctuation during each day are neglected, the Michigan bridges will undergo 2000 cycles of freeze- thaw per year. If temperature fluctuations during the day are considered this number will be more than double (see Appendix B). Freeze-thaw damage can be resisted by proper mix-design with low water-cement ratio (w/c), high quality materials, adequate curing, and special attention to construction practices (ACI, 1992). In patch materials, low permeability and shrinkage can reduce freeze-thaw damage.

Corrosion Deterioration

Corrosion of reinforcing bars in concrete is the most destructive mechanism contributing to damage in reinforced concrete bridges in the U.S (Weyers et al. 1993). Corrosion reduces the strength, durability, and service life of reinforced concrete structures. As the reinforcement corrodes, it expands causing cracking of concrete and spalling. Chloride concentration,

temperature, relative humidity, cover depth, and concrete quality are the major factors affecting the rate of corrosion. The transformation of metallic iron to rust can result in an increase in volume of up to 600%, depending on the final rust form (Mehta. 1993). The deterioration caused by corrosion of reinforcing steel in concrete structures has been recognized as one of the greatest maintenance challenges (Beaudette, 2001). Corrosion should therefore be treated before it becomes a significant problem. Since the presence of both air and water is required for the corrosion activity to continue, corrosion may slow down considerably if a barrier could reduce the diffusion of moisture and harmful ions like chloride and carbonate through the concrete

In many situations, even after repairing damaged concrete, corrosion continues to induce damage. The patch can accentuate corrosion in the adjacent steel bar. This phenomenon is often referred to as "ring anode" corrosion (Beaudette, 2001). Ring anode corrosion results from electrochemical incompatibilities between the repair and the concrete substrate. Differences between the base concrete and repair can create an electrical potential difference, which drives a new corrosion cell across the interface between the patch and the concrete substrate. Factors that can lead to this corrosion problem include differences in chloride ion content, pH, and permeability (Beaudette, 2001). These factors may lead to increased corrosion in the repaired part, especially at the interface of the patch and concrete substrate, and consequently cause damage to the patch material.

Two effects can accelerate the corrosion process:

1. *Carbonation of concrete*: Carbonation of concrete is a reaction between acidic gases present in the atmosphere or dissolved in water and the products of cement hydration (Emmons, 1994; ACI, 1992). Carbonation occurs in concrete because the calcium bearing phases present are attacked by the carbon dioxide in the air and are converted to calcium carbonate. Cement paste contains 25-50 % calcium hydroxide ($Ca(OH)_2$) by weight, which means that the pH of the fresh cement paste is at least 12.5. The pH of a fully carbonated paste is about 7. the chemical reaction corresponding to the carbonation is:

$$Ca(OH)_2 + CO_2 \rightarrow CaCO_3 + H_2O \qquad (2\text{-}1)$$

This reaction produces calcium carbonate ($CaCO_3$) and is accompanied by shrinkage. Concrete carbonation is a function of humidity, concrete permeability, and the concentration of carbon dioxide. Carbonated concrete has properties that can be considered both beneficial and detrimental to concrete performance. Favorable effects of

carbonation can be found in increased strength, hardness, and dimensional stability. Adverse effects of carbonation can be a porous and less wear resistant surface. Probably the most detrimental effect is a reduction in the concrete alkalinity, from a pH of around 13 to a pH of around 10 (ACI, 1992). When the pH of the concrete approaches 10, the passivity of steel is destroyed and more rapid corrosion may occur (Emmons, 1994). Carbonation may be recognized in the field by the presence of a discolored zone in the surface of the concrete. The color may vary from light gray that is difficult to recognize to strong orange that is easy to recognize. Carbonation can be visualized by using phenolphthalein. In the optical microscope carbonation is recognized by the presence of calcite crystals and the absence of calcium hydroxide, ettringite and un-hydrated cement grains. Porosity is unchanged or lower in the carbonated zone

2. *Deicing salt*: Chloride ions have a well-documented detrimental role in reinforced concrete as mentioned earlier. Chloride ions are considered to be the major cause of premature corrosion of steel reinforcement (ACI, 1996). The chloride ions disrupt the performance of the passive oxide film on the reinforcement, in turn promoting corrosion (ACI, 1996).

2.3.2 Cause of Premature Failure

The premature failure of shallow depth patches is a significant problem in concrete bridge rehabilitation. Causes of premature failures are usually not load related failure and arise mostly from a lack of knowledge and experience in this field or the use of poor material for prevailing situation. The repair process usually involves different stages and the omission of any of the patching stages can result in unsuccessful patching and premature failure of the patch. The stages of patching are:

(a) An inspection to document the extent and details of damage.

(b) An evaluation to determine the cause of distress and the as-constructed details for the damaged element.

(c) The selection of the repair materials.

(d) The application of the repair materials in accordance with the standard practice for Portland cement based concrete or in accordance with the manufacture's instruction for commercial repair products (REMR Technical Note, 1994).

2.3.2.1 Construction Related Causes

Construction related damage is independent of material properties and arises form bad working conditions. These can be classified in as (Wilson et al, 1999):

1. Exclusion of some deteriorated concrete from the repair boundaries
2. Incompatible climate condition during the repair placement
3. Insufficient consolidation
4. Improper repair technique
5. Inadequate cure time prior to opening repair to traffic.

Using more experienced workers in the field and more detailed and skilled quality control can reduce construction related of damage in the patch material.

2.3.2.2 Design Related Causes

Design related damage occurs mostly de to improper selection of the repair material for the particular application. As mentioned earlier, the selection of the patch material is typically based on the properties reported in material data sheets by manufacturers, and often that data is incomplete and exclude some of the important properties. Improper choice of a patching material can results in:

1. Lack of bond between the patch and original concrete substrate.
2. Incompatible thermal expansion between the repair material and original concrete substrate (Wilson et al, 1999).
3. Incompatible elastic modulus between the repair and original concrete. (Kelley, 1996)

2.3.2.3 Restrained Shrinkage and Other Causes

Restrained shrinkage is one of the main causes of premature failure of patch material. It is neither design nor construction related, and it is unavoidable for any patching technique and patching material. Repair mortars applied to the hardened concrete substrate have a tendency to shrink during the drying phase. The shrinkage of cement-based material comprises chemical shrinkage, thermal strain and drying shrinkage. The shrinkage of epoxy-based material comprises chemical shrinkage and thermal strain, and no drying shrinkage (Yuan et al., 2003). As a result of restraint provided by the substrate at the interface and/or the periphery for an enclosed patch repair, drying shrinkage cannot proceed freely. These results in the development of various stress components, the interaction of which can lead to premature failure of the patch.

The potential failure modes include vertical cracking due to direct tension, horizontal cracking due to transverse or peeling tensile stresses, and delamination due to interface shear stresses (Rahman et al., 1997). Alternatively, the latter two effects could combine to cause a mixed mode failure of the interface.

2.4 Repair Methods

Repair techniques are considered by some researchers to be those that restore a bridge component to an acceptable level of service (Weyers et al., 1993). Repair strategies can be developed with several or no levels of redundancy to assure durable repairs (Emmons, 1994). Different repair scenarios can be used, depending on the degree of exposure and damage (Xanthakos, 1996). Monitoring of repairs is recommended to improve damage inspection and assessment techniques (Shanafelt and Horn, 1980). The ability to perform maintenance or replacement of repair systems should also be considered (Xanthakos, 1996). For repairing the damaged members there are two different techniques: (1) repair, and (2) replace. This study focuses on repair of the damaged element by patching materials. Repair consists of three different stages: (a) Removal of damaged concrete, (b) patch placement, and (c) curing.

2.4.1 Concrete Removal and Surface Preparation

All damaged, deteriorated, loosened, or unbonded portions of existing concrete should be removed from the concrete substrate. Two different techniques to detecting the concrete that needs to be removed and patched: (a) observation and hammer sounding for shallow removal, and (b) coring and half cell techniques for deep removal. The removal technique should preserve the concrete substrate and provide a good quality surface for bonding the patch material. Each technique has strengths and a weakness (Weyers et al., 1993) is used. Hydrodemolition is a technique in which high pressure water (around 20 to 40-ksi) to remove concrete of any condition. This is an attractive removal option because it cleans the reinforcing bars as it removes surrounding concrete without causing damage to the remaining concrete or steel (Weyers et al., 1993). Other concrete removal methods include the use of pneumatic and electric impactors and rotary hammers. These processes are flexible, but also the most labor intensive, and hence production rates are slow (Weyers et al., 1993).

In addition, all loose scale, rust, corrosion byproducts, or concrete should be removed from exposed reinforcing steel to completely expose reinforcing steel for more than one-third of its perimeter circumference to provide 1-inch minimum clearance between the steel and the concrete. Damaged or deteriorated reinforcing steel should be removed and replaced. For additional protection from future corrosion, the prepared reinforcing steel should be coated with Zincrich Rebar Primer or install Corr-Stops® CM. The edges of the repair locations should be saw cut to a depth of at least 3/8" (10 mm) to avoid featheredging and to provide a square edge. The concrete in complete repair area should be removed to a minimum depth of 3/8" (10 mm) up to the sawn edge.

Any microfractured surfaces resulting from the initial removal process should be eliminated. Diffrent options can be used for preparing the roughened concrete surface. Depending on the requirements of the repair material, surface preparation methods consisting of compressed air blasting, detergent washing, water blasting, grit blasting, sand blasting, scabbling, or mechanical abrasion may be appropriate. One researcher has found that using sandblasting techniques increased the bond strength of overlays when specific contact inhibitors are used (Al-Qadi, 1993).

The surfaces should be cleaned and allowed to dry thoroughly (unless the specific repair technique requires application of materials to a saturated surface). Some material data sheets recommended that the substrate should be saturated surface-dry (SSD) with no standing water (e.g. HB2 repair mortar)

Acids should not be used for cleaning or preparing concrete surfaces for repair. After the concrete is prepared and cleaned, it should be kept in a clean, dry condition until the repair is completed. Any contamination, by oil, solvent, dirt accumulation, or other foreign material should be removed by additional cleaning as stated above.

2.4.2 Application and Finishing

The chosen repair material and repair location will largely govern placement and formwork options. Some options include form-and-pump, form and cast-in-place, hand application, low-pressure spraying and others (Emmons, 1994). For large surface area repairs, spray application may work better compared to other techniques. As a general principle in the repair of buildings (like materials should be replaced with like materials and cementitious-based repair materials are

preferred to epoxy–based repair materials, unless low permeability is desired to reduce the moisture diffusion. The repaired mortar surface should be finished by striking off with a straight edge and smooth with a steel trowel. Wooden or plastic floats or sponges may also be used to achieve the desired surface texture. The completed surface should not be overworked.

The use of stainless steel pins should be considered to secure deeper patches. The Illinois Department of Transportation has used patches that were mechanically anchored to the concrete using pins and welded wire fabric reinforcement (Xanthakos, 1996).

2.4.3 Curing

Proper curing is extremely important. For peak performance the repair should be cured immediately after finishing in accordance with good concrete practices (see ACI 308). Options for curing repair materials consist primarily of moist or membrane curing methods. Moist curing methods (e.g. wet burlap covered with polyethylene sheet) are often viewed as being more efficient than membranes (curing compounds), but for vertical application, and other difficult to access areas such as beam-ends, moist curing may be difficult.

The following practices are recommended for best performance of the patch material:

1. If the patch material sags during application, completely remove it. Properly reprime the substrate and reapply the mortar at a reduced thickness.
2. Dispose of any material that sets prior to application.
3. Try to not apply at ambient or surface temperatures below 50°F/10°C or above 90°F/32°C.
4. Follow the material data sheet and details provided by the manufacturer.

2.5 Numerical Modeling to Evaluate Patching Materials

Analytical and numerical methods can be used is to evaluate the performance of patching materials and assess the effect of different material properties such as strain shrinkage strain and elastic modulus, on their performance. A variety of approaches have been used to evaluate the behavior of patch materials under the different loading conditions. Most of these studies focus on evaluating the risk of cracking in and delamination of the repair material and/or the concrete substrate due to shrinkage effects. The approaches described below are the most general techniques used to simulate shrinkage in concrete. Some were developed specifically to analyze

repair materials, while others may be modified to make them applicable to modeling concrete repairs. Existing methods include:

1. Conproco procedure (Pinelle, 1995)
2. ACI Committee 209 procedure (ACI 209R-92) with new Comité International du Béton (CIB) equations for time-dependent properties
3. Laval University model (Pigeon and Bissonette 1999)
4. Chidiac et al. model(1997)
5. The University of Texas model for polymer concrete repairs
6. 4C-Temp & Stress model (Danish Technical University; Pedersen et al. 1997)
7. HIPERPAV model(McCullough and Rasmussen 1999)
8. Warsaw University of Technology model for polymer concrete repairs (Czarnecki et al.1999).

Most of the above are basically "load-resistance" models that compare the computed stresses in a particular structural configuration with the available strength as a function of time. In addition to these models, a fracture mechanics based model was developed at Northwestern University to analyze the ring test (Shah et al. 1998).

Some more recent studies used finite element analysis to simulate shrinkage in concrete repair material. Since shrinkage occurs due to loss of moisture, shrinkage can be model as a moisture diffusion problem that is coupled with the stress analysis module (Rahman, 2002). In this method a nonlinear differential equation based on Fick's second law describes the diffusion of moisture through cementitus material (Rhman, 1999). Another method incorporates the shrinkage strain as an initial strain, computes the equivalent displacements at the ends, and applies these as a boundary condition (Shambria, 2000).

The research described in this report focuses more on the post shrinkage behavior of the patch materials in terms of debonding and cracking, and not on the details of the shrinkage behavior of the patch materials. Complex diffusion-based techniques are, therefore unwarranted. In this research, the shrinkage strain is applied as a uniform initial strain in the patch material and time-dependency of shrinkage is neglected. Finite element analysis is used to determine stresses not only due to shrinkage, but also due to corrosion and mechanical loads.

Chapter 3
Finite Element Simulation

3.1 Introduction

This chapter presents the development of finite element models to evaluate and predict the effect of restrained shrinkage, corrosion, and mechanical load on the repair materials and the concrete substrate. The ABAQUS general purpose finite element package was used for all the analysis. The main goal of the numerical studies was to choose a layer of FRP that can sustain all the above loading and prevent further damage on the patch material. Figure 3-1 illustrates the various types of analyses performed using 2-D and 3-D finite element models.
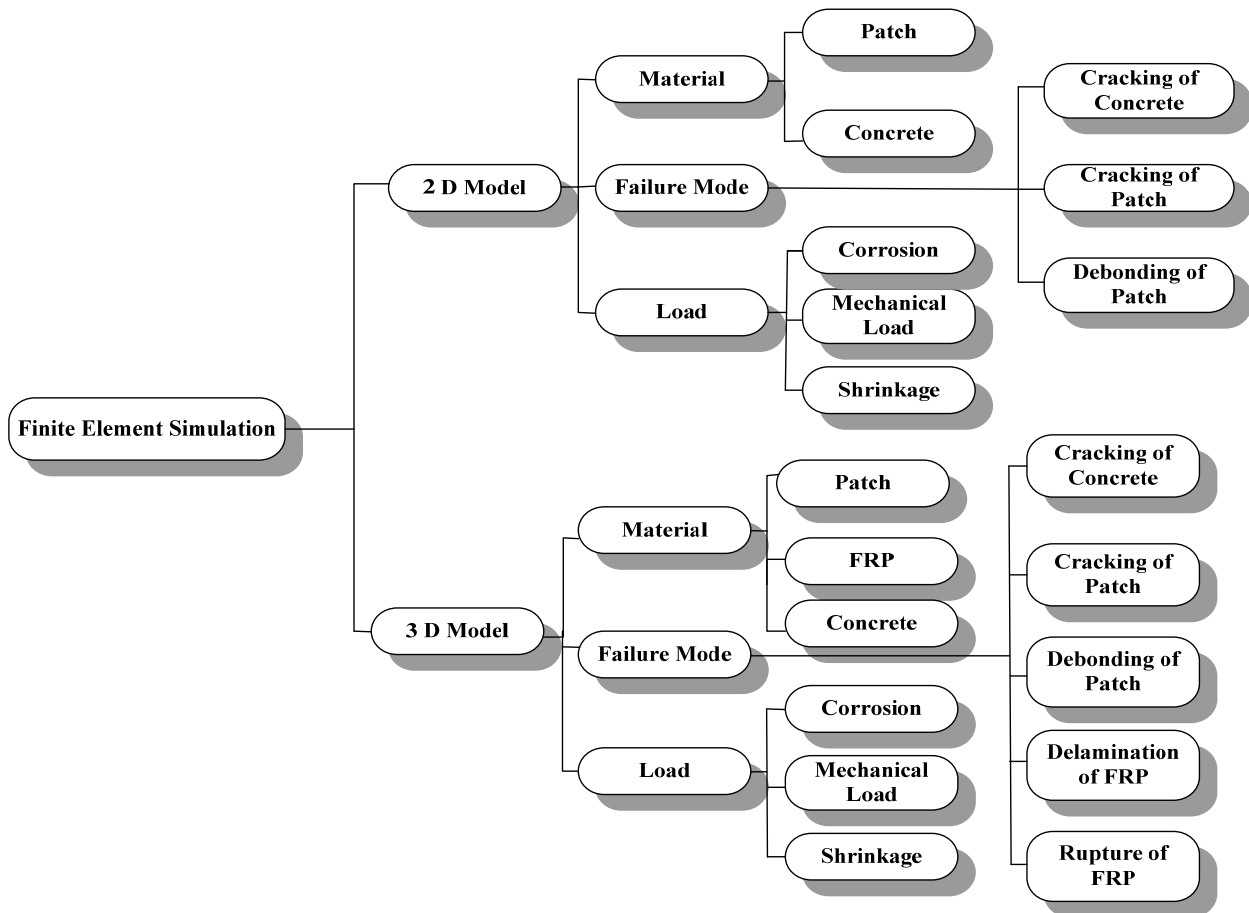
Figure 3-1: Finite element evaluation matrix

2-D models were used to study the effect of different loading on the repair material and concrete substrate when the FRP overlay was not used. 3-D models were used to select optimally configured layers of FRP on damaged patches. The major limitation of experimental investigation is that they cannot provide detailed information regarding the type of damage in the patch material. The experimental results can indicate the amount of damage in the patch, but often micro cracking cannot be detected and more importantly the cause of each type of damage in the patch material such as cracking or debonding cannot be inferred. In light of these limitations numerical models and results can provide a better understanding of the behavior of the patch material and FRP overlay under different loading conditions.

3.2 Geometry, Material and Boundary Conditions

3.2.1 Geometry and Materials

The analyses were conducted on models with the geometry, boundary conditions, and loading to be used in initially envisaged experimental specimens[*]. Simply supported beams with dimension of 16" × 4" × 3" were used in mechanical load and shrinkage tests, and beams with dimension of 12" × 6" × 6" were used in corrosion tests. Both beam geometries were to have a cavity of dimension 4" × 3" × 0.625" and 4" × 5" × 0.625", respectively, on the bottom side. The physical and mechanical properties of the patch and FRP materials used in the FE models are given in Table 3-1 and Table 3-2. The properties of the chosen patch material were extracted from the material data sheets provided by the manufacturer. MDOT requires chosen FRP materials to have Caltran durability approval for different environmental exposures such as freeze-thaw.

Table 3-1: Properties of Patch Materials used in Finite Element Analyses

	Commercial Name (Client Agency)	Elastic Modulus (psi)	Shrinkage Strain (με)	Compressive Strength (psi)	Slant Shear Bond (psi)	Tensile Strength (psi)
Material 1	HB2 (MDOT)	2.0×10^6	350	5000	2700	590
Material 2	R350 CI (MDOT)	2.0×10^6	1410	5000	1500	600
Material 3	VO1 (WvDOT)	3.6×10^6	800	5550	1930	620
Material 4	200 (UDOT)	2.49×10^6	760	5800	2000	800

---

[*] Geometry of the specimens was changed after the first set of tests as explained in Chapter 4.

Table 3-2: Properties of FRP Composites used in Finite Element Analyses

	Type	Commercial Name (Client Agency)	Fiber Orientation	E_{11} (psi)	Ultimate Tensile Strength (psi)	Thickness (in.)
FRP 1	Glass	SHE-51	Unidirectional	3.47×10^6	6.67×10^4	0.05
FRP 2	Glass	Chopped (General)	Chopped	1.17×10^6	1.50×10^4	0.04
FRP 3	Glass	Hex 106 G	Bidirectional	2.47×10^6	4.40×10^4	0.013
FRP 4	Carbon	MBrace CF130	Unidirectional	1.02×10^7	8.00×10^4	0.02
FRP 5	Carbon	Hex 113 C	Bidirectional	6.05×10^6	6.60×10^4	0.01

3.2.2 Material Model

Each material was modeled based on the available data in the literature and appropriate material models in ABAQUS (version 6.3).Unfortunately for some of the materials used the existing data did not provide the best material behavior, and in some cases ABAQUS did not have an appropriate material model.

3.2.2.1 Concrete Material Model

There are currently three different models in the ABAQUS (version 6.3) to model plain and reinforced concrete. These include the smeared cracking model, the concrete damage plasticity model and the cracking model. In this study, concrete damage plasticity model was used for modeling concrete.

The damage plasticity model is very versatile and capable of predicting the behavior of concretes structure subjected to monotonic, cyclic and/or dynamic loading. It assumes the main failure mechanism of tensile cracking and compressive crushing in compression, and uses the multi-axial plasticity model with a non-associated flow rule and isotropic strain hardening. In tension the model uses a multi-axial damage elasticity model. Concrete in tension is considered as a linear-elastic material until the uni-axial tensile stress, f_t, at which concrete crack is attained and softening behavior is assumed thereafter. A linear softening model is used to represent the post-failure behavior in tension.
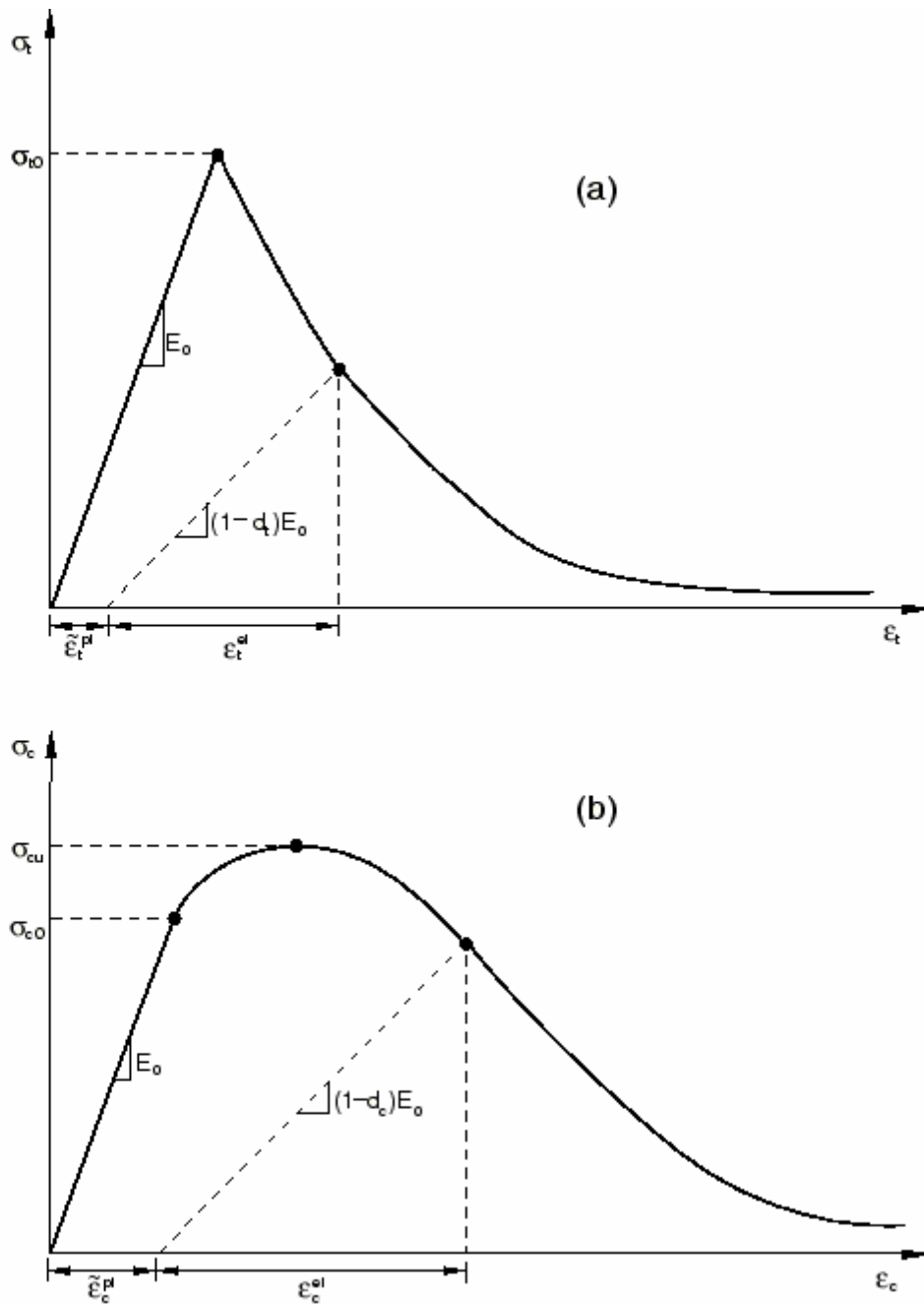
Figure 3-2: Typical concrete uni-axial stress-strain curve in (a) tension and (b) compression
(ABAQUS User Manual)

The softening rate depends on the post-failure behavior in tension. In the analysis for mechanical loading the number of failed elements was large, because of the high tensile stress; ABAQUS does not have any provision to model the possible high crack widths and the analysis

terminated and prematurely. To resolve this problem, a large tension stiffening value was used to continue the analysis up to the failure. It should also be noted that after initial tension cracking in the concrete the tensile strength of the concrete can't be ignored. Therefore the concrete was modeled as an elastic-plastic material with different properties in tension and compression. The behavior of the model in uni-axial tension and compression is shown in Figure 3-2. Figure 3-3 shows the combined uni-axial stress-strain curve.

The input required for defining the concrete material model are: (a) the un-iaxial compression stress-strain curve; (b) the uni-axial tension stiffening stress-strain curve; (c) the volumetric dilation angle ψ; (d) the bi-axial compression ratio; and (d) the ratio of tensile-to-compressive meridian K. These inputs are described as below.

The uni-axial compression stress-strain curve was defined using the Todeschini empirical stress-strain model. A typical uni-axial compressive and tensile stress-strain curve for 3500 psi concrete is shown in Figure 3-3. As explained earlier the concrete is assumed to have elastic-plastic behavior under the tensile loading.

$$f_c = \frac{2f''_c\,(\varepsilon/\varepsilon_0)}{1+(\varepsilon/\varepsilon_0)^2} \tag{3-1}$$

where

$$\varepsilon_0 = \frac{1.71f'_c}{E_c} \tag{3-2}$$

$$f''_c = 0.9f'_c \tag{3-3}$$

The calculation for the dilation angle involves complex mathematical derivations, and assumptions using the yield surface of the concrete damage plasticity model. The dilation angle for unconfined concrete in this study was assumed to be 30 degree (30°). The bi-axial stress ratio and the tensile to compressive meridian ratio were assumed to be equal to 1.16 and 0.667, respectively.
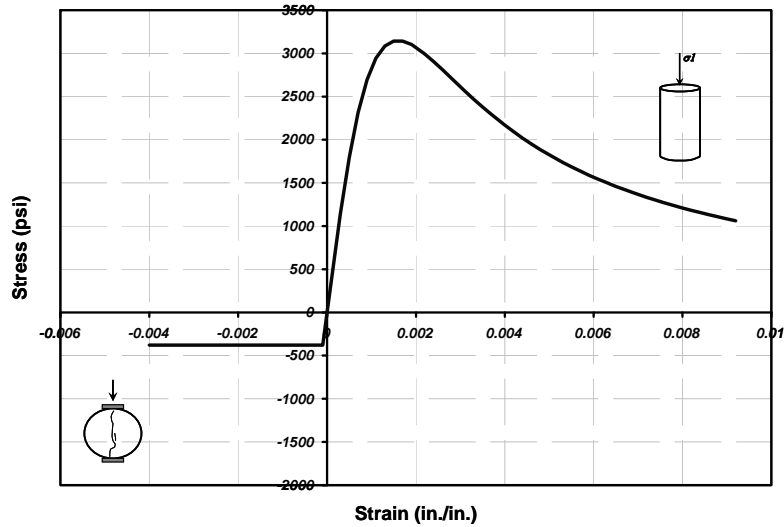
Figure 3-3: Stress-strain curve used for concrete

3.2.2.2 Other Materials

Modeling the Steel Reinforcement

The steel bar was modeled using an isotropic elastic-perfectly plastic multi-axial material model. The elastic modulus used was 29,000 ksi, and the yield and ultimate stresses were 60 ksi and 94.5 ksi, respectively. The yield and ultimate stresses were not required because the mechanical applied load produced only 40% of the yield stress in the steel bars.

Modeling the Patch Material

Since information regarding the plastic behavior of the patch material in tension or compression was not available in the literature or the material data sheets, the patch material was modeled using an isotropic elastic material model. Tension crack opening and crack propagation in the patch material was applied manually in each time step based on a tension crack function. The failure modes in the patch material and concrete substrate are present in detail in the next section.

Modeling the FRP Material

The FRP was modeled as a linear elastic material based on the information provided in the on material data sheet for the fabric and the resin. In ABAQUS, the FRP overlay was

26

modeled using the lamina option. In this option the material can be define as an orthotropic plane stress material.

For the bi-directional FRP overlay, the longitudinal and transverse stiffnesses were calculated using

$$E_L = E_F V_F + E_M V_M \tag{3-4}$$

where E_M and E_F are the matrix and fiber elastic modulus, respectively, and V_M and V_F are the volume fractions of the matrix and fiber, respectively. This equation is commonly called the "Rule of Mixtures" or upper bound theory.
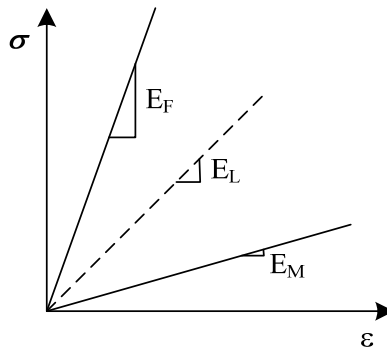
Figure 3-4: FRP stiffness calculation

This equation is accurate for composites under tensile loading, but can have a slight error for compressive loading since the fibers act like long columns that are restrained from buckling by the shear stiffness of the matrix.

The ultimate stress of the FRP overlay was calculated using the same concept:

$$\sigma_L = \sigma_F V_F + \sigma_M V_M \tag{3-5}$$

where σ_F and σ_M are the ultimate stresses of the FRP fabric and the matrix, respectively.

For unidirectional fabric the elastic modulus in the transverse direction was calculated through

$$ET = \frac{E_F V_M}{E_M V_F + E_F V_M} \tag{3-6}$$

3.2.3 Loading Conditions

The effect of three different loading conditions that in practice causes the most damage was studied. As mentioned in the literature review, drying shrinkage, mechanical load, and corrosion causes the most significant loads on the patch material. In addition to the effects of these three individual loading conditions, possible load combinations were also studied.

3.2.3.1 Shrinkage Load

Since ABAQUS (version 6.3) is not able to directly model plastic shrinkage of concrete or any mortar based material, shrinkage was applied as an initial strain in the patch material within the time steps. Shrinkage effects were simulated using a fictitious coefficient of thermal expansion and a reduction in temperature applied uniformly through the patch:

$$\varepsilon_{sh} = \alpha \times \Delta T \tag{3-7}$$

where ε_{sh} = shrinkage STRAIN according to the manufacturer's data sheet, ΔT = change in temperature (assumed to be $100^{\circ}C$), and α = coefficient of thermal expansion = $\varepsilon_{sh} / \Delta T$. Since this research focused mainly on post damage behavior of the patch material, more sophisticated analysis was consider unnecessary.

3.2.3.2 Corrosion Load

When the reinforcement bars corrode, the corroded steel swells to about 4 to 6 times of its initial volume. However, some of the corrosion product is likely to fill pore voids within the concrete. The expansion induced by corrosion can only be obtained by calibrating with experimental data. In a previous MDOT project (Baiyasi, 2000) strains in FRP wraps were measured for wrapped concrete cylinders subjected to accelerated corrosion. Figure 3-5 shows how the measured strain varied with time.
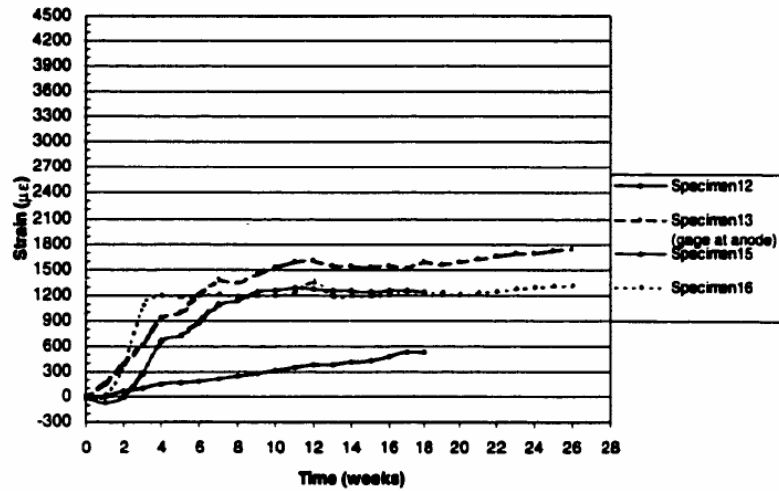
Fig. 3.46 Hoop strains in bonded, carbon-wrapped specimens

Figure 3-5: Hoop strain in carbon-wrapped specimens (Baiyasi, 2000)

A FE model of the carbon FRP wrapped concrete cylinders was developed, expansion strain was introduced into one steel bar (anode in the original experiment), and the hoop strain in the carbon FRP was computed.
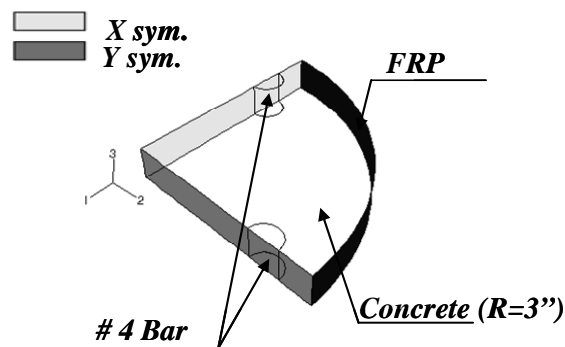
Figure 3-6: Boundary condition and geometry of corrosion specimen
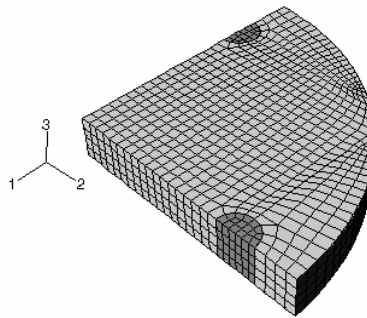
Figure 3-7: 3-D finite element mesh of FRP wrapped concrete cylinder

29

The expansion strain was simulated in ABAQUS using a fictitious coefficient of thermal expansion and a fixed temperature change. The expansion strain was varied until the computed FRP strain was about 1600 $\mu\varepsilon$ (maximum strain in Figure 3-5). The corresponding expansion strain applied to the cross section of the # 4 bar was 17500 $\mu\varepsilon$.

It should be noted that the concrete was modeled using a Drucker-Prager material model to consider the effect of the confinement pressure exerted by the FRP wraps. To eliminate the undesirable strain in the longitudinal direction, an orthotropic material with longitudinal thermal expansion of zero was used. Details of the analysis are discussed in more detail in section 3.3.

3.2.3.3 Mechanical loading

The applied mechanical load was limited to induced a strain in the steel of be about $0.4\varepsilon_y$ as mentioned before. Two concentrated loads were applied at the tired points on the top surface of simply supported beam specimens.

3.2.4 Bond Surfaces and Failure Models

Full bonding between the steel reinforcement and concrete was assumed. Full bonding between the patch material and the concrete substrate was also assumed, but the bonded surfaces were allowed to separate node-by-node to simulate crack propagation in the patch material and debonding along bonded surfaces. Details are provided in the next section.

3.2.4.1 Failure Functions

Patch Failure

Two failure modes were considered in the patch: a) bond failure between the patch and the concrete; and b) tension cracking in the patch.

> *Debonding Index:* Coulomb theory is used to describe the concept of shear bond failure:

$$\tau_n = c + \mu \times \sigma \tag{3-8}$$

where τ_n = bond shear stress, σ = normal stress acting on the bond interface, c = pure shear strength (obtained from a direct shear test), and μ = coefficient of friction between the two surfaces. Coefficients of friction have been determined from studies investigating bond on

various surfaces and are dependent on the surface preparation of the concrete substrate. Table 3-3 gives the coefficient of friction for different surface preparations.

Table 3-3: Coefficient of Friction (Austin, 1999)

Surface Preparation	Coefficient of Friction
Smooth	0.75
Medium Rough	1.00
Rough	1.25

Bond failure was characterized by the debonding index:

$$\text{DI} = \sqrt{\left(\sigma_{ii}/\sigma_n\right)^2 + \left(\tau_{ij}/(\tau_n)\right)^2} \qquad (3\text{-}9)$$

where τ_n = shear bond strength obtained from equation 3-1, σ_n = tensile or compressive strength of the patch material, τ_{ij} and σ_{ii} = shear and normal stresses acting on the bond interface, respectively. Debonding occurs when DI > 1.

Figure 3-8 shows the bond strength envelope for Material 2 based on information in the manufacturer's data sheet for three different surface preparations. The parameter c for Material 2 according to the material data sheet is 400 psi (obtained from direct Shear test-MDOT). Since the tensile and compression strength of Material 2, 600 psi and 5000 psi respectively, exceed the tensile and compression strength of the concrete substrate, 378 psi and 3500 psi respectively, σ_n in equation 3-6 is assumed to be 378 psi or 3500 psi, and failure is assumed to occur in the concrete rather than the patch material. The curves in Figure 3-8 represent the combination of τ_{ij} and σ_{ii} that yield DI=1 ,where τ_n is computed using equation 3-8.

$$\text{DI} = \sqrt{\left(\sigma_{ii}/\sigma_n\right)^2 + \left(\tau_{ij}/(C + \mu \times \sigma_{ii})\right)^2} \qquad (3\text{-}10)$$
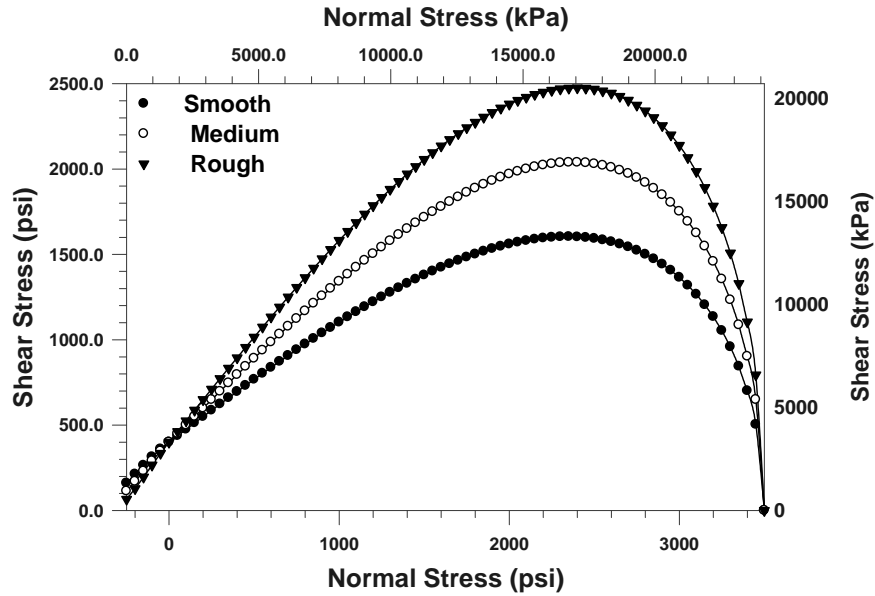
Figure 3-8: Bond failure envelope

Tension Crack Index: As mentioned earlier, the other potential failure is tension cracking of the repair material itself due to shrinkage. The potential for tension cracking can be assessed using the principal tension stress at a point. A tension cracking failure function is defined as:

$$\text{TCI} = \sigma_{p\,\text{max}} / f_t \tag{3-11}$$

where σ_{pmax} = maximum tension principal stress and f_t = tensile strength of the patch material. Tension cracking occurs when $\text{TCI} > 1$

FRP Failure

Two failure modes were considered for FRP material: a) rupture of the FRP fibers or matrix depending on the loading and direction of unidirectional FRP (FRP1, FRP4), and b) bond failure between the patch and the FRP overlay.

Rupture Index of FRP/Matrix: The potential for rupture in the fibers or matrix can be assessed using the fibber/matrix rupture index.

$$\text{F/MRI} = \sigma_{ii} / f_{ultimate} \tag{3-12}$$

where σ_{ii} = stress in direction of fibers or matrix and $f_{ultimate}$= ultimate tensile strength of the FRP. Rupture occurs in the FRP when F/MRI> 1

Debonding Index: The potential for debonding of the FRP was assessed using the debonding index, DI, defined earlier for the patch. However, since the normal stresses acting on the bond is very small for the FRP it can be neglected, and only the shear stress was used in computing DI.

$$DI = \sqrt{\left(\tau_{ij} / (\tau_n)\right)^2} \qquad (3\text{-}13)$$

where τ_n = shear bond strength, τ_{ij} = shear stress acting on the bond interface. Debonding occurs when DI >1

Bond Length. The required extension of each FRP overlay beyond the dimensions of the patch was calculated using:

$$L_e = \frac{2500}{(ntE_f)^{0.58}} \qquad (3\text{-}14)$$

where L_e = effective bond length needed for the FRP to transfer all the stresses to the concrete substrate when fully stressed, n = number of layers, t = thickness of a layer, and E_f = elastic modulus of the FRP layer (Khalifa, 1998). It should be noted that since the full capacity of the FRP overlay is not likely to be required when it is used as an overlay, the chosen extension length could be less than L_e.

3.3 Two-Dimensional Finite Element Model

Two-dimensional FE analysis was conducted to evaluate the behavior of the patch material and detect the type of damage under each type of loading. Since the results of FE analysis were used in the laboratory investigation, the boundary conditions and the geometry of the first set of experimental specimens were used in the analysis. The beam was evaluated under three different loading conditions: a) mechanical loads (four point bending) b) shrinkage of the patch material, and c) corrosion load. Combination loads were not used in the 2-D analysis.

The model consisted of a simply supported beam with a #3 bar as flexural reinforcement for the shrinkage and mechanical load analysis. For a corrosion case, a concrete block with three #4 bars, two bars as anodes (corroding bars) half in patch and half in concrete, and one as a cathode (non-corroding bar) in concrete were used. Both models had a cavity at the bottom to model the patch. The mid-section of the beam was modeled in 2-D.

The geometry, boundary condition and repair patch are shown in Figure 3-9 and Figure 3-10 for mechanical, shrinkage and corrosion loads.

(a)

(b)

(c)
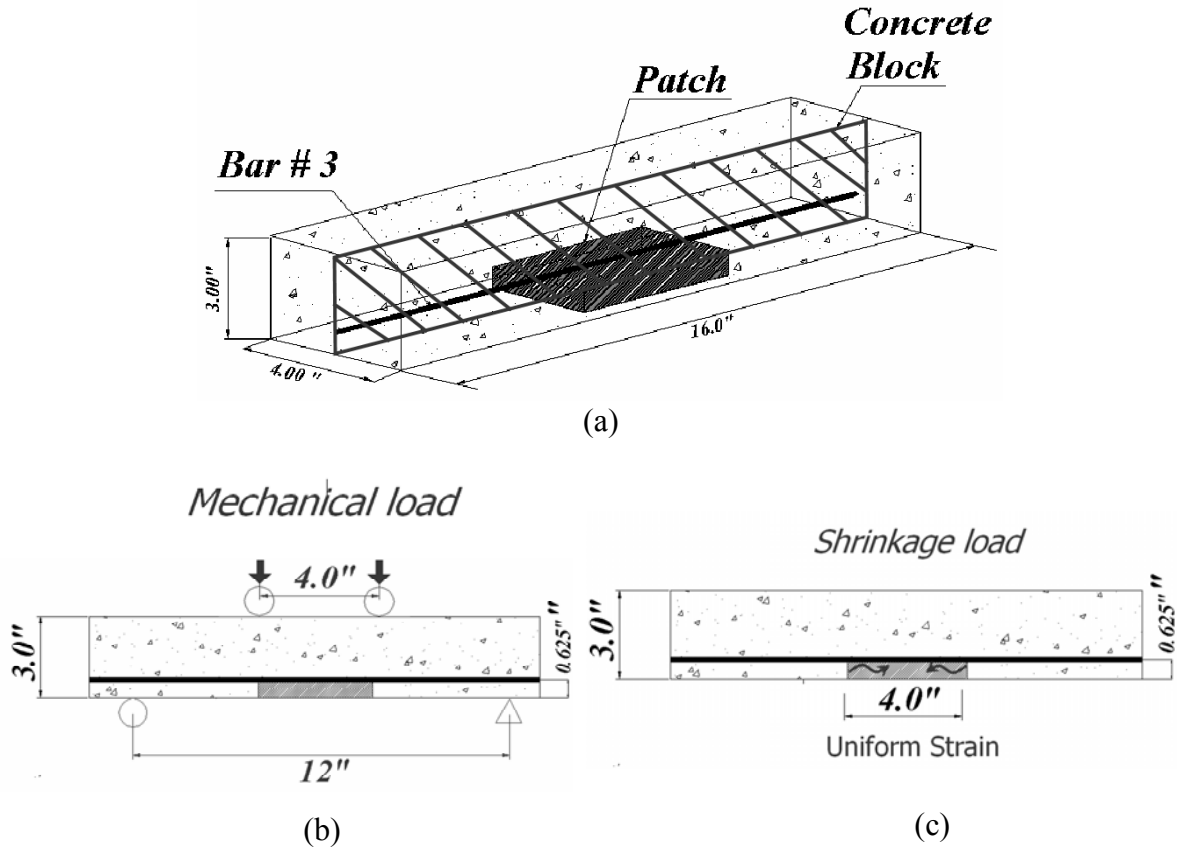
Figure 3-9: Shrinkage and mechanical load: (a) experimental unit, (b) mechanical load model, and (c) shrinkage load model
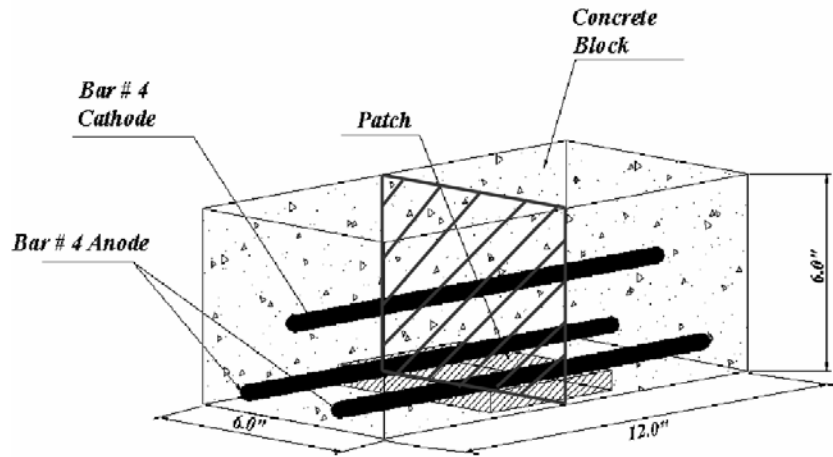
(a)
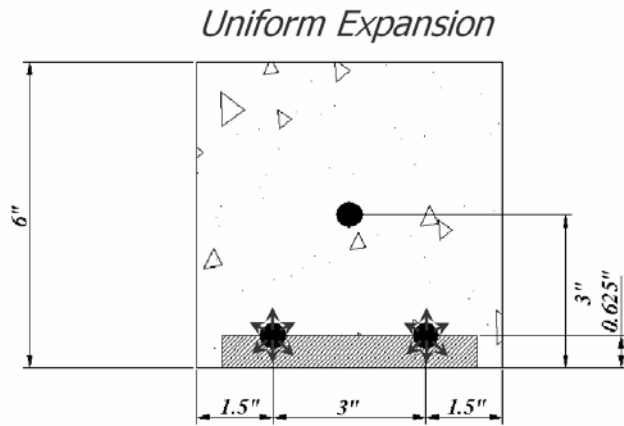
(b)

Figure 3-10: Corrosion load: (a) experimental unite, and (b) 2-D model

3.3.1 Element Selection

Figure 3-11 (a) and (b) shows typical 2-D FE mesh discretizations of the beam. The models consist of: a) a concrete part modeled with 4-node plane stress quadrilateral reduced integration elements (CPS4R), b) a repair patch with 4-node plane stress quadrilateral reduced integration elements (CPS4R), and c) a steel reinforcement part modeled with 2-node truss elements (B21) for the mechanical and shrinkage models and a 4-node plane stress quadrilateral reduced

integration element (CPS4R) for the corrosion model. CPS4R elements are versatile and can be used in simple linear analysis or complex nonlinear analysis involving contact plasticity.
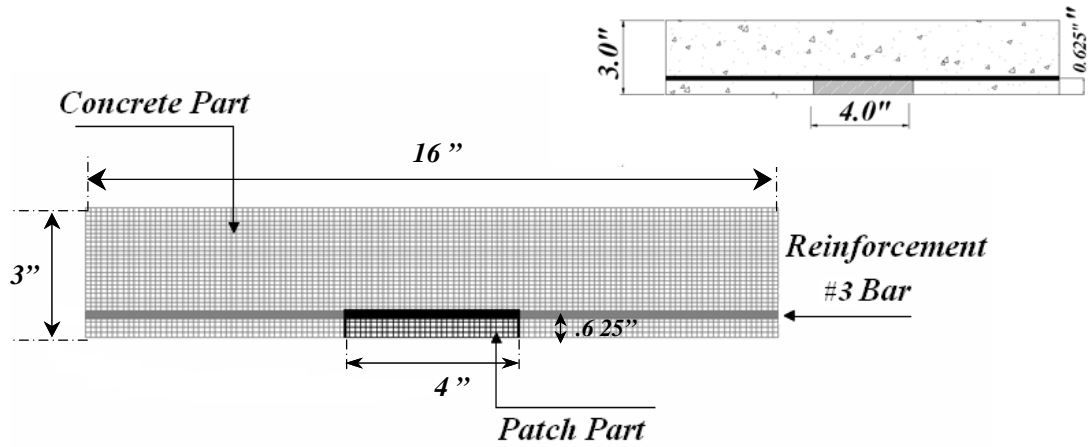
(a)
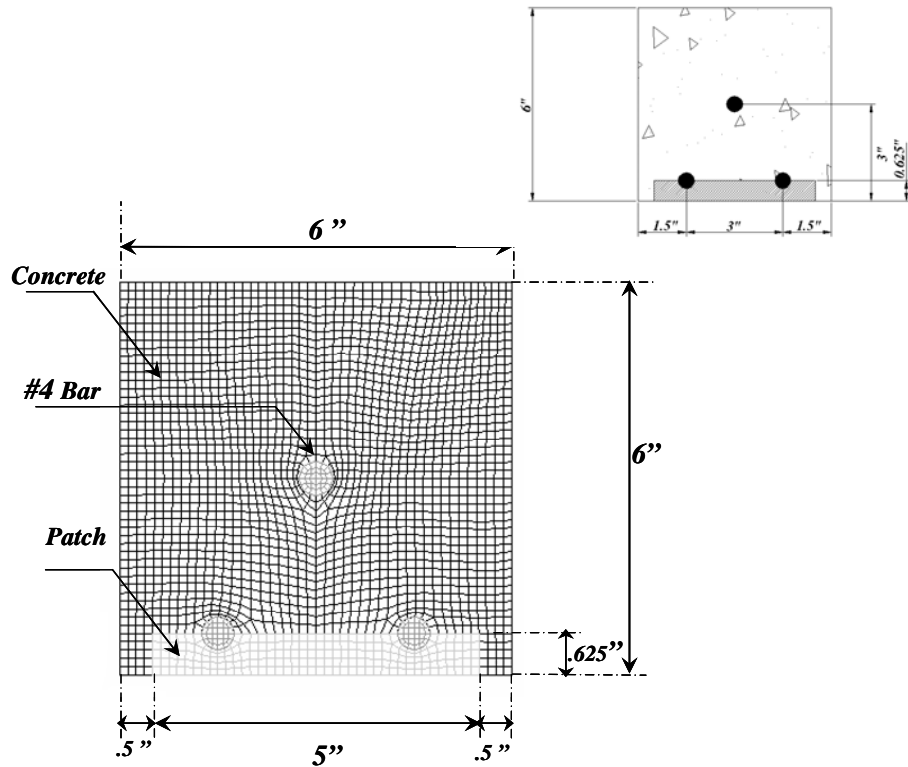
(b)

Figure 3-11: 2-D finite element model discretizations: (a) shrinkage and mechanical model, and (b) corrosion model

3.3.2 Results of 2-D Analysis and Discussion

3.3.2.1 Shrinkage Load

The stresses inside the patch and the status of the bond between the patch and concrete substrate were assessed by using debonding and tension crack failure indices. When the failure indices exceed unity, failure will occur. Figure 3-12 and

Figure **3-13** shows the FE results due to shrinkage along the patch. The debonding index (DI) is shown along the side and top bond surface, and tension crack index (TCI) is shown along the most critical vertical path located mid length of the patch. By comparing these figures it can be seen that tension-cracking failure occurs before debonding for Materials 2, 3, and 4. No debonding or tension crack failure is observed for Material 1.

The behavior of the patch bond status and the likelihood of other crack opening after initial cracking were studied by using the model with a pre-opened crack at the most likely location (path h).The conditions along the bond surfaces and inside the patch were evaluated by computing the debonding and tension crack indices.
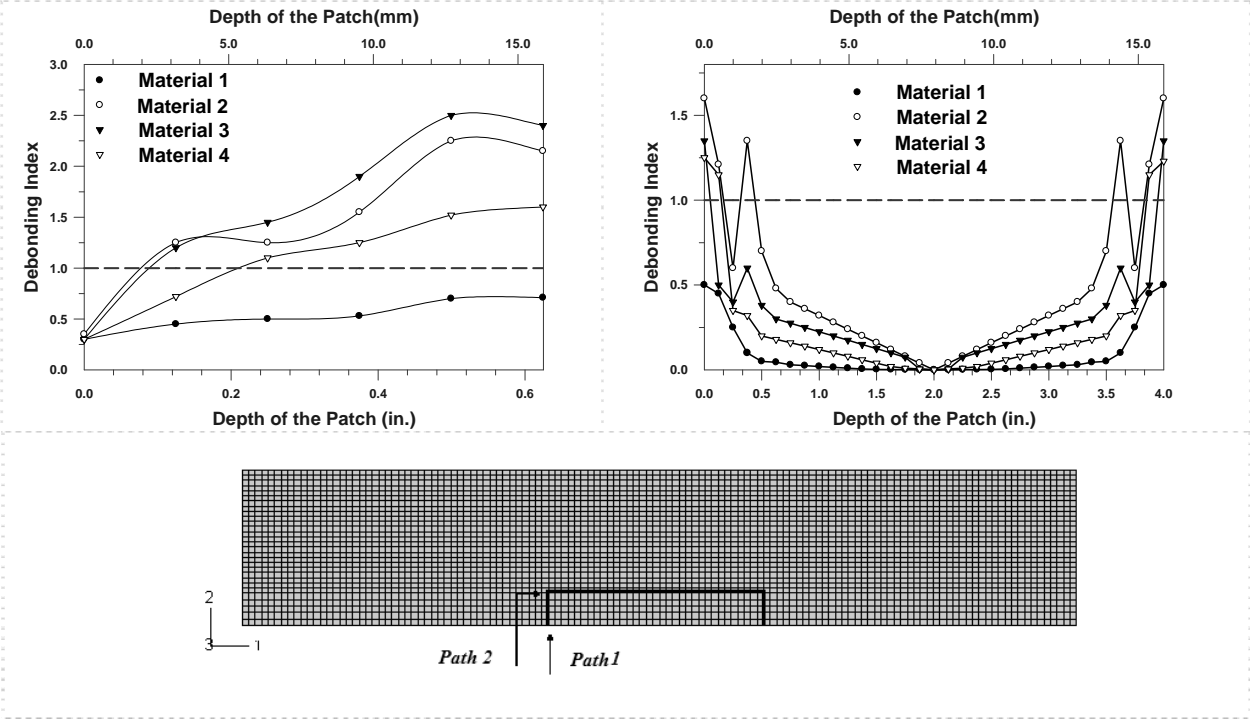
Figure 3-12: Debonding index along bond surfaces due to shrinkage
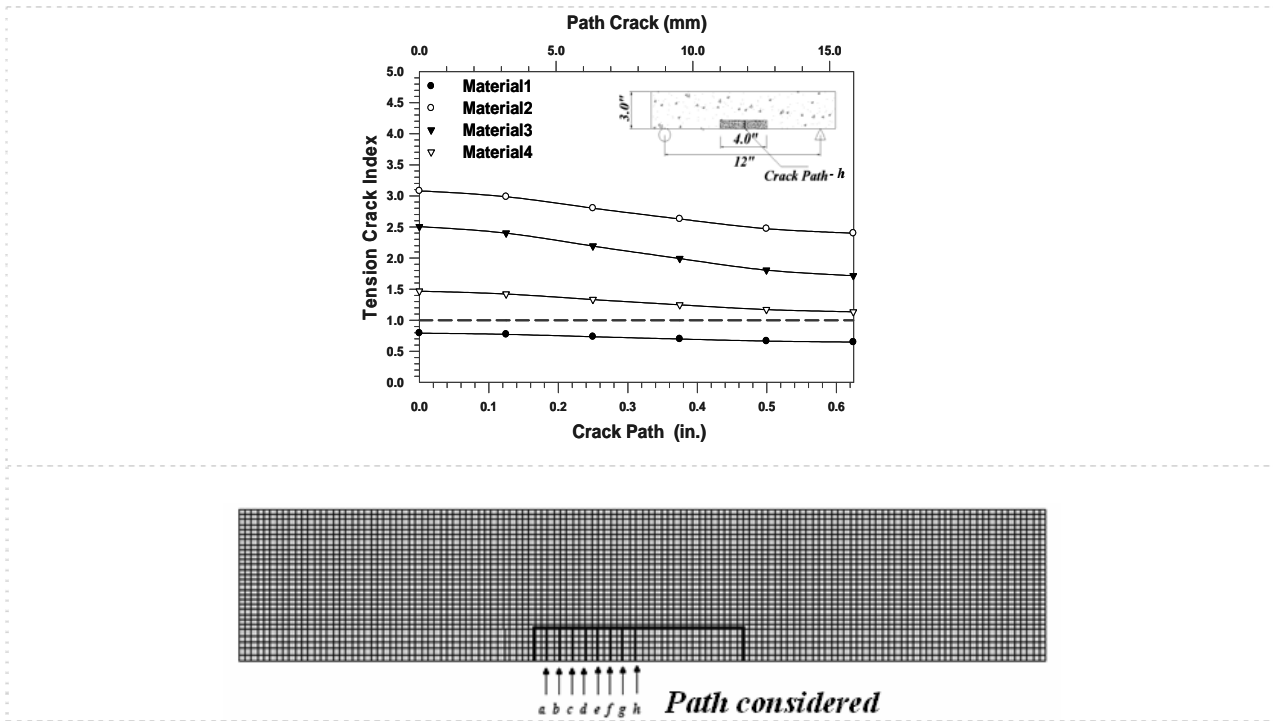
Figure 3-13: TCI along the most critical path (h)

Since Material 1 did not show any tension cracking or debonding in the first analysis, only materials 2, 3 and 4 were considered in the second analysis. The DI, and TCI along paths 1, 2, and a through g are shown in Figure 3-14 and Figure 3-15, respectively.

Figure 3-14 and Figure 3-15 show that except for Material 2, which has a higher shrinkage strain compared to the other repair materials, the potential for multiple tension cracks on the top face of the patch is larger than the potential for debonding. Therefore, tensile cracks are likely to open randomly and prevent debonding on the bonded surfaces. However, the analyses indicate that not all of the cracks will reach the outside surface of the repair material. For Material 2, the risk of delamination along the top surface is higher than cracking at the side of the patch. The results of the 2-D FEM model under shrinkage loading compares well with the results of the laboratory investigation performed at Michigan Technological University (Ahlborn, 2002) for the two chosen MDOT repair materials (R350 CI and HB2) under shrinkage. Since there is no material data sheet available for the third MDOT material (Sika top 126), this material was not studied.
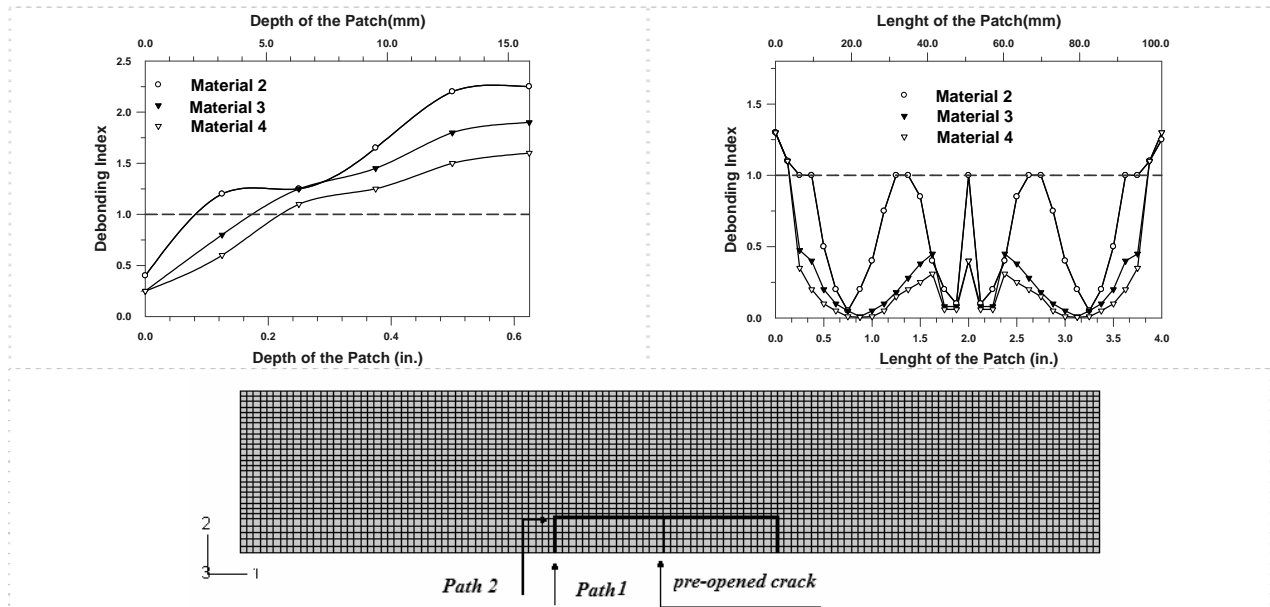
Figure 3-14: Debonding Index on the bond surfaces due to shrinkage after first crack

3.3.2.2 Mechanical Load

Under mechanical loads, the elastic modulus has more influence than the other parameter on the stress distribution, and consequently on debonding or tension cracking.

Figure 3-16 and Figure 3-17 show the debonding and tension crack indeces under mechanical load at different locations. Since materials 1 and 2 have the same elastic modulus, they show the same stress distribution under the mechanical load, However because Material 1 has better bond strength according to the manufacturer's data sheet it should behave better and not debond. Except for Material 3, the potential for debonding along the side surfaces (Path 1) is higher than the potential for tension cracking inside the patch. Material 3 shows the worst condition for both failure modes. No tendency for debonding was observed at the top surface of the patch due to mechanical loads. Repair material 1 showed the best behavior under mechanical load as well as shrinkage effects because of its high bond strength and low elastic modulus. Figure 3-18 shows the location having the highest potential for the first crack due to applied mechanical load. This location is most critical because of the geometry of the patch and location of the applied load.
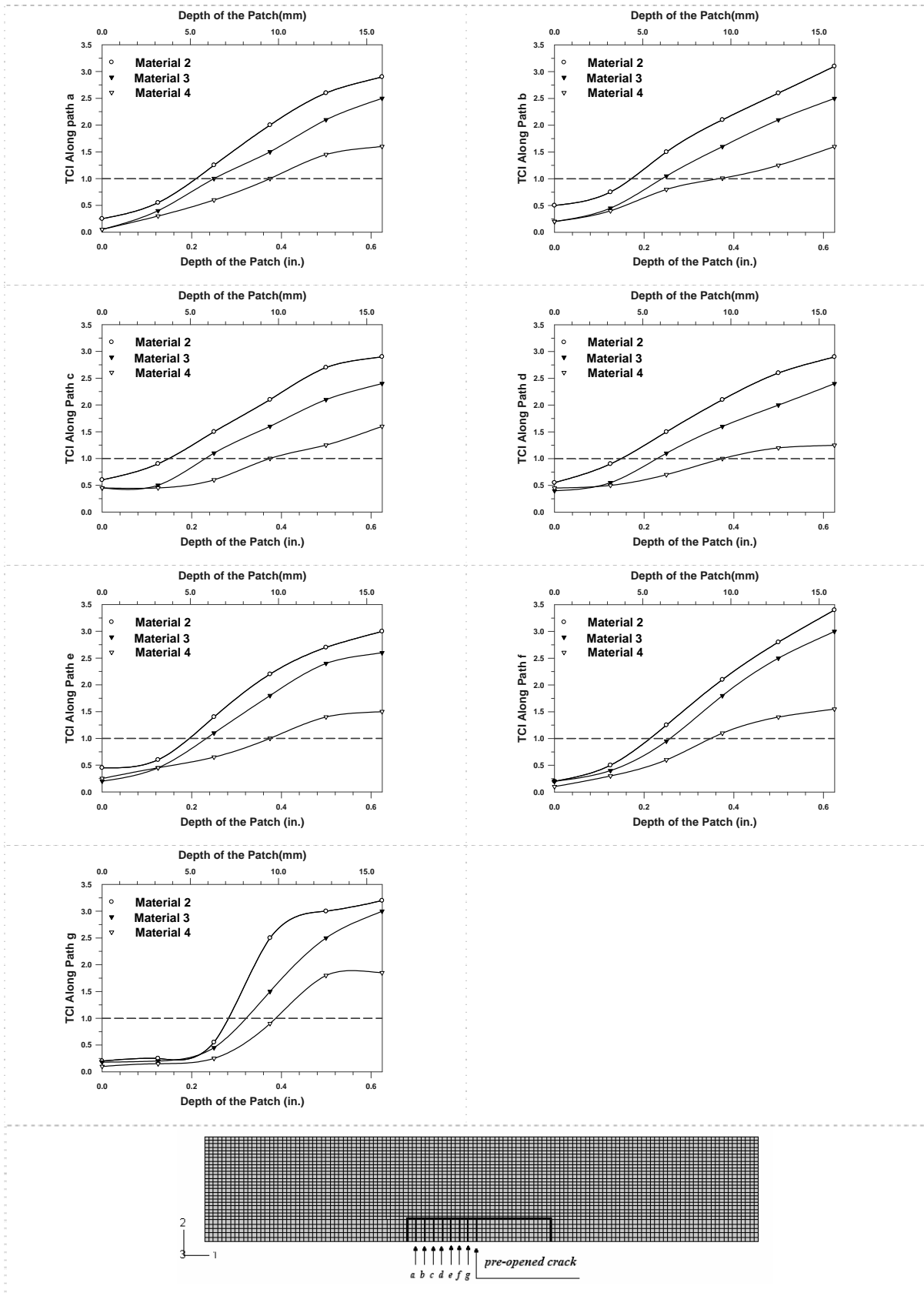
Figure 3-15: Tension crack index along the patch due to shrinkage after first crack
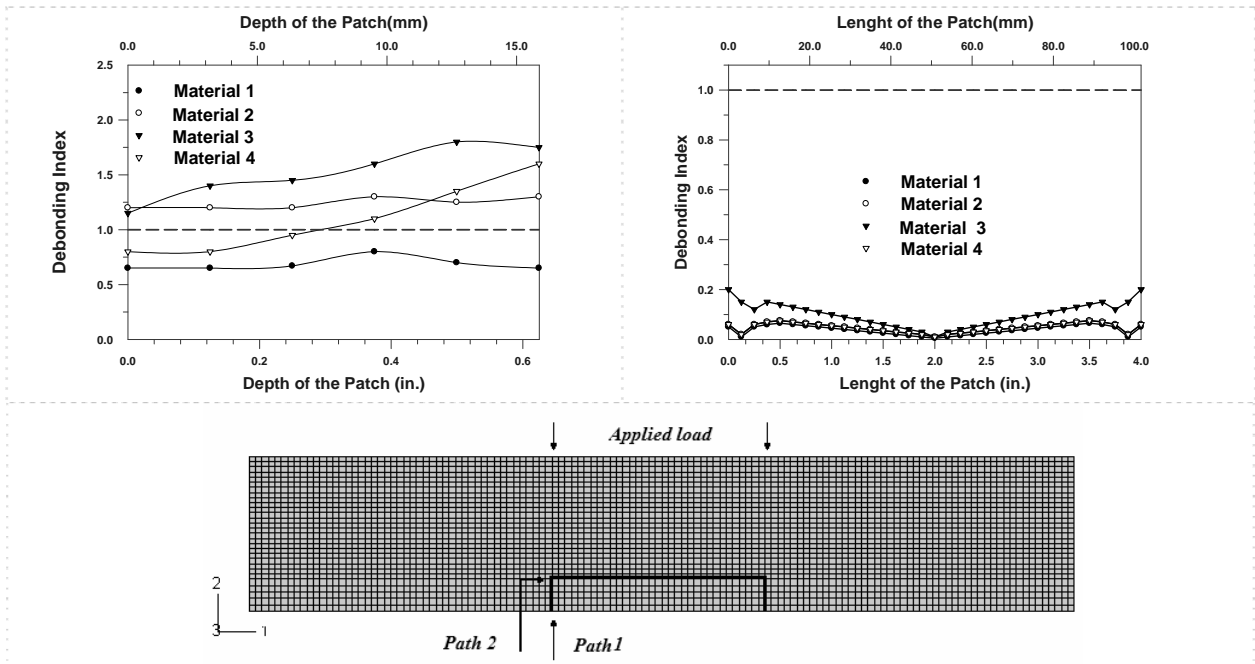
Figure 3-16: Debonding index on bond surfaces due to the mechanical load
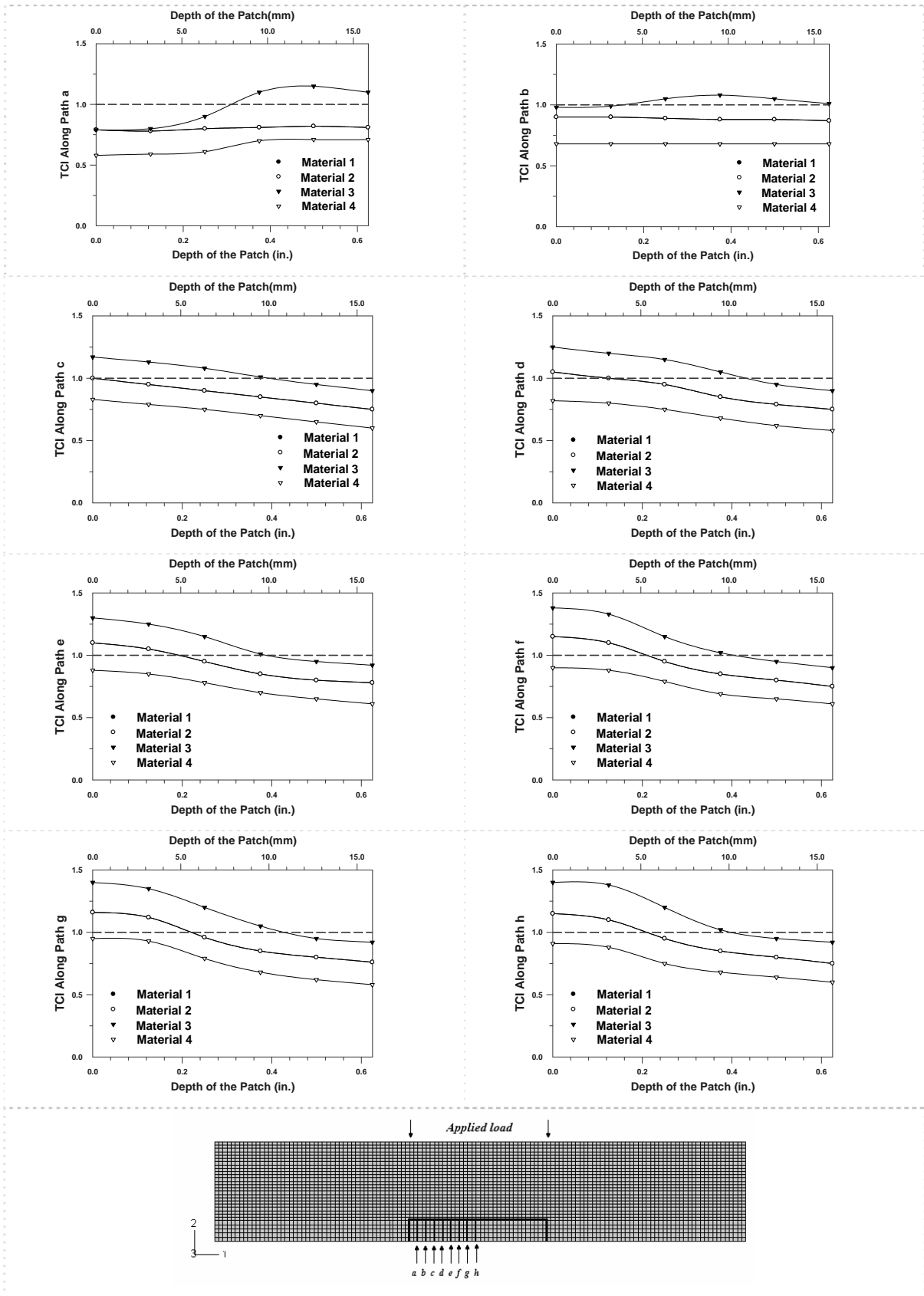
Figure 3-17: Tension crack index along the patch due to the mechanical load
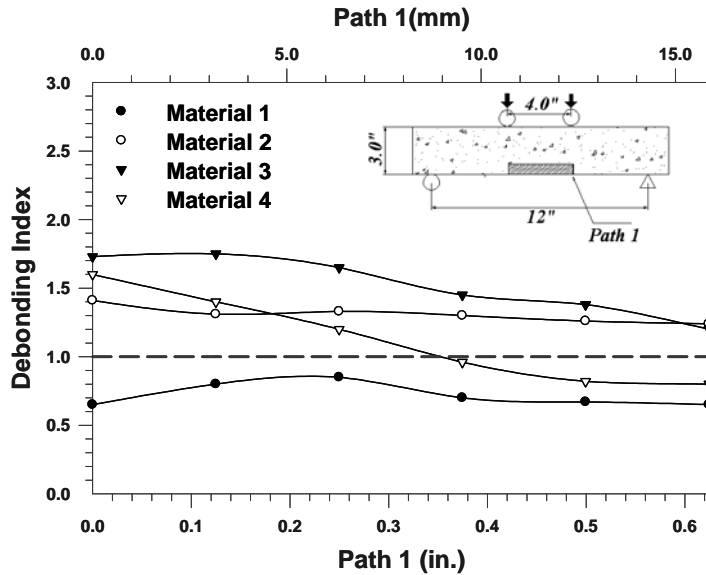
Figure 3-18: DI along location of the first likely crack due to mechanical load

The post-debonding behavior of the patch materials under mechanical load was studied by defining a debonded region between the repair material and the concrete substrate where the debonding index in Figure 3-18 exceeded unity.

Figure 3-19 and Figure 3-20 shows that after initial debonding no major damage occurs for Materials 2 and 4. However, because of its high elastic modulus, Material 3 had the potential of further tension cracking in the patch.

Only the strongest (Material 1) and the weakest (Material 2) patching materials were used for the subsequent parts of the research. The physical and mechanical properties of these two materials are given in Table 3-1.

3.3.2.3 Corrosion Load

As mentioned earlier, when reinforcement bars corrode the corroded steel swells up to about 4 to 6 times of its initial volume. However, some of the corrosion products are likely to fill pore voids within the concrete. The expansion due to corrosion was therefore estimated by calibration with available experimental data for FRP wrapped concrete cylinders subjected to accelerated corrosion (Baiyasi, 2000) as explained before. Based on this calibration, an expansion strain of 17,500 $\mu\varepsilon$ was applied to the cross section of the #4 bar. Figure 3-21 shows the tension crack index along different paths for patch material 2. Both patch materials behave the same way because their elastic modulus is the same. The Figure 3-21 indicates that since the

TIC >1.0 for all the paths, the patch will have several cracks radiating outward from the corroding steel bar. The first crack will occur along path 1.

3.3.3 Conclusion

Material 1 showed the best performance under both shrinkage and mechanical loads because it has the most desirable combination of mechanical properties (lower elastic modulus, lower shrinkage strain, and higher bond strength, etc.) compared to the other repair materials considered in this study. On the other hand Material 2 showed the worst behavior. Under mechanical loads the cracks propagate from the bottom surface of the patch, while under shrinkage the cracks propagate downward from the top surface of the patch. Therefore, the combination of these two cases (mechanical load and shrinkage) represents a more severe condition than either of them alone, and the combined case will be studied using a 3-D FE model for selecting the FRP fabric. Corrosion load was the most severe loading and all the patch materials will show extensive cracking. To evaluate the behavior of the shallow repairs using Material 1 and 2 in more detail, a 3-D FE model was developed with the same assumptions as for the 2-D model.
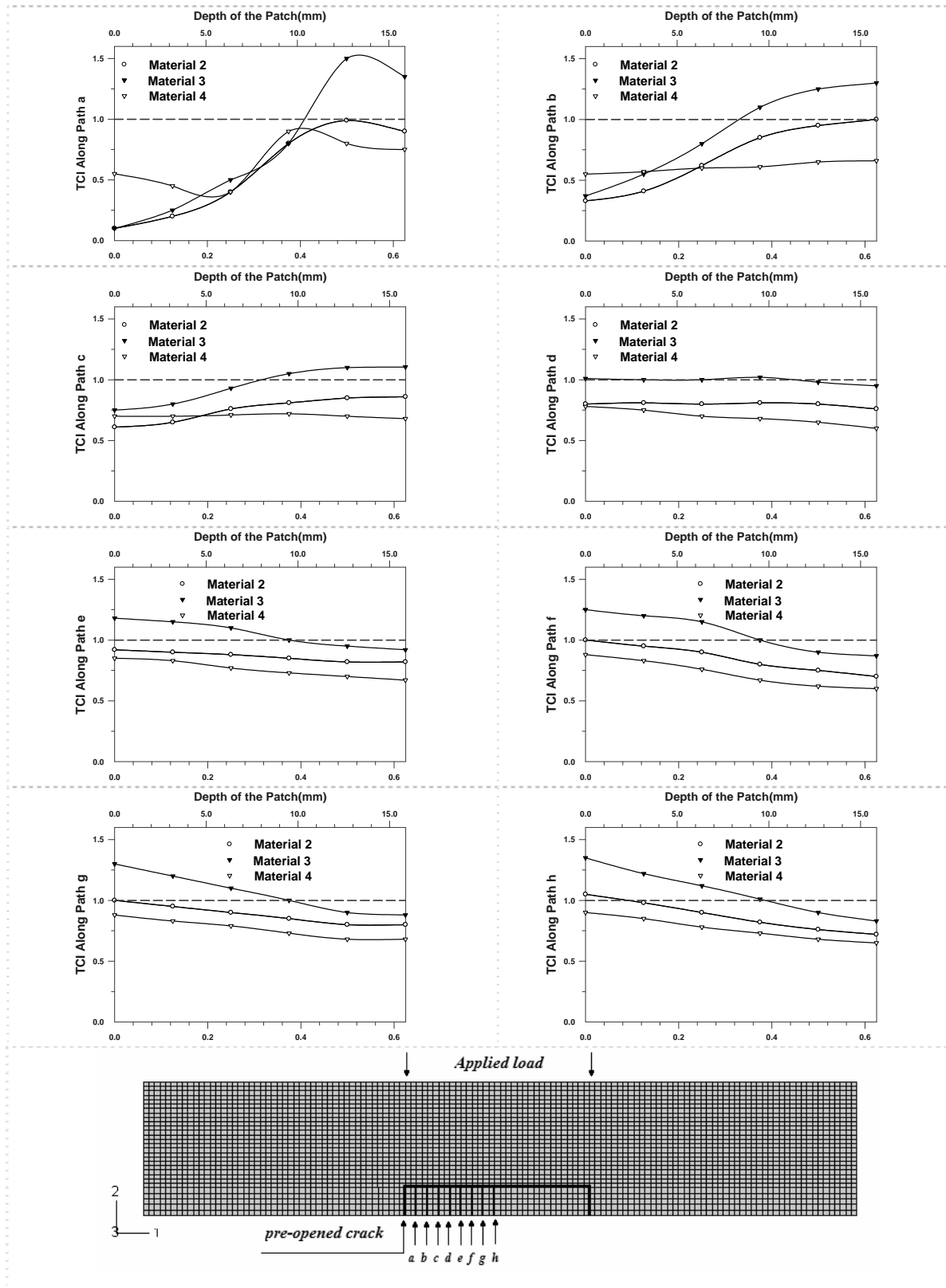
Figure 3-19: Tension crack index along the patch due to the mechanical load after debonding along path 1
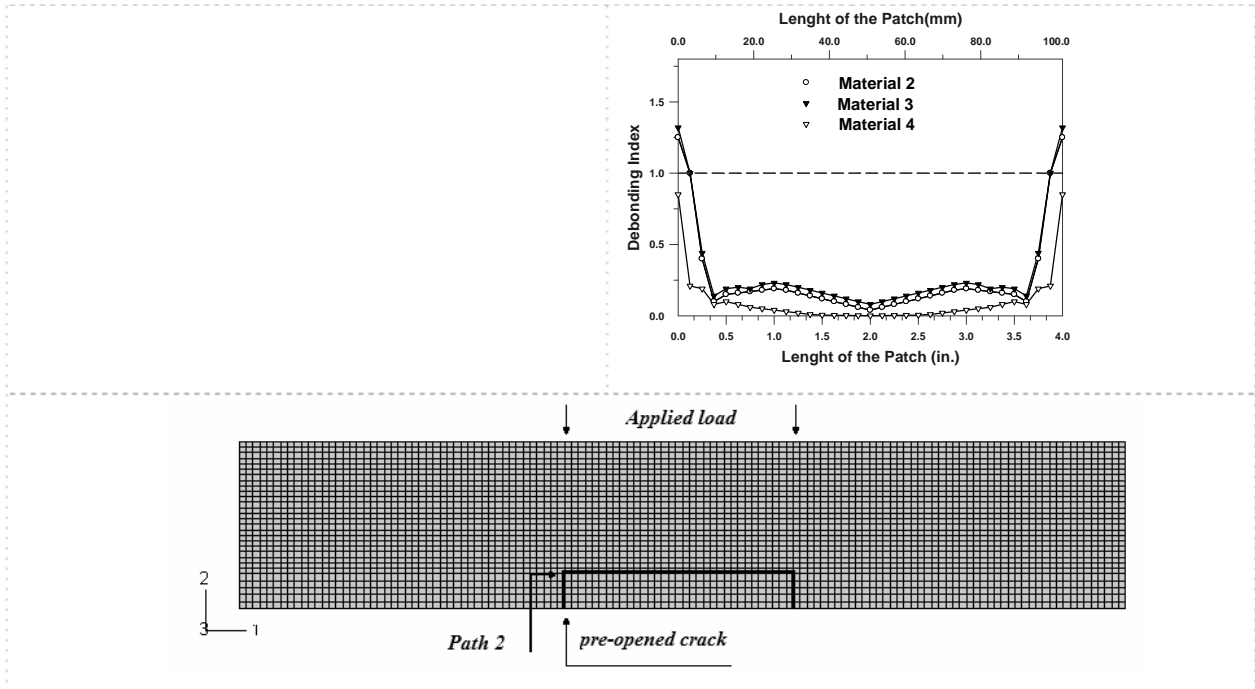
Figure 3-20: Debonding index on bond surface due to mechanical load after debonding along path 1
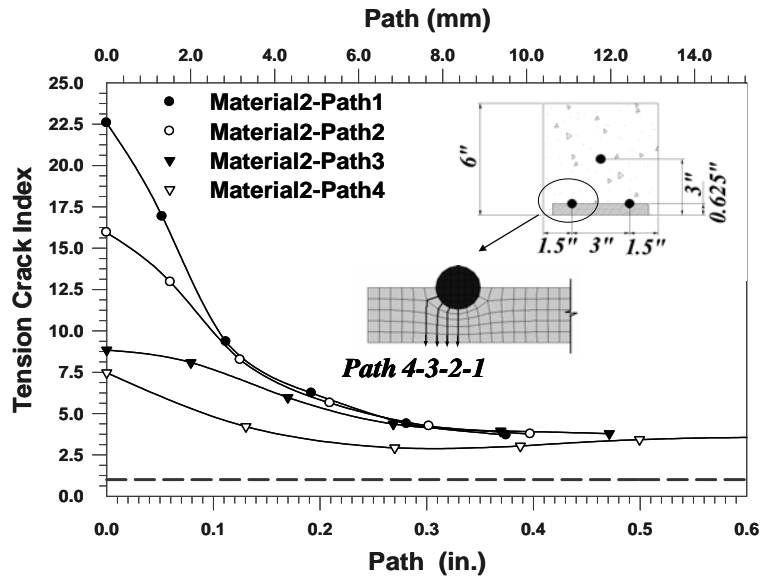
Figure 3-21: Tension crack index due to corrosion along the various paths

3.4 Three-Dimensional Finite Element Models

The purpose of the 3-D analysis was to choose the best FRP overlay and its orientation over the patch. The beam was evaluated under three different loading conditions: a) mechanical loads (four point bending), b) shrinkage of the patch material, and c) corrosion load. The combination of loads was also studied. The dimentions of the beams were the same in 2-D analysis, and in some of the 3-D analyses a layer of the FRP was used over the patch as shows in

Figure **3-22** and

Figure 3-23. To reduce computational effort, only a quarter of the beam was modeled for
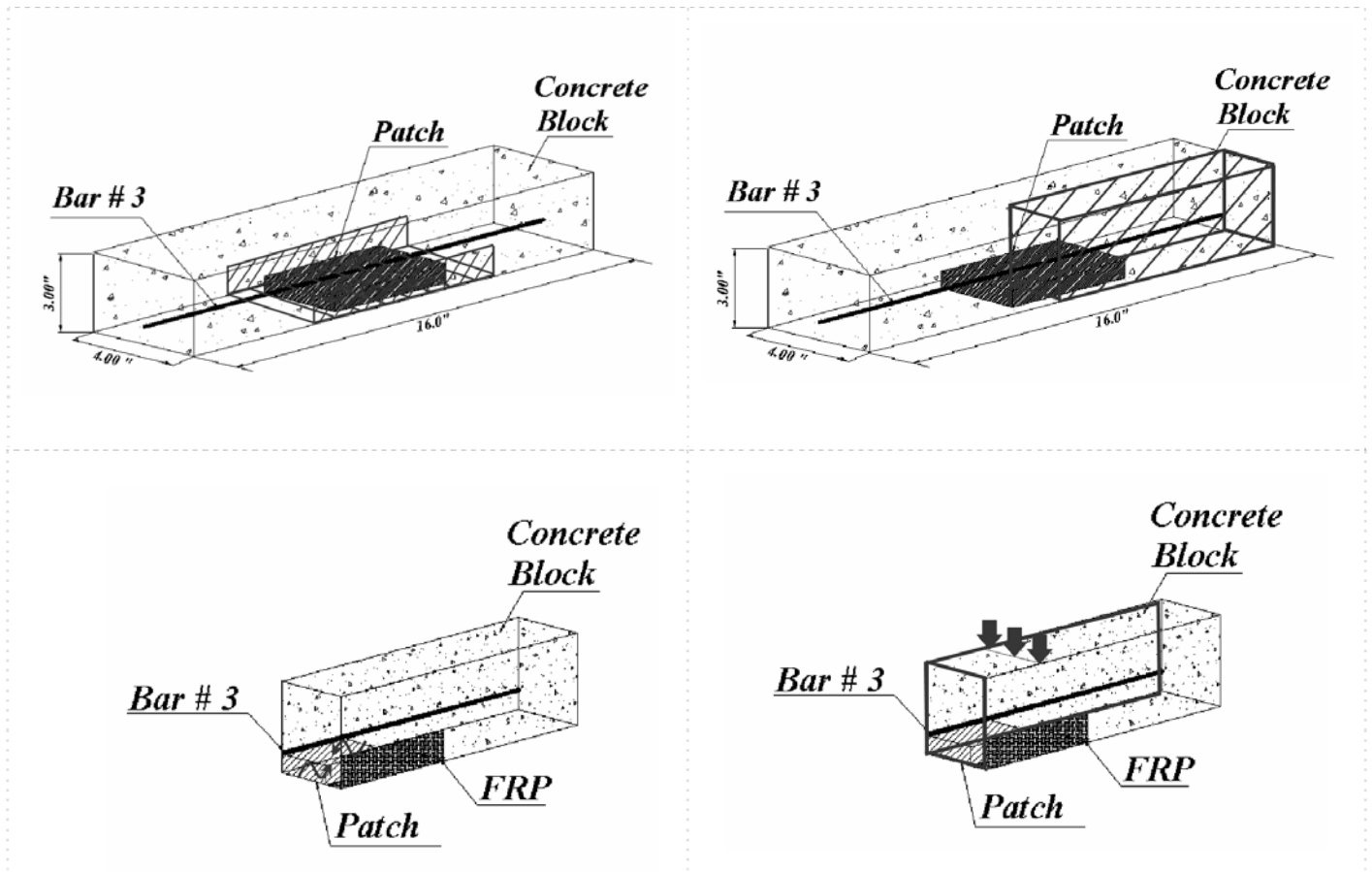
all cases. The model geometries are shown in Figure 3-22 and **Figure 3-23**.

Figure 3-22: 3-D shrinkage and mechanical model
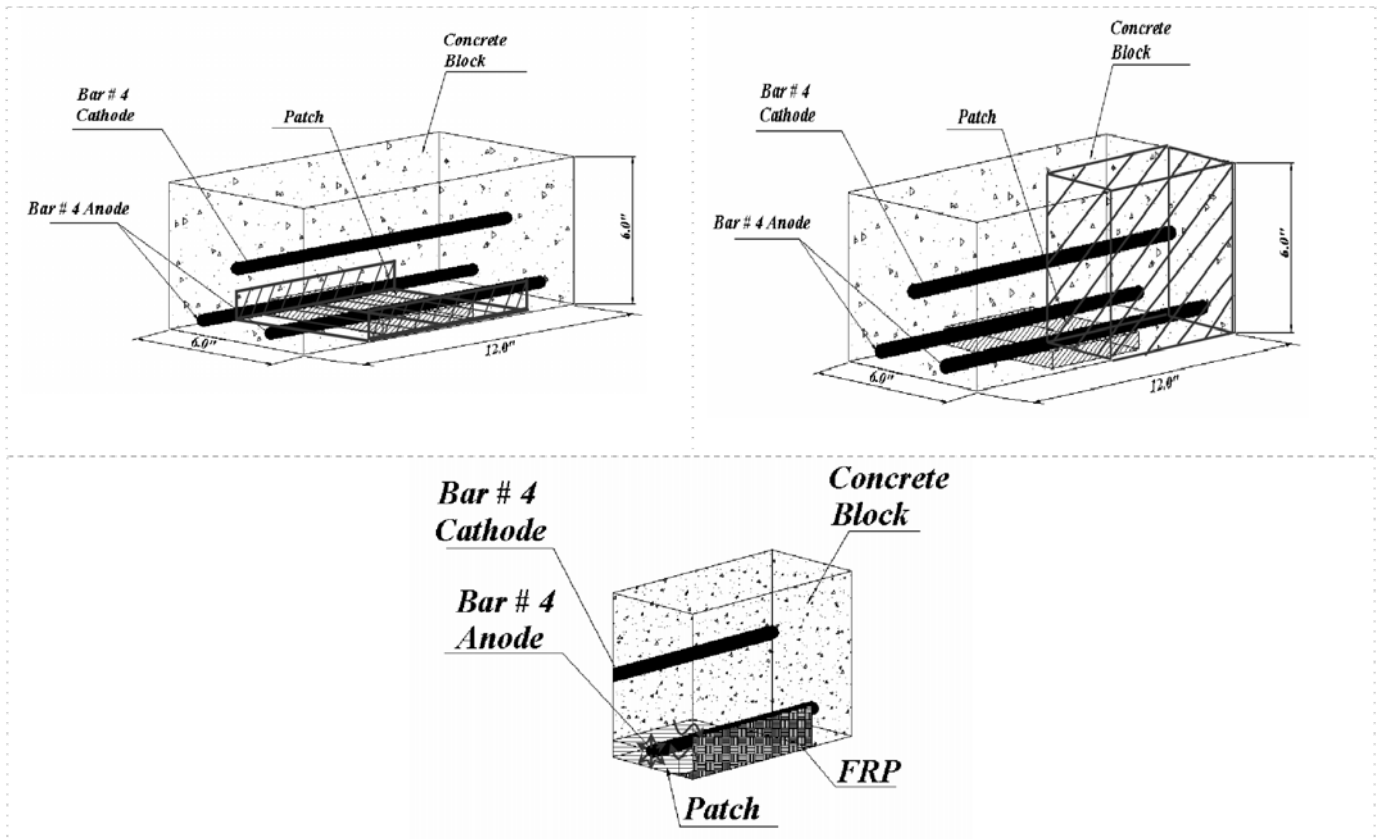
Figure 3-23: 3-D corrosion model

3.4.1 Element Selection

The typical 3-D FE mesh discretization of the quarter of the beam is shown in Figure 3-24 (a) for the mechanical and shrinkage loads and Figure 3-24 (b) for the corrosion load. The model includes: a) a concrete and repair patch part modeled with 8-node reduced integration brick elements (C3D8R), b) a steel reinforcement part modeled with 2-node truss elements (B21) in the mechanical and shrinkage models, with 8-node reduced integration brick element (C3D8R) for corrosion model, and c) an FRP overlay part modeled with 4-node, quadrilateral reduced integration shell element (S4R). These brick elements (C3D8R) are versatile and can be used in models for simple linear analysis or for complex nonlinear analysis involving contact plasticity.
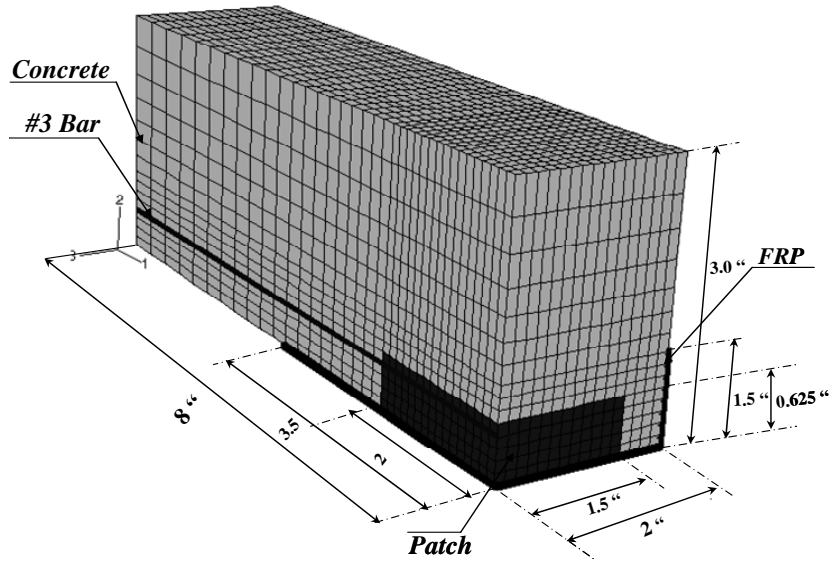
(a)
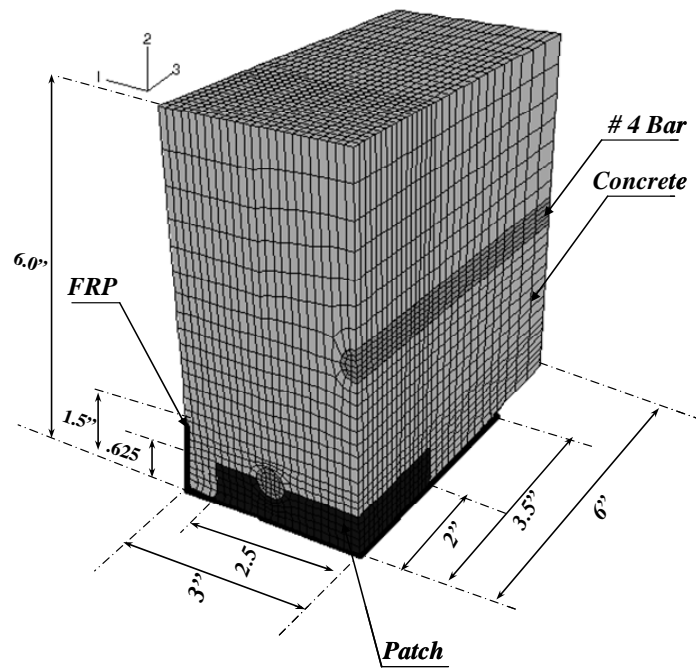
(b)

Figure 3-24: 3-D finite element model discretization: (a) shrinkage and mechanical model, and (b) corrosion model

3.4.2 3-D Results and Discussion

The main objective of the 3-D analysis was to choose the best fabric and orientation of a single layer of FRP overlay that could sustain all possible loading conditions and damage on the patch material and limit further damage. Three different loads and their combinations were considered together with the most pprobable crack path and debonding associated with the chosen loading. Two bidirectional, two unidirectional, and one chopped FRP fabrics were chosen. See Table 3-2 for details on the FRP material properties.

Tabl1: FRP Material Properties

	Type	COMMERCIAL NAME (Client Agency)	Fiber Orientation	E11 (psi)	Ultimate Tensile Strength (psi)	Thickness (in.)
FRP 1	Glass	SHE-51	Unidirectional	3.47×106	6.67×104	0.05
FRP 2	Glass	Chopped (General)	Chopped	1.17×106	1.50×104	0.04
FRP 3	Glass	Hex 106 G	Bidirectional	2.47×106	4.40×104	0.013
FRP 4	Carbon	MBrace CF130	Unidirectional	1.02×107	8.00×104	0.02
FRP 5	Carbon	Hex 113 C	Bidirectional	6.05×106	6.60×104	0.01

Since corrosion expansion is a transverse loading and mechanical load is a longitudinal loading, two types of analyses were performed for the unidirectional FRPs to determine whether it is possible for the matrix alone to carry load the direction transverse to the fabric.

In the initial analysis for FRP 1 and FRP 4 (unidirectional) the direction of the fiber was assumed to be along the load direction. For example, in case of mechanical load the fibers were directed in longitudinal direction, and for corrosion load they were directed in the Transverse direction. For both cases in the direction transverse to the fibers, the shrinkage load was carried only by the matrix. In the second analysis, the most critical case obtained from the initial analysis was used with just FRP 1 and FRP 4 (unidirectional) with fibers oriented in the opposite direction to choose the most efficient direction for the FRP overlay.

Since the applied mechanical load and corrosion load are perpendicular directions, and the less severe load might be able to be carried by the matrix alone. This was the main reasons for the follow up analysis. The following notation is used in figure caption:

TCP: Transverse crack path

LCP: Longitudinal crack path.

UL: Unidirectional FRP with fibers in the longitudinal direction

UT: Unidirectional FRP with fibers in the transverse direction

It should be noted that the small arrow in the figures shows the direction of the path in each case.

3.4.2.1 Shrinkage and Mechanical Load

The results of the analyses indicated that even with the best patching material, some small debonding and shrinkage cracking is unavoidable, and it is also possible that environmental exposure could have some negative effects on the patch that the FEM analyses were unable to detect. In order to perform the comprehensive analysis, 18 different models with different loading conditions and crack paths were chosen for 3-D analysis, with the FRP overlay applied over the damaged patch. Based on the loading condition and the potential of cracks opening at different locations, one or more pre-opened cracks or debonding faces were introduced into the patch at prior to the analyses. Figure 3-25 shows the patches in the different models used, with the location of pre-opened cracks shown in gray. Cracks were introduced within the patch or at the concrete/patch interface (debonding). It should be noted that in the FE model, only the symmetric quarter of the figures (patch) shown was modeled.

The failure of the FRP overlays was characterized by the fiber/matrix rupture index (F/MRI), and the debonding index (DI) given in equation 3-12 and 3-13. When the indices exceed unity failure will occur by rupture of the fiber/matrix, or debonding between the patch and FRP overlay.

It should be noted that GFRP is likely to lose up to 20% of its strength under wet -dry cycles, but the strength of the CFRP will not be effected by different environmental conditions (Bayasi, 2000). Freeze-Thaw cycles do not affect the strength of the FRP significantly, therefore the strength of the GFRP were reduced to 80% of their initial values to account for the effect of wet-dry cycles on the FRP overlay.
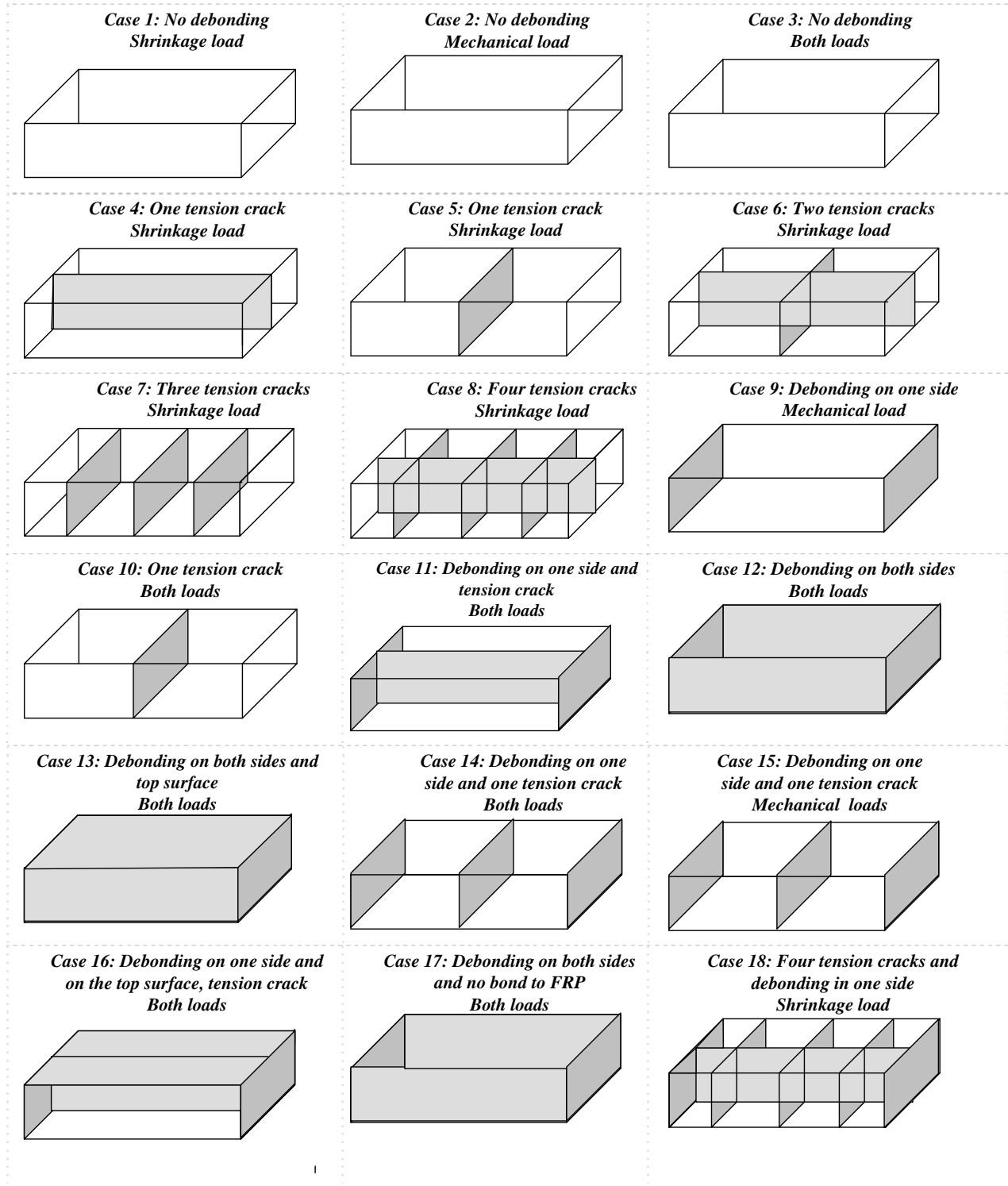
Figure 3-25: Models used for 3-D analysis

Figure 3-26 and Figure 3-27 show the fiber/matrix rupture indices along the transverse and longitudinal crack paths for the critical cases (Case 10, and Case 4) in both directions,

respectively. Figure 3-26 shows that FRP 2 with patch Material 2 is likely to rupture under the applied load (Case 10). All other FRPs do not fail with either patching materials. Figure 3-27 indicates that FRP 1, and FRP 4 (unidirectional) with patch Material 2 showed the worst behavior under the applied load (Case 4), but was still well below failure

All of the FRP fabrics perform satisfactorily with either patching material. Figure 3-28 to Figure 3-31 show the FE results for most of the cases shown in Figure 3-25.
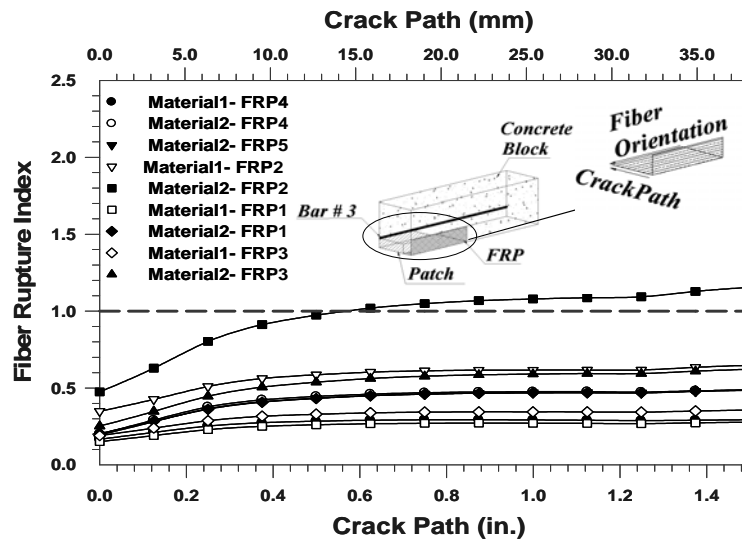
Figure 3-26: Fiber rupture index – Case 10 (TCP, UL)
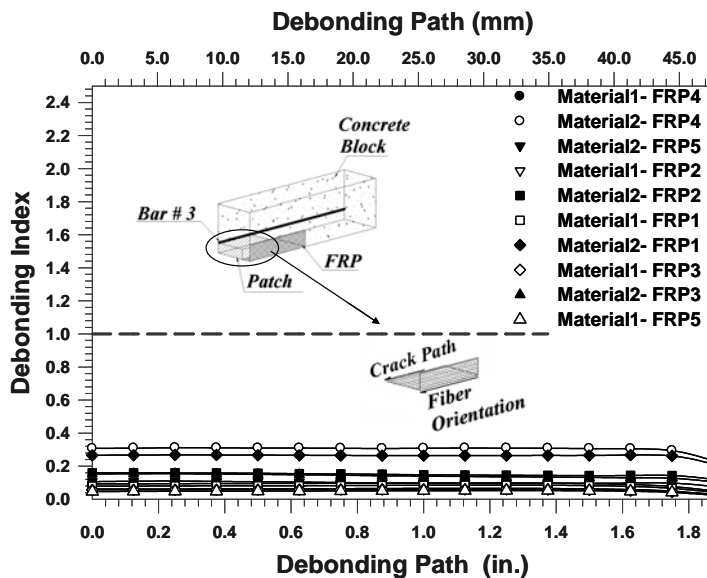
Figure 3-27: Fiber/Matrix rupture index – Case 4 (LCP, UL)
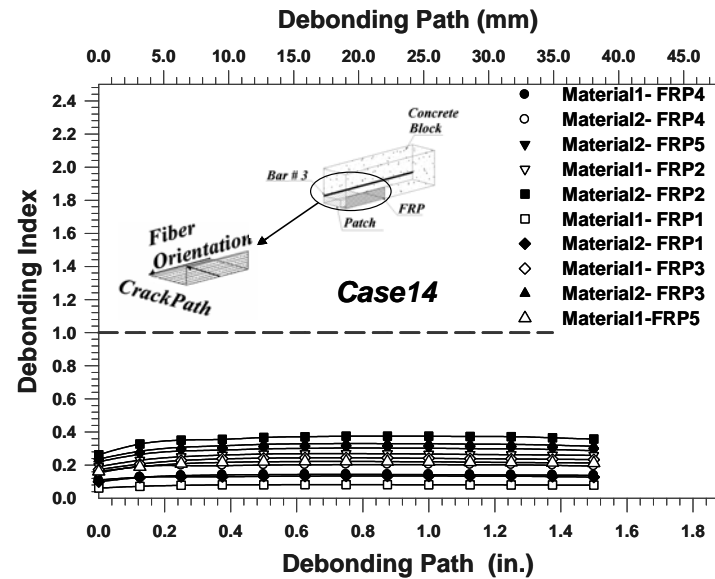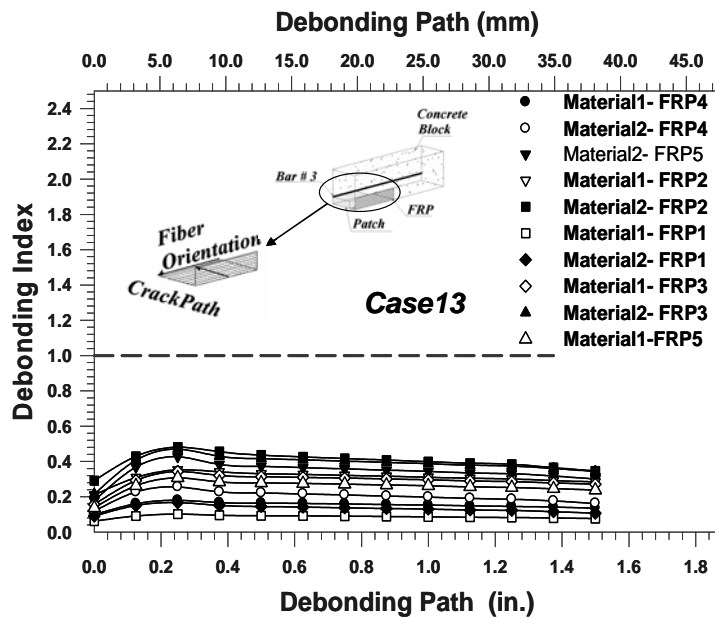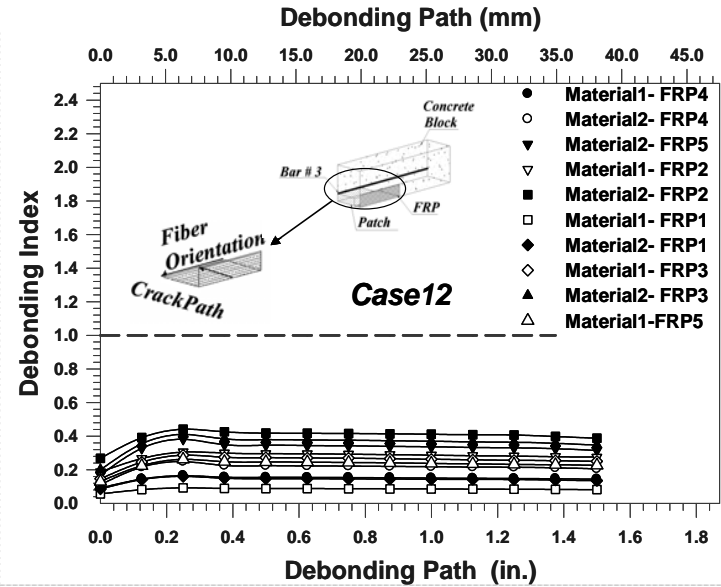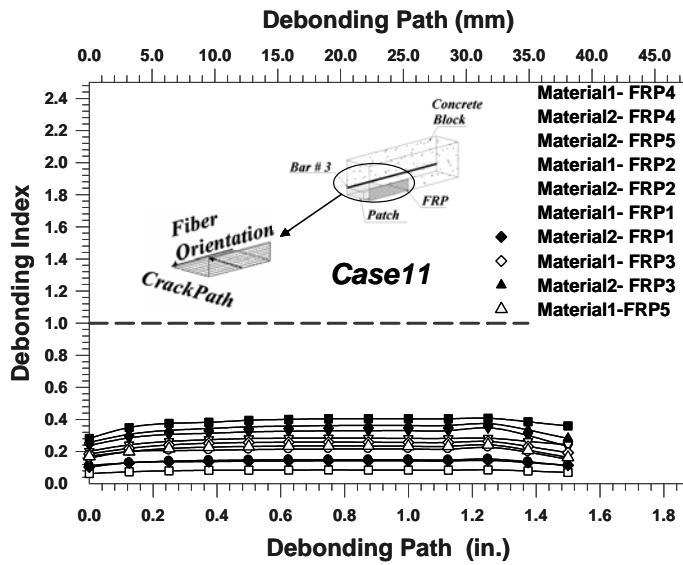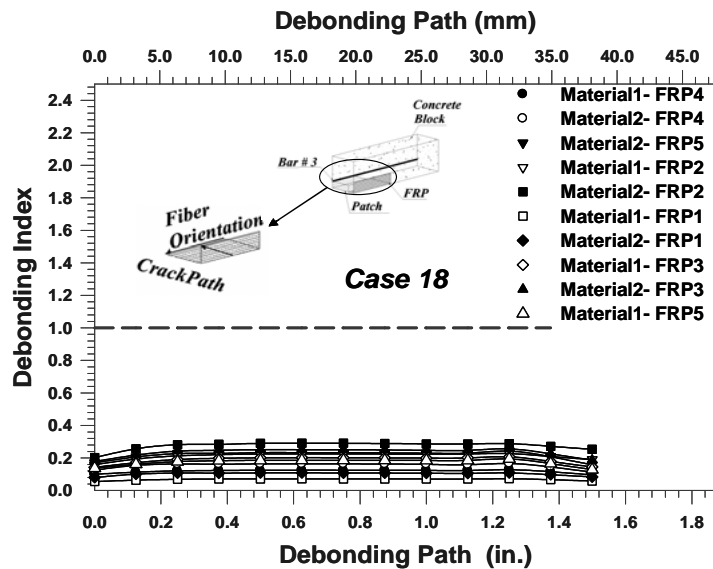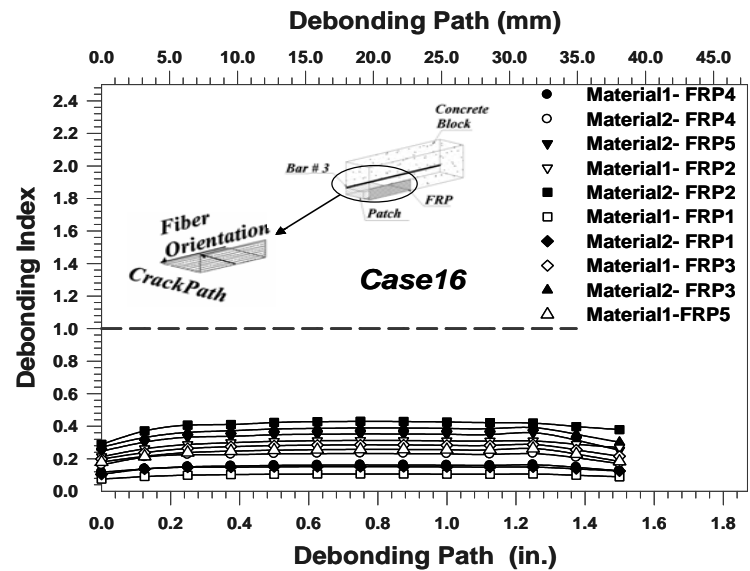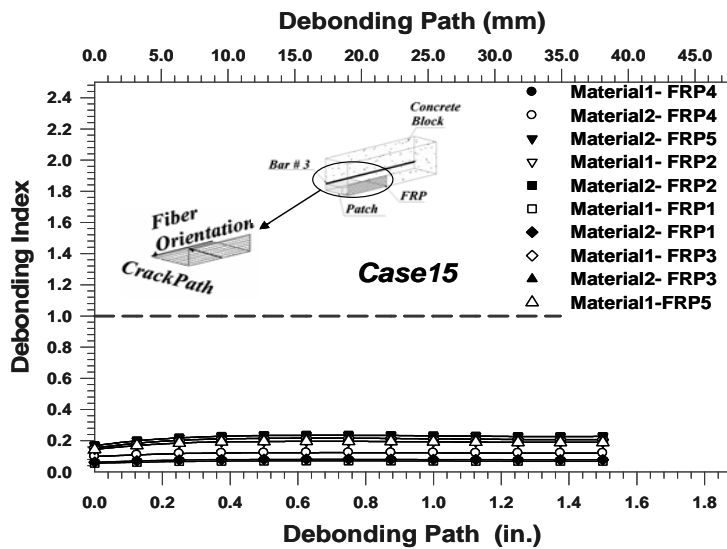
Case11, Case12, Case13, Case14 — Debonding Index vs Debonding Path
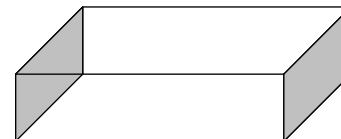
Figure 3-28: M/FRI for different loading conditions along path 1

Debonding Path (mm)

Case6

| Material1- FRP4 |
| Material2- FRP4 |
| Material2- FRP5 |
| Material1- FRP2 |
| Material2- FRP2 |
| Material1- FRP1 |
| Material2- FRP1 |
| Material1- FRP3 |
| Material2- FRP3 |
| Material1-FRP5 |

Debonding Path (in.)

Debonding Path (mm)

Case8

| Material1- FRP4 |
| Material2- FRP4 |
| Material2- FRP5 |
| Material1- FRP2 |
| Material2- FRP2 |
| Material1- FRP1 |
| Material2- FRP1 |
| Material1- FRP3 |
| Material2- FRP3 |

Debonding Path (in.)

Debonding Path (mm)

Case11

| Material1- FRP4 |
| Material2- FRP4 |
| Material2- FRP5 |
| Material1- FRP2 |
| Material2- FRP2 |
| Material1- FRP1 |
| Material2- FRP1 |
| Material1- FRP3 |
| Material2- FRP3 |
| Material1- FRP5 |

Debonding Path (in.)

Debonding Path (mm)

Case16

| Material1- FRP4 |
| Material2- FRP4 |
| Material2- FRP5 |
| Material1- FRP2 |
| Material2- FRP2 |
| Material1- FRP1 |
| Material2- FRP1 |
| Material1- FRP3 |
| Material2- FRP3 |
| Material1-FRP5 |

Debonding Path (in.)

56

Figure 3-29: M/FRI for different cases along path 2
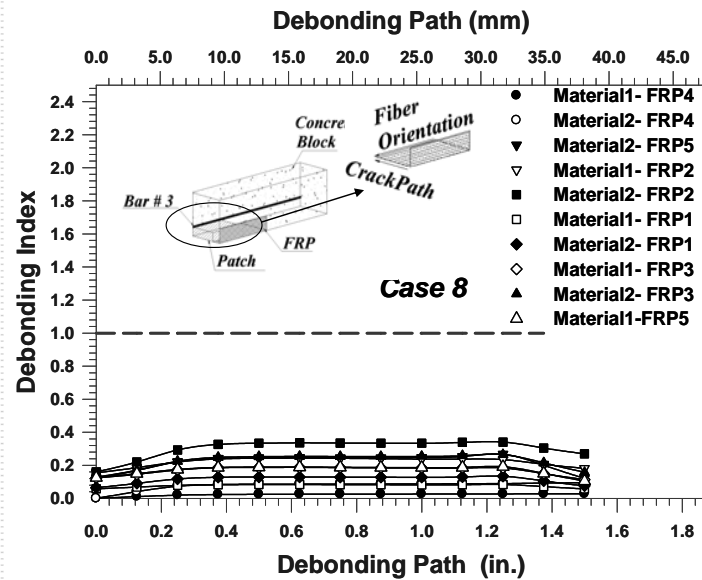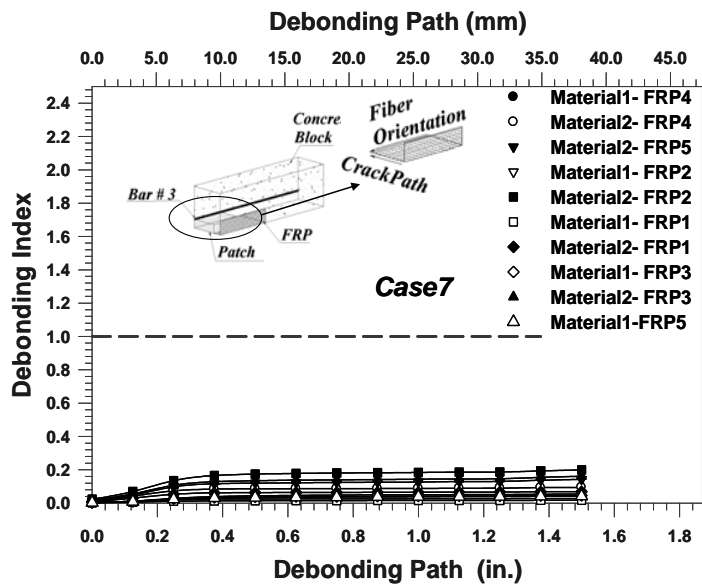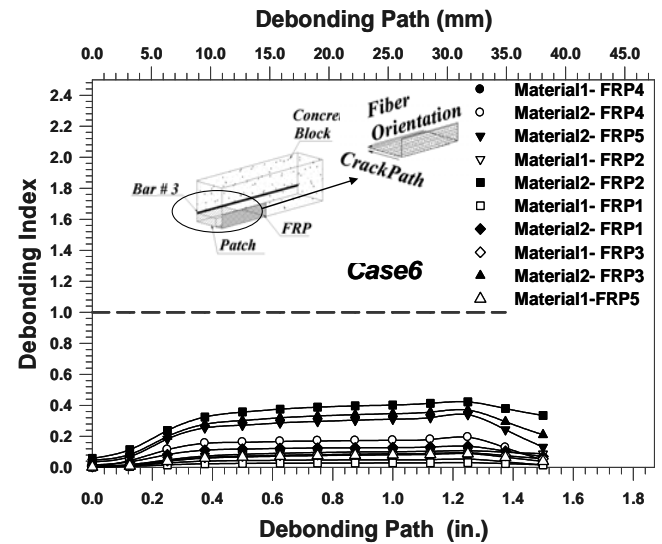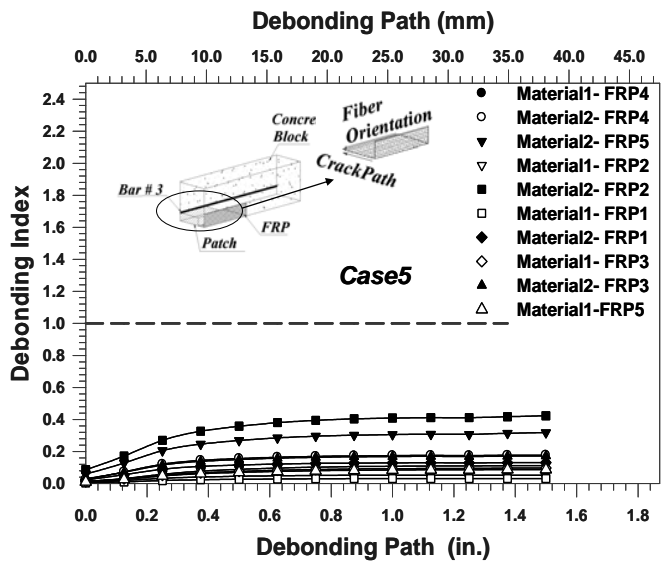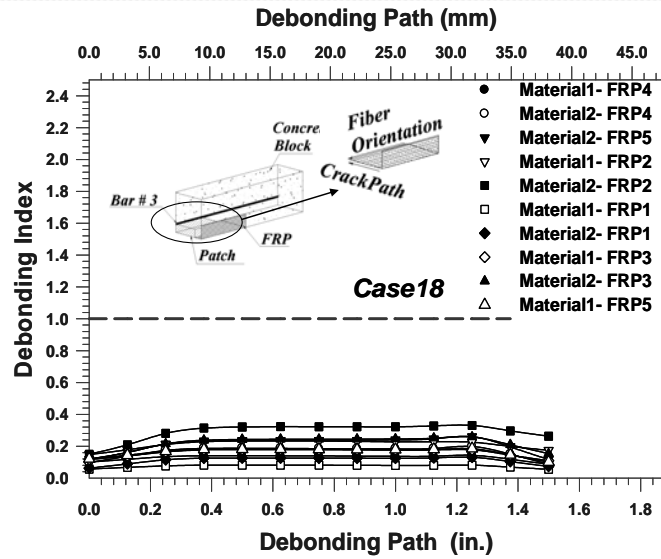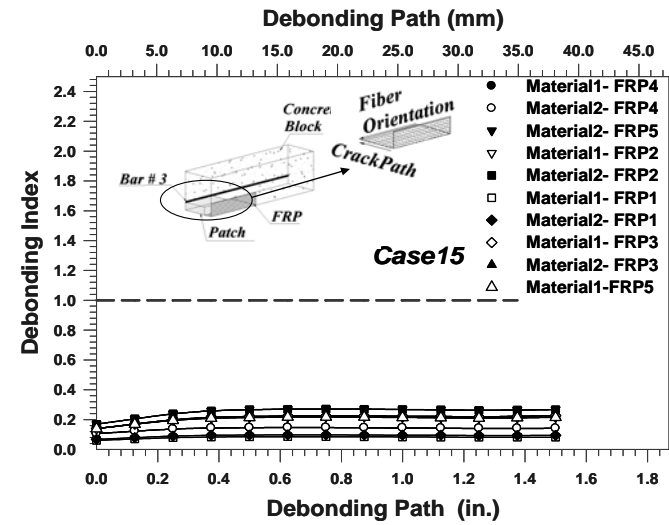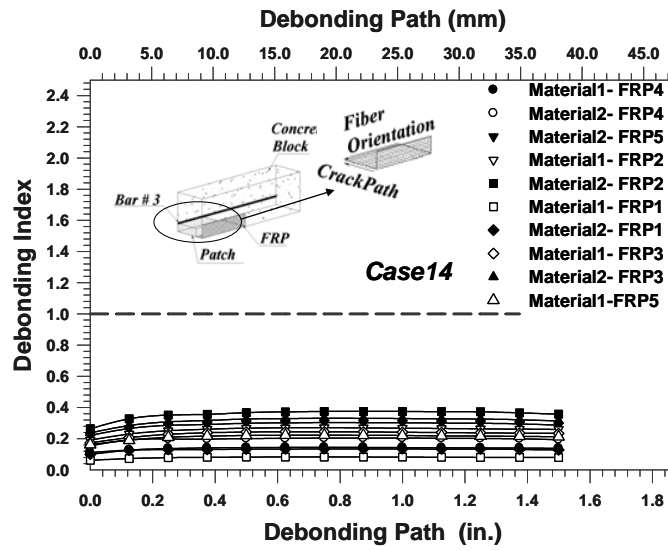
Case5

Case6

Case7

Case 8

58
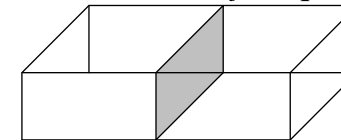
Figure 3-30: M/FRI for different loading conditions along path 4
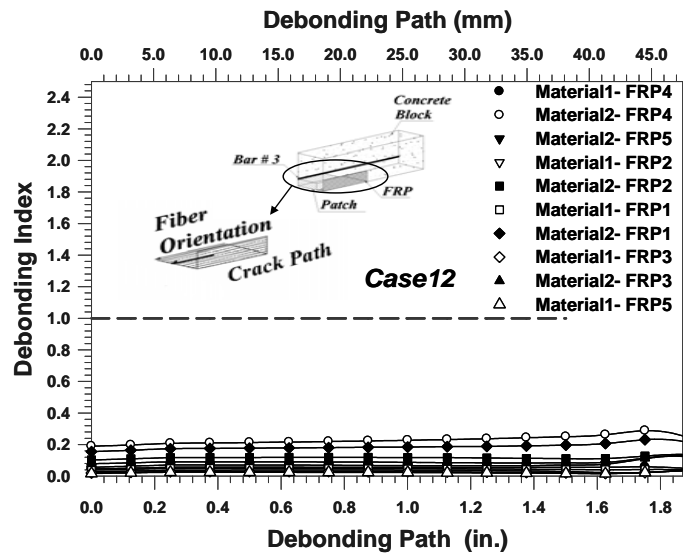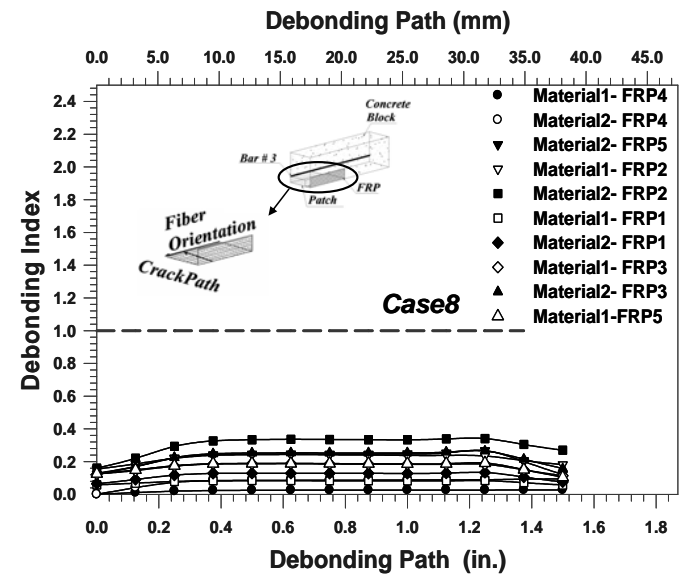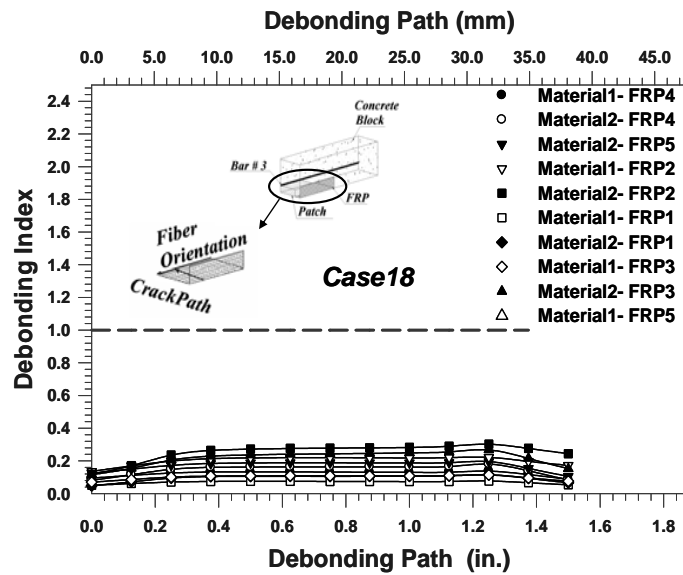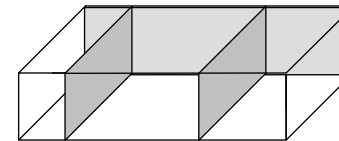
Figure 3-31: M/FRI for different loading conditions along path 3 and 5

The debonding index was calculated to evaluate the state of the bonding between the FRP overlay and the patching materials along in the path perpendicular to the crack. This should indicate how far the debonding of the FRP will propagate from the crack location. Since no information about the shear bond strength between the FRP material and concrete was available, it was assumed that failure initiates in the patching material.
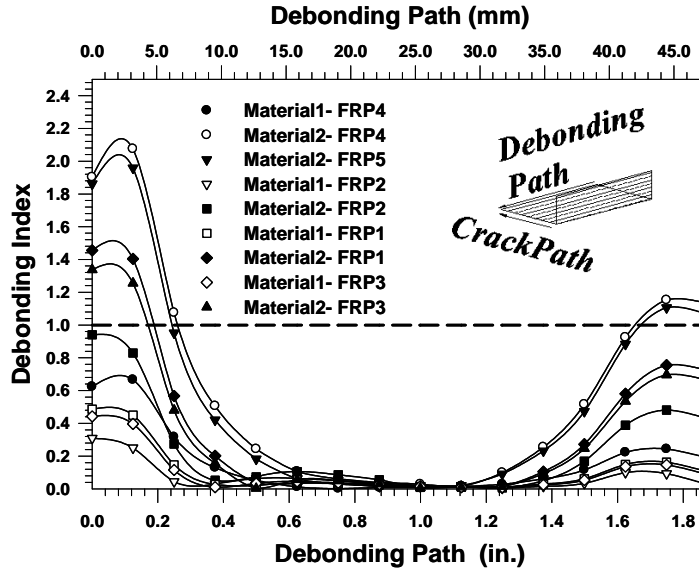
Figure 3-32: Debonding index for Case 10 (TCP, UL)
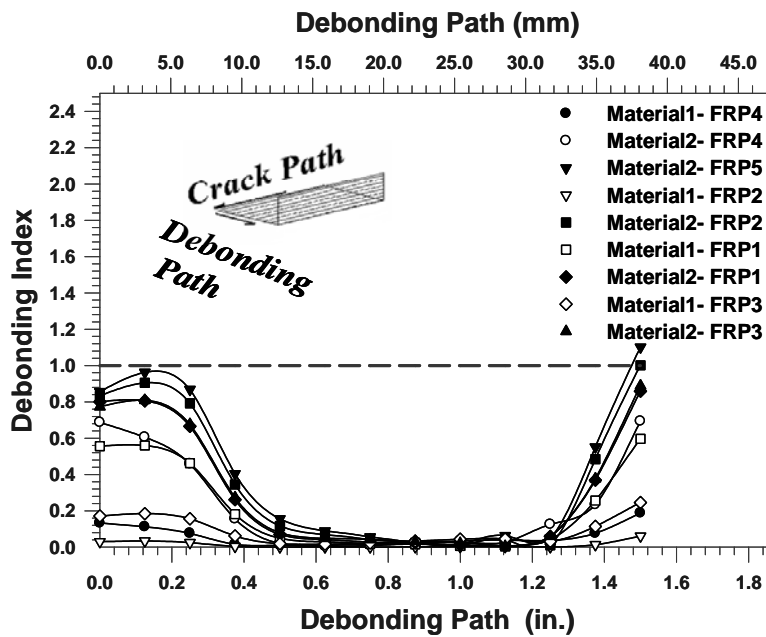
Figure 3-33: Debonding index for Case 4 (LCP, UL)

Figure 3-32 and Figure 3-33 show the calculated debonding index for debonding transverse to the crack paths for the critical cases in both direction (Cases 10 and 4), respectively. Figure 3-32 indicates that there is some debonding between the patch and the FRP near the ends of the patch when patch material 2 is used. Figure 3-33 shows that there is no significant debonding between the patch and FRP for the LCP with either patching material.

In a follow-up analysis, the critical case obtained from the initial analysis (Case 10, Figure 3-25) was evaluated again with the opposite orientation of the fibers for the unidirectional FRP 1 and FRP 4. The loads carried by the fibers in the initial analysis were now carried by the matrix and vice versa. As Figure 3-34 indicates, both FRP 1 and FRP 4 failed due to the applied load in Case 10 when used with patch material 2, but do not show any damage when used with patch material 1.
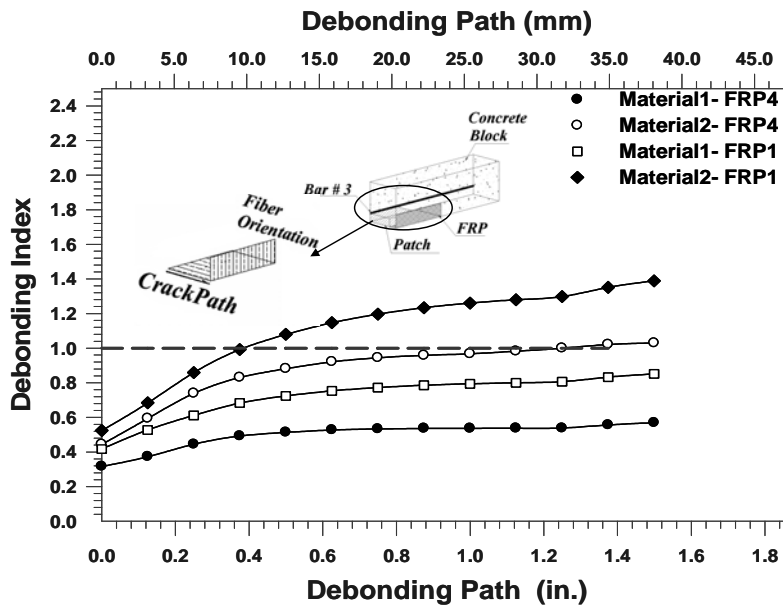
Figure 3-34: Fiber rupture index -Case 10 (TCP, UT)
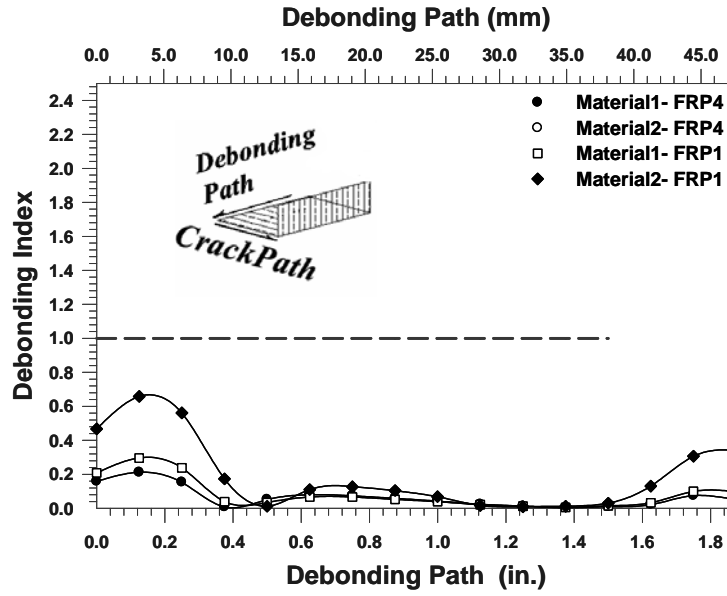
Figure 3-35: Debonding index -Case10 (TCP, UT)

Corrosion Load

Only two different loading conditions were studied in this section (1) corrosion load, and (2) the combination of corrosion and shrinkage loads. Based on the results from 2-D analyses, a vertical pre-opened crack was introduced in the 3-D model radiating downward from the bar along Path 1, (see Figure 3-36 and Figure 3-21). The model was studied under corrosion load (with FRP fibers oriented in the transverse direction for uni-directional FRP).
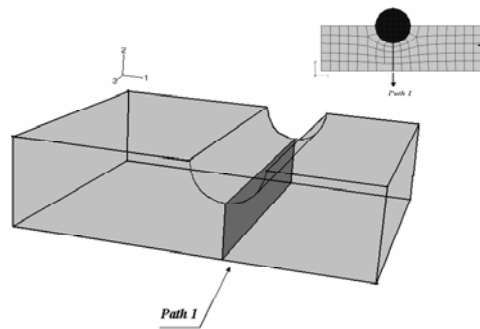
Figure 3-36: Location of the pre-opened crack in the corrosion model

63

Since both chosen patch materials (Material 1 and 2) have the same elastic modulus, they will behave identically under the corrosion loading, and consequently only one of the results is presented here. Figure 3-18 shows the fiber rupture index of the FRP overlay along the critical points (crack path) under the corrosion load. The Figure 3-37 indicates that under corrosion load some of the chosen FRP fabrics are close to failure, but none will actually fail.
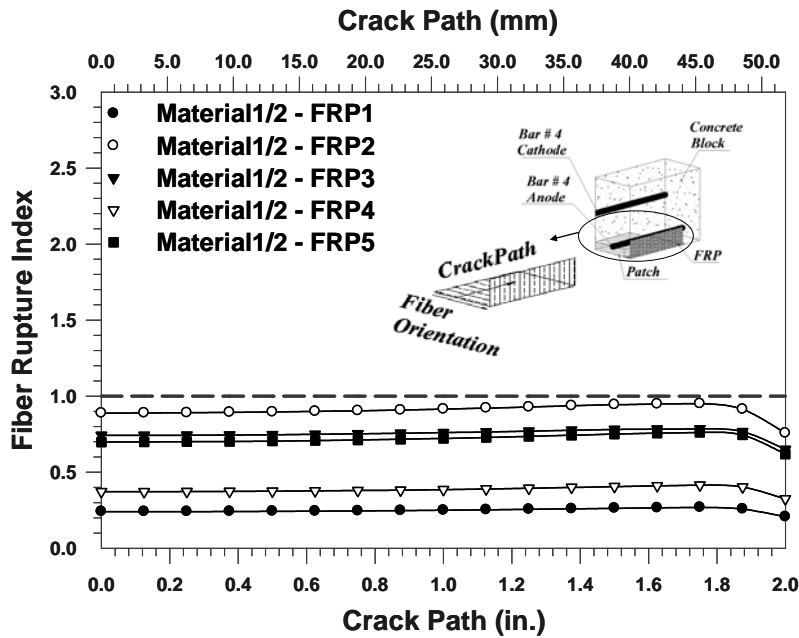
Figure 3-37: Fiber rupture index due to applied corrosion load (LCP, UT)

It should be noted that the combined load case was studied only for Material 2 (highest shrinkage), for comparing the behavior of the FRP overlay under the extreme loading situation. Figure 3-38 shows the fiber rupture index along the crack path and indicates that FRP 2 (chopped glass) showed the worst behavior under the combined load and is expected to fail. The other FRPs do not fail under the combined load.
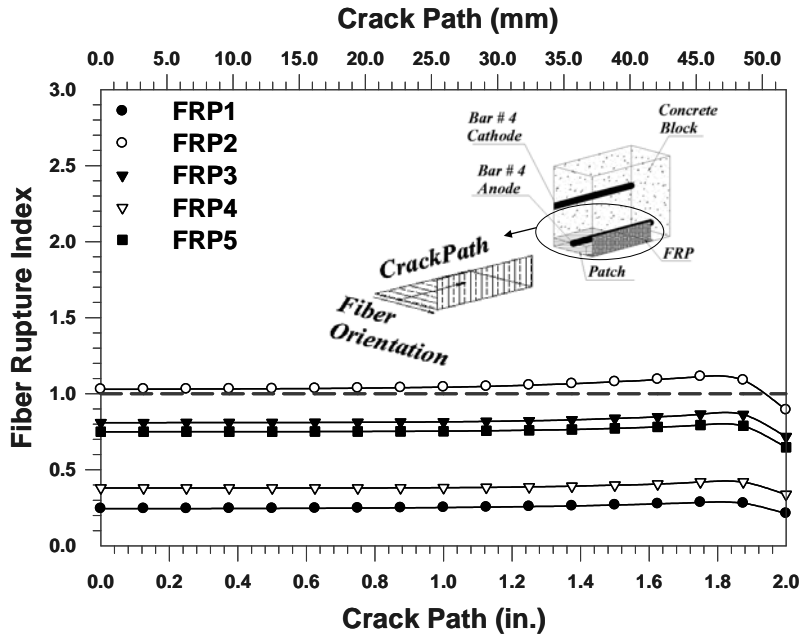
Figure 3-38: Fiber rupture index due to combined loads (LCP, UT)
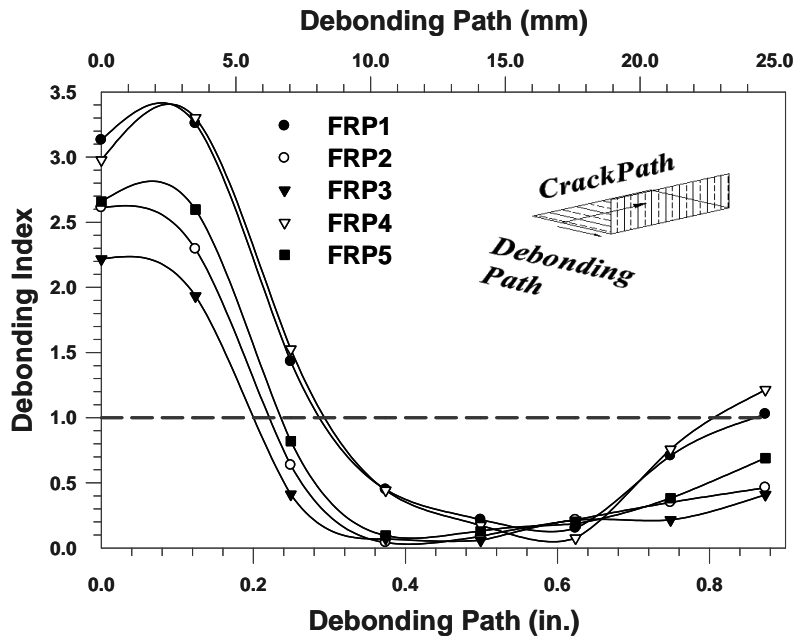
Figure 3-39: Debonding index due to combined load (LCP, UT)

Figure 3-39 shows the DI-values calculated to evaluate the state of the bond between the FRP overlay and the patching material. It was assumed that bond failure initiates in the patching material. The calculated DI-values transverse to the crack path indicate that there will be debonding near the crack location over a 0.2-0.3 in. length for all FRP overlays (left side of Figure 3-39), and debonding near the patch/concrete

interface at the ends of the patch over a 0.1-0.2 in. length for FRP 1 and FRP 4 (right side of Figure 3-39).

Crack pattern: In the experimental part discussed in next the chapter, the specimens with and without FRP showed very different crack patterns and measured strains under the accelerated corrosion test. 3-D FE analysis of these specimens was conducted to understand why the FRP overlay changes the crack pattern and reduces crack widths. These analyses and results we explain more in next chapter.

3.4.3 Conclusions

Numerical results for mechanical, shrinkage, corrosion, and combined loading effects on patch repairs with an FRP overlay show that one layer of uni-directional fabrics (FRP 1 and FRP 4), with fibers oriented either in the transverse or longitudinal direction, are insufficient to withstand the combined load. One layer of the chopped glass fabric (FRP 2) also is inadequate. However, one layer of the bi-directional fabrics (FRP 3 and FRP 5) is sufficient to resist all loading effects with either of the patching materials considered. Since glass FRP is more economical than carbon FRP, one layer of FRP 3, or any other bi-directional glass reinforced FRP with similar mechanical properties, should be an effective solution for use as an overlay for improving the performance and durability of shallow depth patches in concrete structures.

Chapter 4
Experimental Investigation

4.1 Introduction

A comprehensive laboratory experimental investigation was carried out to study the advantage of the proposed dual patch and FRP system compared to applying just the plain patch material on the concrete structure. The concrete beams were subjected to different environmental exposures of freeze-thaw, wet-dry, and accelerated corrosion. This chapter presents the experimental plan, type of exposure, materials used, problems encountered, test results, and observations. The patching materials and FRP overlay used in this part of the research were chosen based on the FE analysis. The concrete was cast using Michigan Department of Transportation approved mix design for bridge decks and girders. Due to problems encountered with initial patch geometry in specimens subjected to freeze-thaw and wet-dry exposure, the patch geometry was subsequently enlarged as described later.

4.2 Experimental Plan

An extensive experimental investigating was carried out to study the effect of the FRP overlay on durability of the patch material. Laboratory investigation was focused on determining and characterizing the durability and damage tolerance of the selected dual repair system compared to the conventional approach of using only filler. The original experimental plan included three subtasks to evaluate the durability of the repair under:

- Swelling strains induced by the corrosion of steel reinforcement;
- 300 freeze-thaw cycles followed by cyclic loading simulating traffic;
- 300 wet-dry cycles followed by cyclic loading simulating traffic.

To evaluate the advantages of the selected repair system, the durability studies were conducted on test units that simulate "undamaged" and "damaged" conditions. The "undamaged" specimens were cast with the full cross section over the entire length. The "damaged" specimens were cast with a rectangular cavity (4" × 3" × 0.625") at mid-span as shown in Figure 4-1 and

Figure 4-3 for freeze-thaw, wet-dry and corrosion tests, respectively. The "damaged" specimens were repaired using two methods: (1) with the filler material only, and (2) with the filler and FRP overlay. Specimens repaired only with the filler material were originally expected to deteriorate significantly when subjected to cyclic fatigue loading following environmental exposure. However as described later, this did not occur.

A second test set of "exposed" and "non-exposed" specimens were therefore fabricated. In this set the cavity size was increased to 9" × 4" × 0.625" at mid-span as shown in Figure 4-2 . "Exposed" specimens were repaired with the two methods mentioned above and subjected to only to the more aggressive freeze-thaw exposure and "non-exposed" specimens were repaired with the filler material only. "Undamaged" and "exposed" specimens are henceforth referred to as Group 3 specimens or control specimens and specimens repaired with the filler material only and with the filler and FRP system are henceforth referred to as Group 2 and Group 3 specimens, respectively. A summary of the test matrix for each of the subtasks outlined above is given in Table 1. Detailed descriptions of the methods to be followed in each of the tests are given in the respective sections that follow. The number of specimens exposed to each environment is shown in Table 4-2. Figure 4-4 illustrates the evaluation matrix of the experimental program.
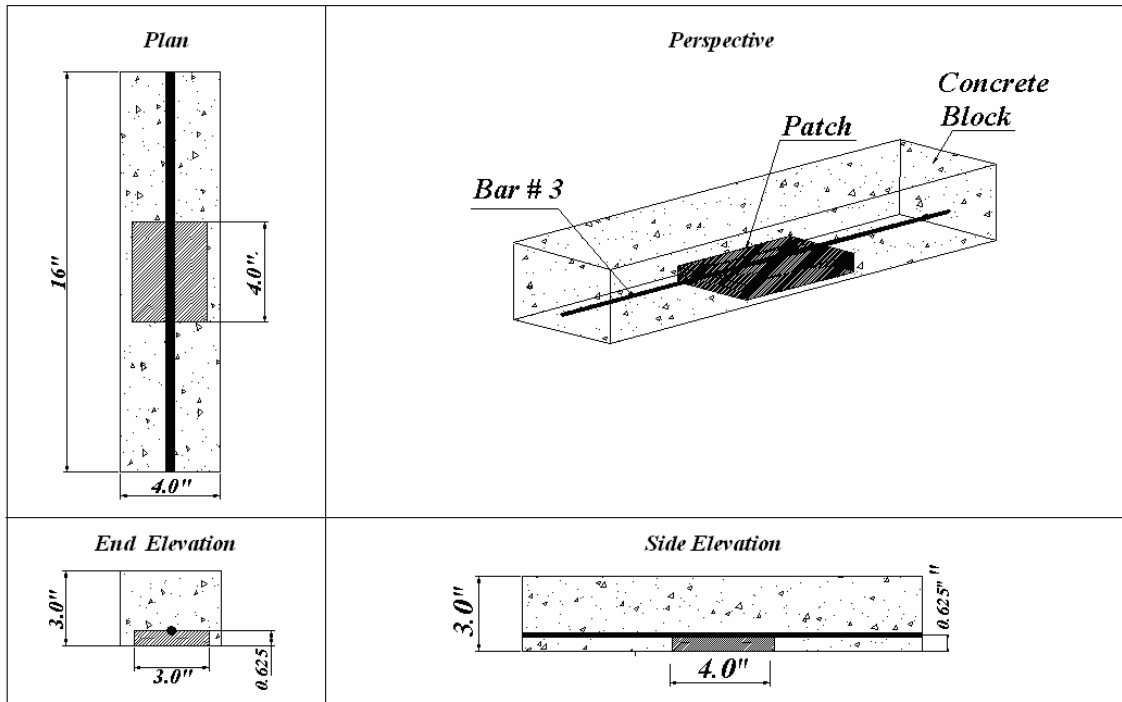
Figure 4-1: Geometry of first set of freeze-thaw and wet-dry test specimens
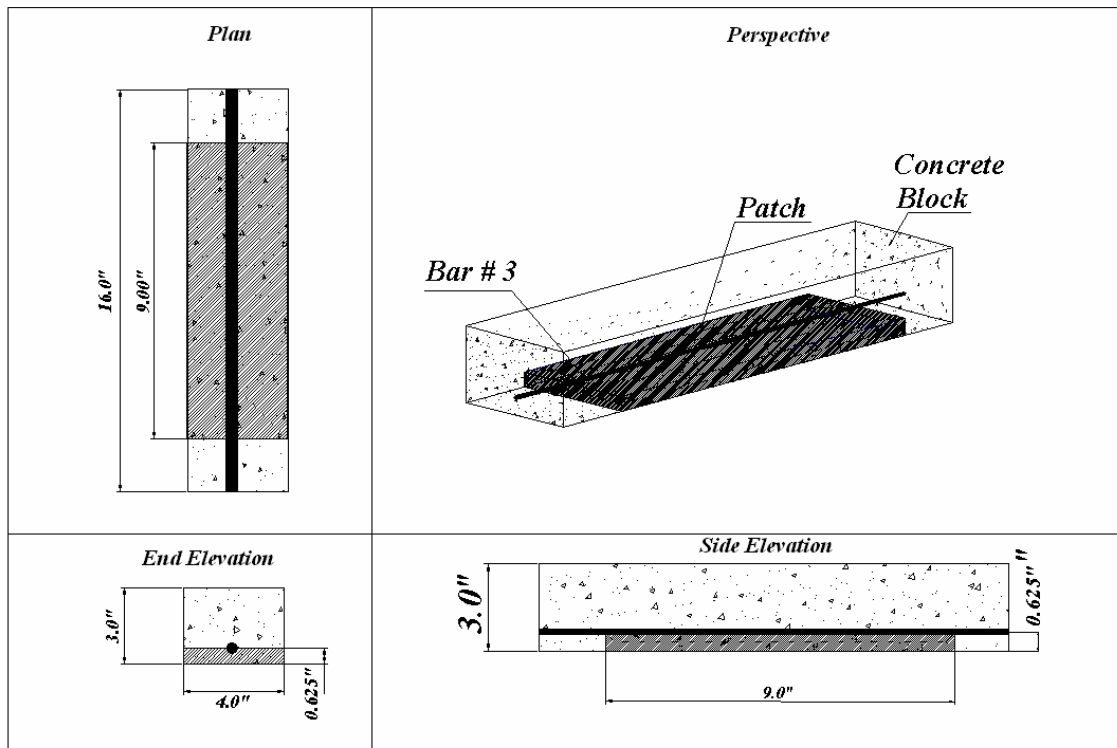
Figure 4-2: Geometry of second set of freeze-thaw test specimens

69
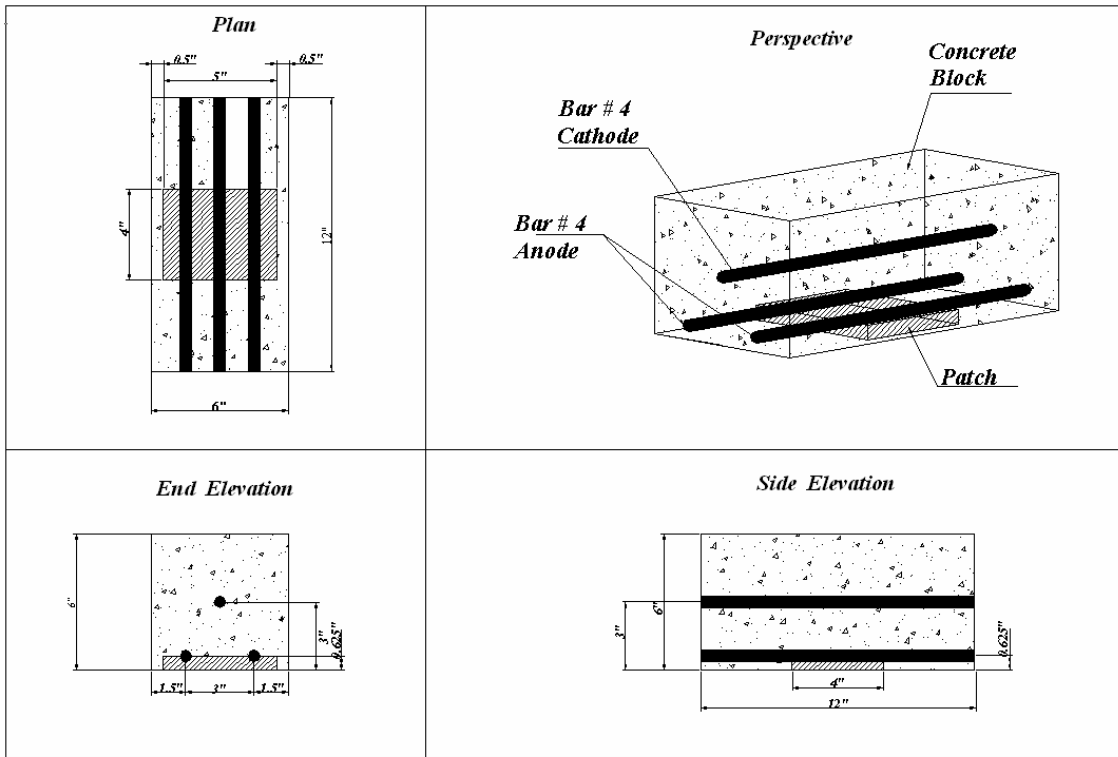
Figure 4-3: Geometry of the corrosion test specimens
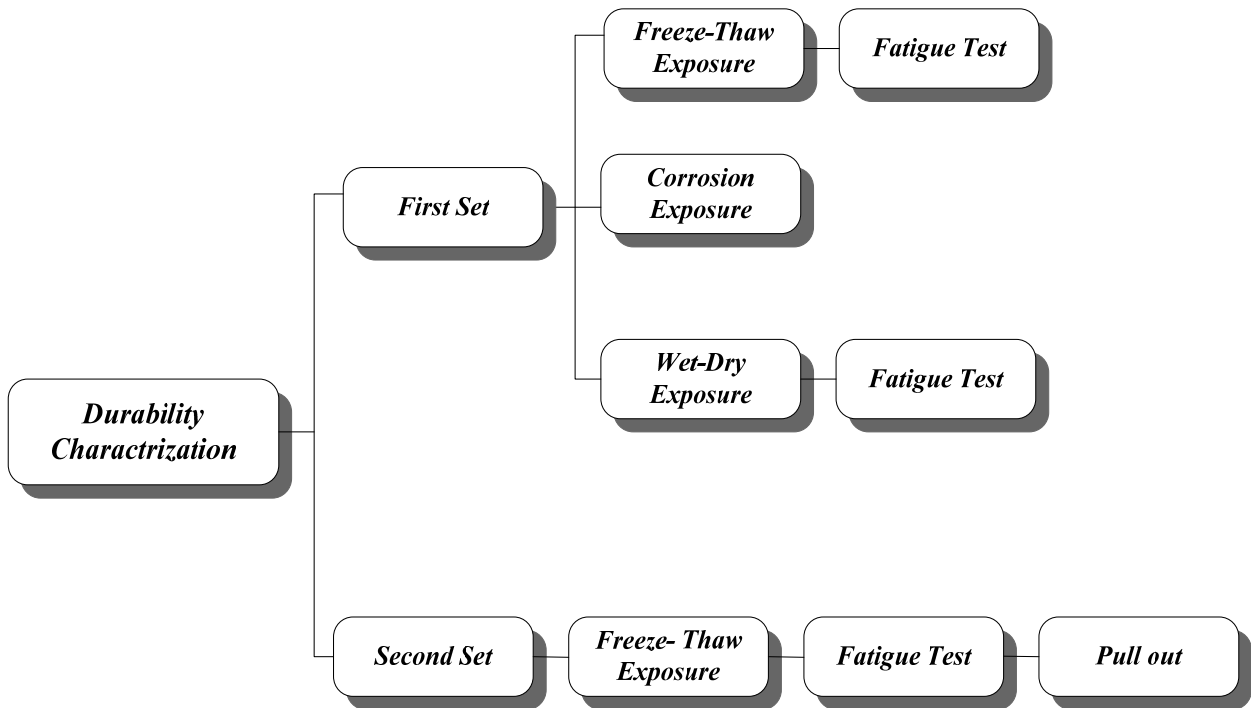
Figure 4-4: Experimental evaluation matrix

Table 4-1: Test Materials

FRP		Patch	
Bidirectional Glass FRP	All tests	HB2 (Material 1)	All tests
		R-350 (Material 2)	Freeze-Thaw

Table 4-2: Test Specimens

	CORROSION (SUBTASK 3-1)	FREEZE-THAW (SUBTASK 3-2)	WET-DRY (SUBTASK 3-3)	UNEXPOSED (Control)
No patch (Control)	3 (1st set)	5 (1st set)	5 (1st set)	
Patch	3 (HB2; 1st set)	10 (HB2 & R-350; 1st & 2nd set)	5 (HB2; 1st set)	10 (HB2 & R-350; 2nd set)
Patch & FRP	3 (HB2; 1st set)	10 (HB2 & R-350; 1st & 2nd set)	5 (HB2; 1st set)	

4.2.1 Deterioration Due to Corrosion

Cracking of the concrete surrounding the reinforcement due to the volume expansion associated with corrosion will stress the patches and possibly cause spalling. An accelerated corrosion experiment was used to study the effect of corrosion on the durability of the patches.

For the corrosion study, concrete specimens (6" × 6" × 12") with three reinforcing bars, two near the bottom face (anode or corroding bars) and one near the top face (cathode), were used. The bottom bars were placed such that half of each bar cross section is exposed to the patching material as described in the FE modeling, and the cathode was placed at the middle of the specimens. A constant voltage of 12 V was supplied from the single bar (cathode) to the other two reinforcing bars (anodes) using an external power source. A 3.5 percent sodium chloride solution (by weight) was used to wet the concrete specimens for one hour in each 12-hour period. The moisture in the concrete specimens and the applied current induced corrosion in the anodic reinforcing bars in an accelerated fashion. Figure 4-5 shows the experimental setup for the corrosion test. The specimens were subjected to accelerated corrosion for three weeks. The applied current was monitored at of two-minute intervals with a voltage data-logging unit

(Omega Engineering Inc., AD128-10T2), since this can be used to estimate the total corrosion in the reinforcing bar.

As shown in Figure 4-5 the specimens were connected in parallel and hence the applied voltage was equal for all specimens.
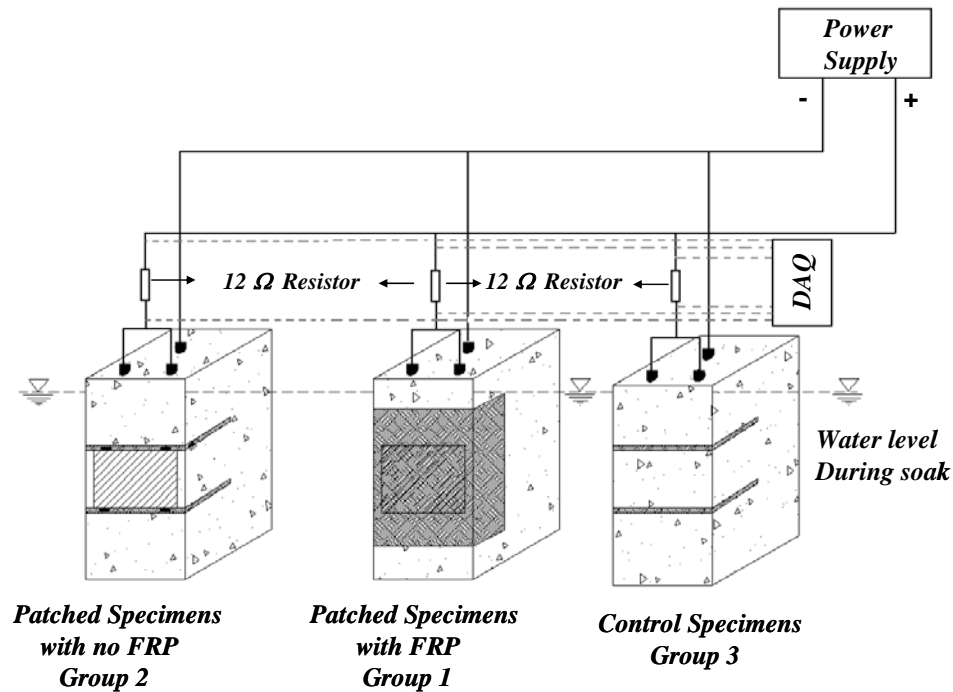
Figure 4-5: Accelerated corrosion test setup

4.2.2 Deterioration Due to Freeze-Thaw Cycles

Concrete bridges in Michigan undergo freezing and thawing cycles in winter that are likely to cause deterioration of patched repair. To examine the effect of freeze-thaw cycles on the durability of patches, both sets of specimens were subjected to 300 cycles of freeze-thaw. The ASTM C-666 Procedure B (freezing in air, thawing in water) was used in which each freeze-thaw cycle consisted of a one-hour and fifty minutes freezing period at $0^{o}F$ and a one-hour and ten minutes thawing period at $40^{o}F$. The test was performed in the Michigan Department of Transportation freeze-thaw machine. In some cases, specimens were subjected to cycling loading before the freeze-thaw exposure, to introduce some cracking in the patch material to better simulate the real field condition. Following freeze-thaw conditioning, the specimens were subjected to cyclic loading.

4.2.3 Deterioration Due to Wet-Dry Cycles

Concrete bridge structures experience cycles of wetting and drying on a continuous basis. The expansion and shrinkage resulting from wetting and drying cycles is likely to cause deterioration of the patches. A wet-dry experiment was used to study the durability of the patches. The first sets of specimens were subjected to 300 wet-dry cycles. Each wet-dry cycle consisted of a one hour wet period followed by a 12-hour dry period. A 3.5% NaCl solution was used to wet the specimens.

4.2.4 Cyclic Load Test

I n addition to environmental demands, repeated load-induced strains can further deteriorate the repair patch leading to bond and tensile failures. The durability of the repair was investigated by subjecting the weathered wet-dry and freeze-thaw specimens to cyclic loading. Since there is no standard test for this evaluation, a custom protocol was used. Cyclic testing was done through four and three point flexural test on the first and second set of freeze-thaw test units (3" × 4" × 16"), respectively. The cyclic load magnitude was selected to produce tensile strain demands on the repair similar to that caused in a typical highway bridge girder under full service loads. It was estimated that the bottom flexural reinforcement in bridge beams are strained about 20% of the yield strain. But this value took up to 60% of the yield strain for both sets of specimens to induce noticeable damage. This test was not intended to be a fatigue test and hence the number of load cycles will was limited to 1000 for the pre-loading prior to environmental exposure and 500,000 cycles following environmental exposure. In the second set of specimens the patches were then subjected to the pull out test explained in the next section.

4.2.5 Pull Out Test

After the second set of specimens were exposed to freeze-thaw and subjected to 500,000 cycles of load, a pull-out test was carried out to determine the bond strength between the patch and the concrete. This test was devised to characterize the deterioration of the bond due to weathering are as well as the improvement in the bond due to the use of the FRP overlay. Since no standard procedure exists for the pull out test, a pull-out device was made for this test. Additional details are provided later in this chapter.

4.3 First Set of Specimens

The set of specimens had the dimensions shown in Figure 4-1 and Figure 4-3. These specimens had a smaller cavity that was patched, and the patch bonded to concrete substrate on all but the bottom surface.

4.3.1 Sample Preparation

Fabrication of the specimens consisted of making wooden molds, casting the concrete specimens, surface preparation, patching the specimens, and applying the FRP overlay. Each of these above mentioned steps are explained in more detail below.

4.3.1.1 Preparing the Molds and Casting

Wooden molds were constructed for fabricating the specimens to be used for experimental studies. A piece of wood with the same dimension of the patch was used to create a cavity in the concrete substrate, and the reinforcing bars were placed in the molds so that they were half in the patch and half in the concrete.

Figure 4-6 shows the molds the location of the patch part and the steel bar inside the molds for the test specimens before casting. A total of 60 specimens were cast for the freeze-thaw and wet dry tests (10 extra) and 12 specimens were cast for the corrosion test (3 extra).

Figure 4-7 shows the molds before and after casting and the casting procedure. The specimens were cast on June 3, 2005. The ready-mix concrete used was supplied by Consumer Concrete and the mixture proportion was according to the M-DOT Grade S2 concrete with a water reducer. This concrete mix is usually used for bridges. The fresh properties of the concrete were determined at casting. The fresh properties of the concrete mix as well as some mechanical properties of the cured concrete are given in Table 4-3.

Table 4-3 : Mechanical and Fresh Properties of Concrete

	Fresh	**7 Days**	**14 Days**	**28 Day**
Compression Strength (psi)	-	3789	4647	4896
Tensile Strength (psi)*	-	306	316	371
Slump	3.5-in.-max	-	-	-
Total Air Content	7	-	-	-

*From split tensile test

Freeze-thaw and wet-dry test specimens

Corrosion test specimens
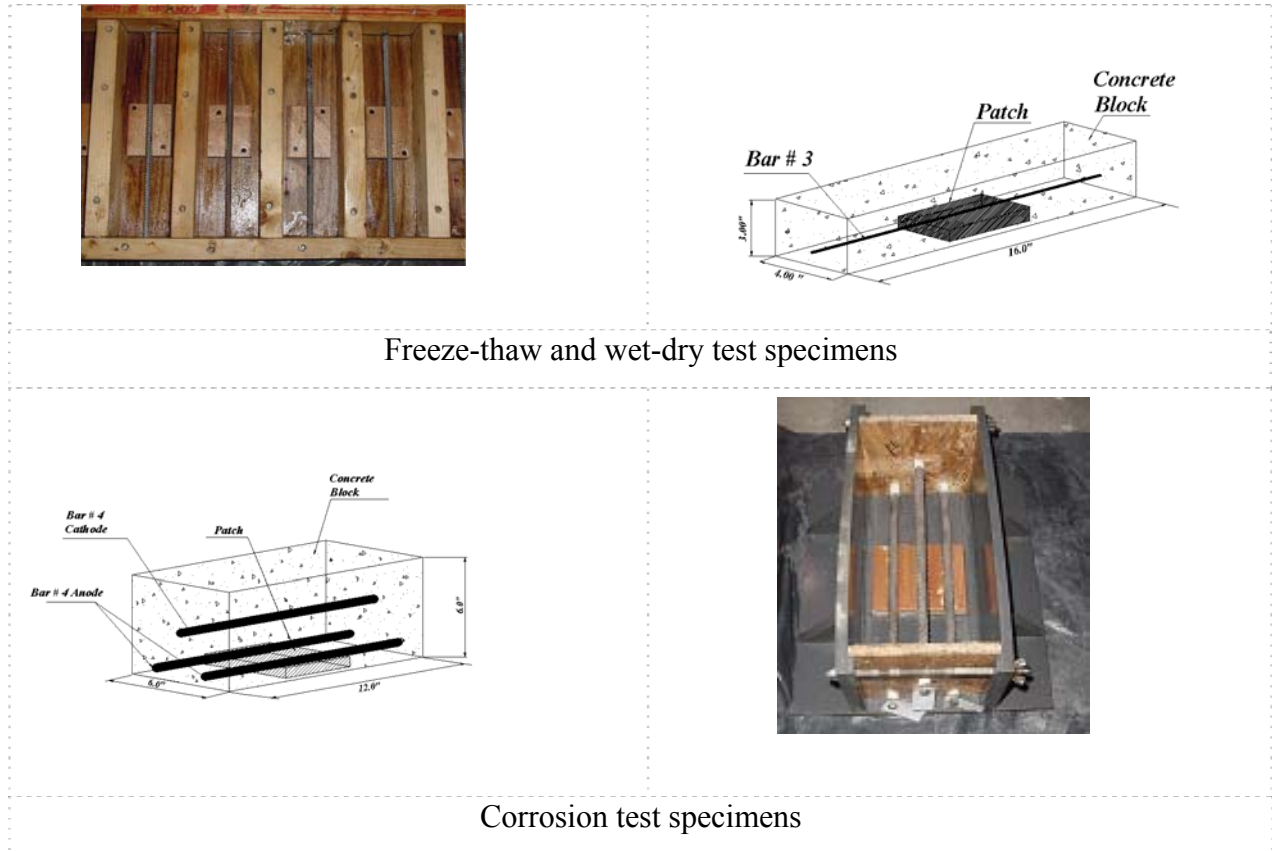
Figure 4-6: Schematics of specimens and photographs of mold

The reinforcement bar for the corrosion test needed to be cleaned to remove all the rust and all other particle the surface of the bars before casting. The bars were weighed after cleaning so that mass loss could be measured after the corrosion test. The ASTM G1-90 (preparing cleaning, and evaluating corrosion test specimens) procedure was used. Following the ASTM procedure the steel bars first were degreased by soaking in saturated lime solution ($CaCO_3$) and then was pickled in a acid solution (HCl 5%), as recommended . After weighing of each bar they named with unique name and tagged. Figure 4-8 shows the corrosion steel bar before and after cleaning.

| a) Wooden molds before casting | b) Measuring the fresh properties of concrete |

| c) Casting | d) Specimens after casting |

Figure 4-7 : Photographs of molds and casting

| (a) After degreasing | (b) After cleaning with acid |

Figure 4-8 : Steel bars after degreasing and cleaning

After casting, the specimens were immediately covered with polyethylene sheets which remained in place for more than 24 hours before demolding. After demolding the specimens were transferred to the curing room.

4.3.1.2 Surface Preparation

Repair practices commonly require that surface preparation techniques consist of high pressure water blasting, abrasive blasting or other techniques mentioned in Chapter 2. The surface preparation will improve the bond strength between the patch and concrete substrate explained in Chapter 3.

The specimens to be filled with a patch were sand blast on all of the cavity sides. Sandblasting was performed with the nozzle nearly perpendicular to the surface and was continued for at least 1 minute until no visible change on the surface was observed. After sand blasting the surface was blown with compressed air and then washed.

Figure **4-9** shows the cavity in the specimens before and after sand blasting.

(a)   (b)
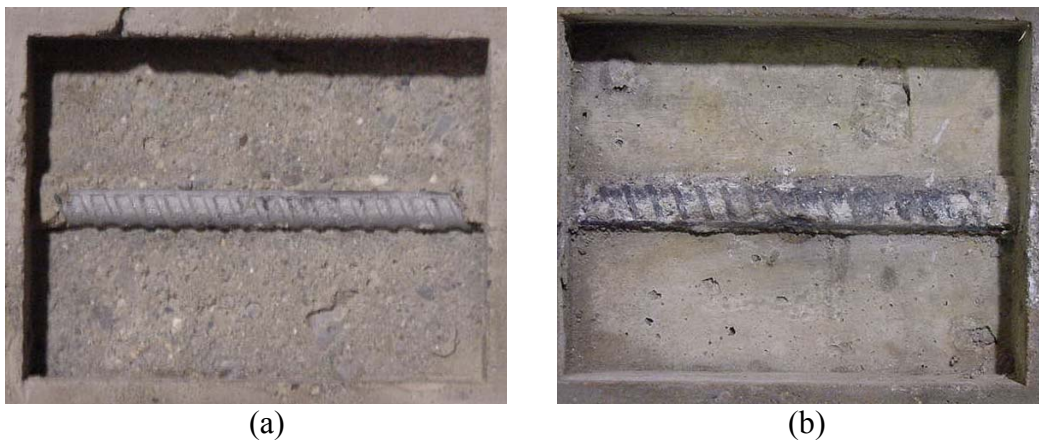
Figure 4-9 : Specimens (a) before and (b) after sand blasting

4.3.1.3 Screen Test

Before applying the patch material and FRP overlay to the specimens, a screen was performed to assess how quickly after the patch the FRP could be applied without compromising bond strength. A short time interval between application of the patch and FRP could reduce the time for the repair.

Time intervals of one hour and 24 hours were used in the screen test. Table 4-4 shows the number of specimens tested with two different patch materials. The following notations are used:

NS: one hour set (No set)

LS: 24 hours set (Long term set)

Table 4-4: Number of Specimens Tested

Time Interval	Hb2-Hex 106	R350-Hex106
1 Hour (NS)	2	2
24 Hours (LS)	2	2

To investigate the bond strength between the FRP overlay and the patch, the specimens were tested under three-point bending. Figure 4-10 shows the details of the test setup.
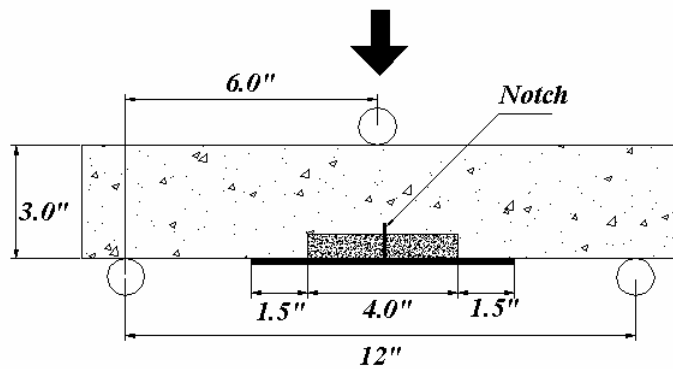
Figure 4-10: Test set up

Preparation of Test Specimens

All the fabricated specimens had a #3 bar as reinforcement. To best test for bond strength between the FRP and patch, the tension strength provided by the #3 bar was removed by cutting a notch through the beam until the bar was completely cut as shown in Figure 4-10. Thus all the tension force was carried by the FRP overlay. After making a one-inch in deep notch exactly at the middle of the beam, the patch material was applied followed by the FRP overlay with a time interval of one hour, and 24 hour intervals between the application of the patch and FRP. Figure 4-11 shows the preparation procedure for the test specimens.

Step 1: Make notch and cut bar | **Step 2**: Apply patch | **Step 3**: Apply FRP overlay after 1 hour or 24 hours
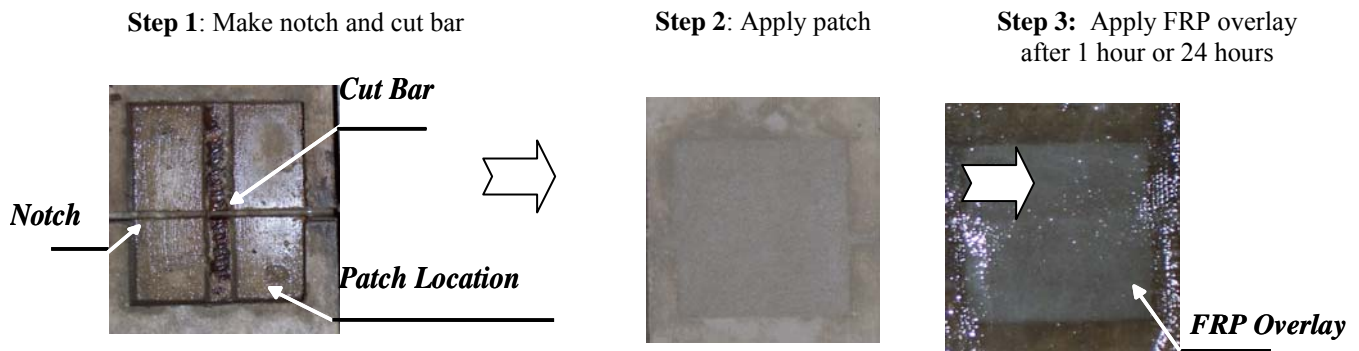
Figure 4-11: Preparation of the screen test specimens

Test Method and Measurement

The specimens were tested under three point bending after ten days of applying the patch material and the FRP overlay. These ten days allowed the patch material and FRP overlay to cure completely. The load was applied to the specimens by the displacement control method. The rate of displacement was 0.02 mm/s. The displacement and the applied load were measured automatically by the MTS machine, and specimens were loaded up to failure.

Test Results and Recommendation

The FRP overlay usually failed in one of two typical modes: premature failure of the FRP (debonding and rip-off), or rupture of the FRP. If the bond between the FRP overlay and patch material is strong enough, the failure should occur by rupture of the FRP.

All but one LS specimens failed due to rupture of the FRP. One specimen failed by debonding of the FRP from the patch and the concrete substrate. The specimen that failed by debonding of the FRP overlay did so because of accidental asymmetry of the applied load during the test. All NS specimens also failed due to rupture of the FRP. It should be noted that in both cases debonding was observed adjacent to the crack after the crack opened at the notch. The extent of debonding in the LS specimens was noticeably less than in the NS specimens.

Figure 4-12 and Figure 4-13 show the force displacement curve for patch materials 1 and 2, respectively.
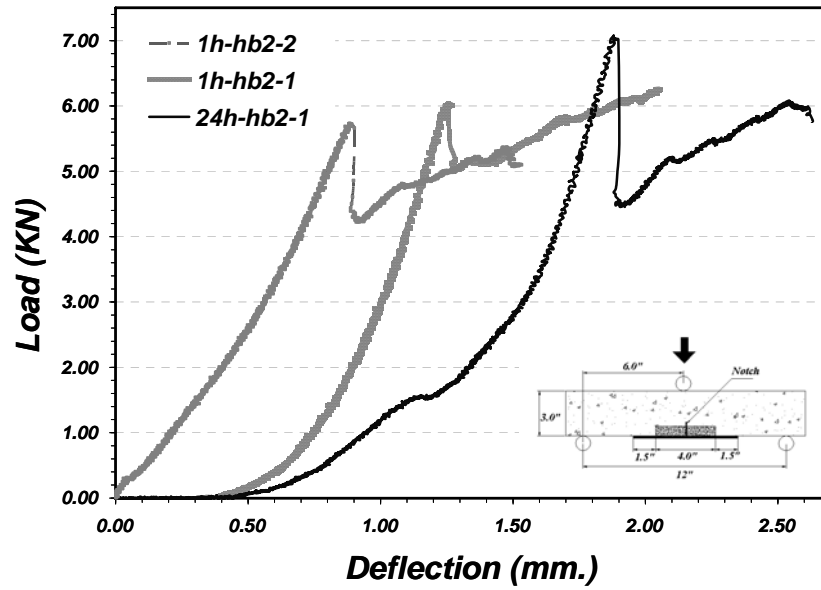
Figure 4-12: Load-deflection curves for Material 1
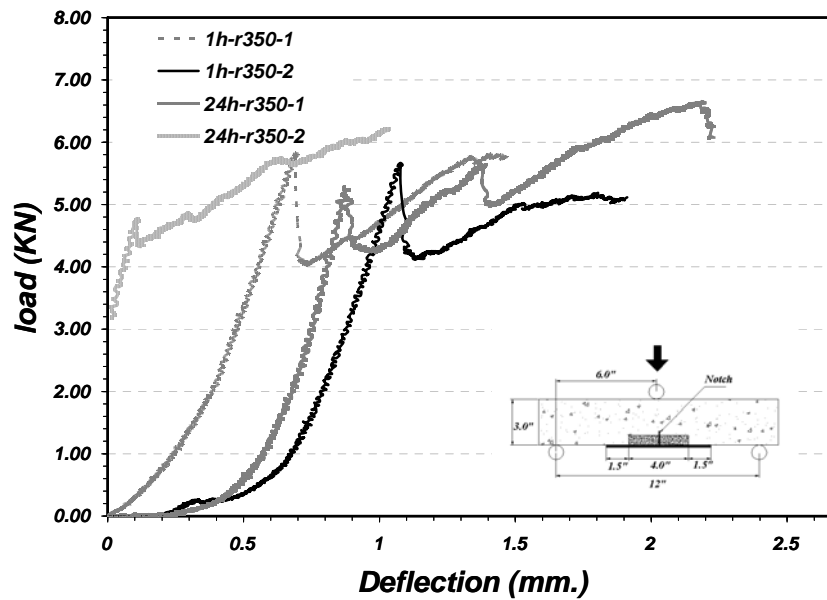
Figure 4-13: Load-deflection curves for Material 2

As Figure 4-12 and Figure 4-13 indicate, there is no significant difference between the overall FRP bond strength for both time intervals. Since the final failure mode in both cases (one hour and 24 hours intervals) occurs due to rupture of the FRP overlay, it is more economical to apply both the patch material and the FRP overlay within an hour of each other. It should be

noted that more care is needed to obtain a good finish when the FRP overlay is applied while the uncured patch is still soft, especially when the area to be patched is large.

4.3.1.4 Repair of the Specimens

Two patch materials and one FRP fabric were used to fill the cavities. The patch and FRP application were done according to the material data sheets.

General Practices

According to the material data sheet, the concrete surface should be "saturate dry" before applying the patch material. To accomplish this, the cavity was filled with water for about 8 hours before applying the patch material. However, when applying the patch the surface was still dry and water was sprayed on the surfaces to moisten them. The specimens were placed in an overhead position before applying the patch to simulate real field conditions.

Patch Material 1 was a two-component polymer-modified, lightweight mortar, and patch Material 2 was a one component low density, polymer-modified mortar. Both patch materials were mixed according to the material data sheet. Table 4-5 shows the mixture proportion for both patching materials. Since the quantity needed for each material was less than the minimum recommended in the data sheet, the mixture quantities were reduced in proportion to the required amount, and repair mortar was mixed in partial batches.

Table 4-5: Mixture of Patch Materials

	Component One	**Component Two**	**Mixing Time**
Material 1	45 (lb)	3.8-2.8 polymer (lit)	3-5 (min)
Material 2	55 (lb)	3.8-4.1 Water (lit)	3-5 (min)

A slow-speed drill (400–600 rpm) with a Jiffy-type paddle was used to mix the mortars for 3 to 5 minutes. Mixing for more than 5 minutes was not recommended in both material data sheets. The quantities of the liquid component and dry component were pre-measured. For both patching materials, the liquid component was always added prior to the dry component.

Ten specimens with dimensions of 3" × 4" × 16" were patched with Material 2 (weakest material in FE analysis) for the freeze-thaw tests, 20 specimens with the same dimensions were patched with Material 1 for the wet-dry and freeze-thaw tests, and 6 specimens with dimensions

of   6" × 6" × 12" were patched with Material 1 for the accelerated corrosion test. All the specimens were patched at the same day. Figure 4-14 shows mixing of the repair mortar with a slow-speed drill.

Figure 4-14: Preparing the repair mortar

The patch mortar was placed into the cavity by hand and compacted with fingers and pressure from the putty knife. Specimens were finished with a steel trowel. The finishing operation was kept to the minimum required to obtain a smooth surface. Since the working time for both patch material was between 30 to 45 minutes, the specimens to be exposed to the same environmental condition were patched from the same batch of patch mixture to avoid variation in the patch mixture.

After applying the repair mortar to all the specimens, the FRP overlay was placed over the uncured repair mortar for half of the specimens from each batch. After placing the FRP overlay, the specimens were kept in an overhead position for curing.

Mortar Application

The mortar was initially placed at the top surface of the cavity and build up toward the finishing surface. In a few cases, the bond between the mortar and concrete was very weak when

the repair material was applied to the totally dry surface, and the patch fall off immediately after application, especially for Material 1. After a few such occurrences, water was sprayed onto the concrete surface to improve the bond. The water was sprayed to wet the surface area, and as stated in the material data sheet, water was not allowed to stand on the patching surfaces. No sagging was observed in the repair material after application of the water spray. The specimens were kept in the overhead position for two days for curing at room temperature.

As mentioned in both repair material data sheets proper curing is extremely important and should be conducted in accordance with ACI 308, "Standard Practice for Curing Concrete". A curing compound that complies with the moisture-retention requirements of ASTM C 309 or ASTM C 1315 should be used. A curing compound was applied to the surface as soon as the surface could not be marred by the application.

FRP Application

As recommended in the screen test, the FRP overlay was applied within 1 hour after applying the repair mortar to all the specimens. The FRP overlay was applied only to half of the repaired specimens (Group 2).In general the FRP overlay can be applied to the concrete surface by two methods: (1) wet lay- up and (2) dry lay-up.

Wet Lay-up: The FRP wrap should be first impregnated using epoxy. For best results, the impregnation process should be accomplished using an automated fabric saturating device. Once saturated, apply fabric to the sealed concrete surface and smooth out any irregularities or air pockets using a plastic laminating roller. If required, apply additional layers of fabric while epoxy on the previous layer is still tacky.

Dry Lay- up: Apply the mixed resin directly onto the substrate at a rate of 1.2 kg/m^2, depending on the surface profile. Carefully place the fabric into the resin with gloved hands and smooth out any irregularities or air pockets using a plastic laminating roller. Allow the resin to squeeze out between the rovings of the fabric. If more than one layer of fabric is required apply additional epoxy at a rate of 0.5 kg/m^2 and repeat as above. Apply a final coat of epoxy to the exposed surface at a rate of 0.5 kg/m^2.

In this experimental test the dry lay up method was used. First the epoxy was applied to the concrete over the uncured patch with a brush and after that dried, the FRP overlay was placed. The FRP overlay was cut to the appropriate size with heavy duty scissor. A 2 to 2.5 inch extension of the FRP overlay beyond the patch material as it was calculated in Chapter 3 was

used. A smooth steel bar was used as a roller to squeeze out all the air bubble and extra resin. After applying the FRP overlay, one more epoxy layer was applied with the bush over the FRP. After 24 hour of curing the third layer of resin was applied to protect the FRP overlay from environmental conditions as recommended in the material date sheet. These specimens also were cured in an overhead position at room temperature for two days. After two days the specimens were back turned upside down and cured for 10 more days. Figure 4-15 shows the specimens after curing. The specimens were inspected visually after 10 days of curing to detect cracking, spalling, or debonding of the patch mortar.

Figure 4-15: Specimens after 10 day of applying the patch and FRP

A unique specimen identification system consisting four alphanumeric characters was used for each specimen as shown in Table 4-6. For example, R2F9 would be number specimen 9 with patch Material 2 (Emaco R350-CI) without FRP overlay, and exposed to freeze-thaw. It should be noted that the second set of specimens the fifth digit of (-2) was added to the specimen name. Also, since the corrosion test was done in two batches, a fifth digit was used to identify the batches.

As mentioned earlier in this chapter, the specimens were divided into three groups: (1) patched specimens with FRP overlay; (2) patched specimens without FRP overlay; and (3) control specimens without any cavity or repair. The behaviors of these three groups are compared in the next section.

Table 4-6: Specimen Naming Convention for Repairs

LABEL	DESCRIPTION
First Digit: Patch Mortar Type	**H**: ThoRoc's HB2 **R**: Emaco R350-CI **N**: none
Second Digit: With or without FRP	**1**: With FRP **2**: Without FRP **3**: Control Specimens
Third Digit: Subtask	**C**: Subtask 1: corrosion **F**: Subtask 2: Free-Thaw **W**: Subtask3: Wet-Dry **N**: no exposure
Fourth Digit: Specimen Number	**1**: Specimen No1 **2:** Specimen No 2 …….

4.3.2 Experimental Results and Observation

In this section the results and observation of the experimental study on the first set of specimens are presented. In addition to the numerical data and analysis, the results presented in this chapter are mostly based on the observation of durability of the patch material under the applied load and environmental conditions. The test procedure used in this part of the study is explained along with the results.

4.3.2.1 Initial Inspection

Initial inspections of the specimen showed some small surface cracking for patch Material 2 in two specimens after curing (Figure 4-16). Patch Material 1, however, displayed no cracks. The cracking in Material 2 could be due to surface tearing and is suspected to be due to over finishing the repair material after it had hardened. The cracking also could be due to the larger drying shrinkage of Material 2 compared to Material 1, as predicted by the FE analysis. None of the specimens displayed any sagging or debonding of the patch material after curing.

Figure 4-16: Comparison of surface cracking in the two patch material after curing

According to the material data sheet, the repair mortar reaches almost 80% of its ultimate strength after 10 days of curing. The environmental exposure of some of the specimens was initiated after 10 days of curing, while others had a longer curing time.

4.3.2.2 Corrosion

Test Set-up

For the corrosion study, concrete specimens with dimensions of $6'' \times 6'' \times 12''$ with a $4'' \times 5'' \times 0.625''$ cavity on the bottom side, patch Material 1, and three #4 reinforcing bars were used. The anode bars (see Figure 4-3) were corroded in an accelerated fashion using an external power supply. The specimens were soaked in salt water for 1 hour during every 12 hour period. The applied voltage and strain in the concrete cover and sides were monitored.

Mass loss: The mass loss was calculated using two methods. The first method measured the real mass loss of the steel bar by weighing the bars before and after the corrosion test. The second method estimates the mass loss with using the recorded current and using the Faraday Law. (Philips 1992, Pantazopoulou 2001):

$$\Delta W = \frac{A_m}{Z \times F} \times \int_0^T I(t)\,dt \qquad (4\text{-}1)$$

where

ΔW = steel loss in grams

$I(t)$ = measured current at time t

t = duration of the test in seconds

A_m = is the atomic mass of the F_e

86

z = valency (assuming that the rust product is mainly

Fe(OH)$_2$, 2 is used for the z value)

F = Faraday's constant

The results of these two methods are compared at the end of this chapter.

Strain readings: Strain gages were used to monitor the strain in the FRP overlay and concrete due to corrosion-induced radial expansion. For specimens with an FRP overlay the strain gages were mounted on the overlay. For specimens without an FRP overlay, (Group 2 and 3) a ½-inch wide strip of FRP was bonded around the specimens at specific locations and strain gages were mounted on these strips. The strain gages were applied on the specimen sides, and also on the bottom surface of the patch exactly below of the steel reinforcement. Figure 4-5 shows the location of the FRP strips and strain gages used in the accelerated corrosion test. Strain measurements were taken on two sides of the specimens at the level of the rebar. The strain was monitored every other day at the same time for all specimens.

Since the available data logging only had 6 analog voltage channels, the corrosion test was conducted in two separate batches. In first batches one specimen from each group was chosen. Specimen H1C5-1, H2C4-1, and H3C3-1were chosen for the first batch and others were in the second test batch.

Test Results

As expected and shown in Figure 4-17, all specimens suffered severe cracking, but in Group 1 specimens (with FRP) the crack propagation and damage was much less than in Group 2 and Group 3 specimens (without FRP). The crack pattern due to the corrosion-induced expansion was monitored in more detail for each group of specimens.

Crack Path: Two different crack patterns were observed. Figure 4-18 shows a schematic and a photograph of the two crack patterns.

Two of the specimens with FRP overlay, H1C5-1 and H1C9-2 (Group 1) had a single dominant crack along the side surface of the specimens parallel to the FRP overlay and reinforcing bar as shown in Figure 4-18(a). This crack path is henceforth referred to as a Pattern 1 crack. Some cracks were observed in the concrete cover but they did not extend to the patch. Also some debonding of the FRP overlay was observed around the crack path as predicted by the FE analysis.

(a) Sample from Group 3   (b) Sample from Group 2   (c) Sample from Group 1
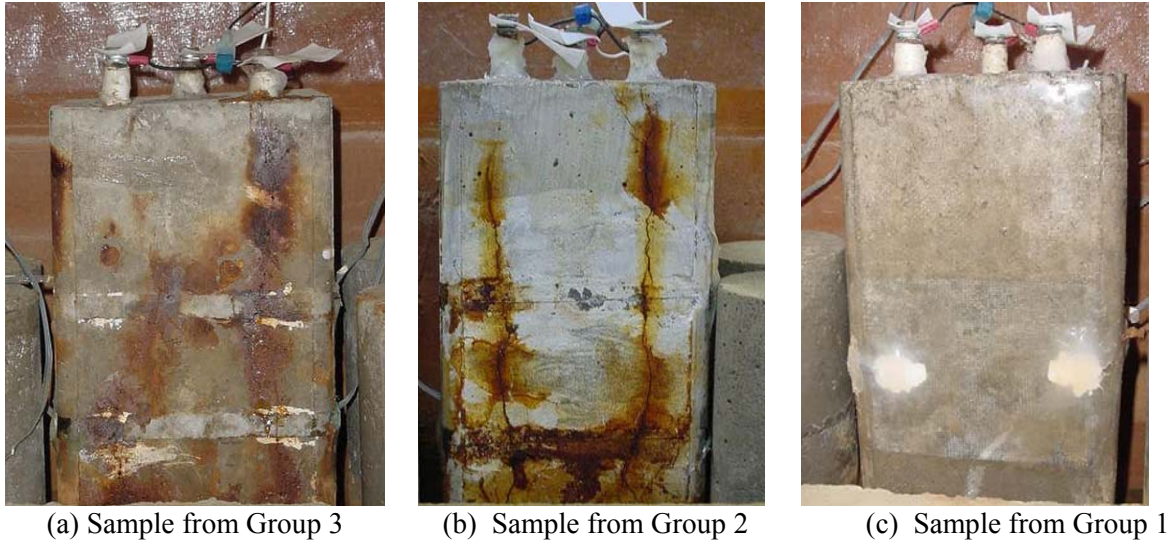
Figure 4-17: Samples from each group after 6 weeks of accelerated corrosion test
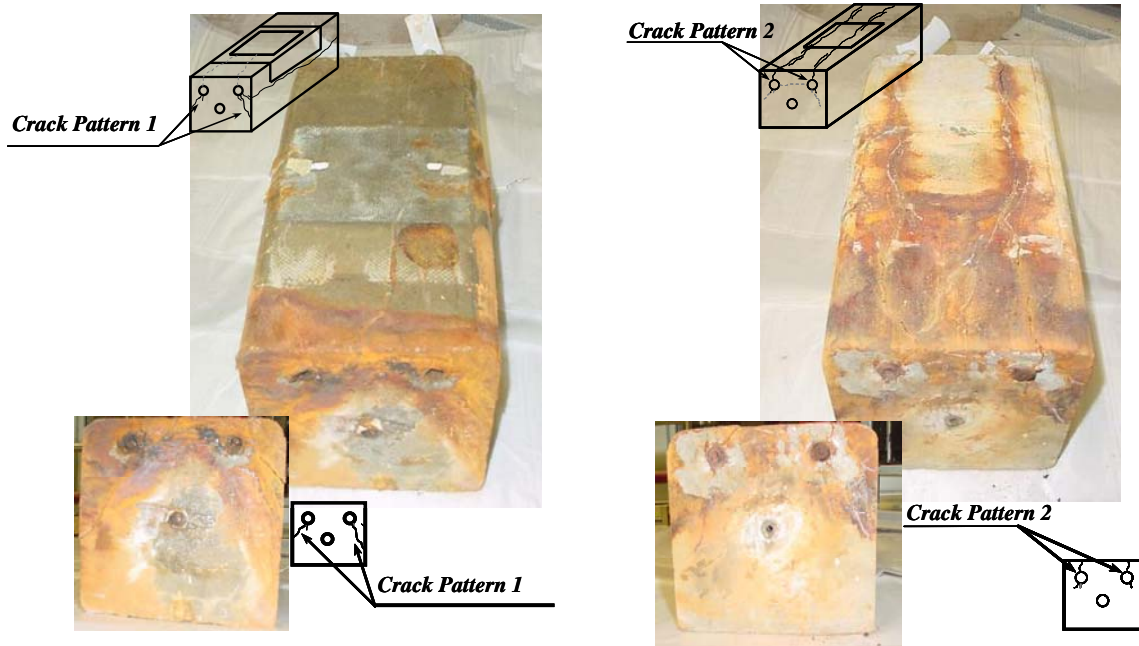
(a) Group 1 crack pattern   (b) Group 2 & 3 crack pattern

Figure 4-18: Crack pattern due to corrosion

Specimens with a patch and no FRP overlay (Group 2), and control specimens with no patch or overlay (Group 3), had a dominant crack at the bottom surface of the specimens parallel to the reinforcing bar. This crack is henceforth referred to as a Pattern 2 crack. In Groups 2 and 3 some specimens also had internal cracks from one corroding bar to the other (anodes), and some internal cracks radiating outward from the reinforcing bar into the concrete.

Strain gage reading: Figure 4-19 and Figure 4-20 show the maximum strains on the sides and bottom of the specimens as a function of time for typical specimens in all three groups. It should be noted that strain readings were initiated after the first two weeks of corrosion when the rebar started to swell and strains began to develop on the concrete and patch material. Figure 4-19 shows that the strain on the sides is largest for Group 1 specimens (with FRP overlay) which had Pattern 1 cracks (i.e., cracks that propagated to the sides). Figure 4-20 shows that the strain at the bottom is largest for specimens in Groups 2 and 3 (without overlay) which had Pattern 2 cracks (i.e., cracks that propagated to the bottom). The strain levels on the bottom and sides are different and this could be because the strain gages on the bottom were mounted at the crack locations while those on the side were not.
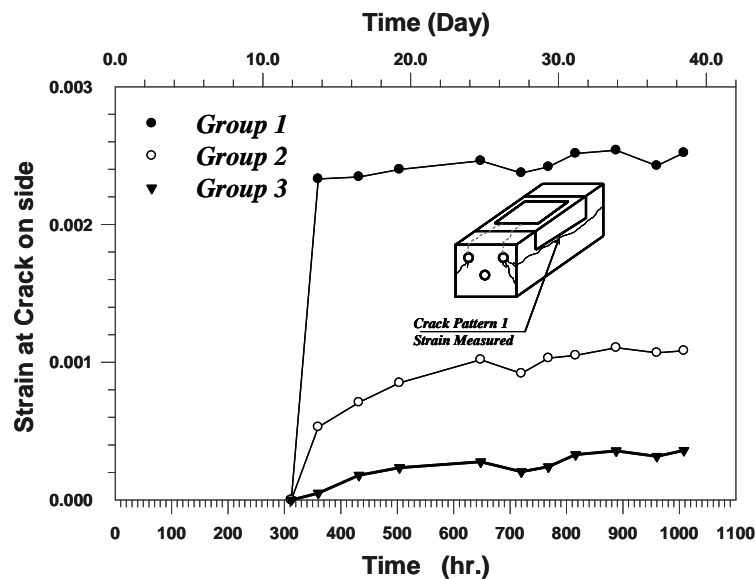
Figure 4-19: Maximum strains in the corrosion test along the crack path for crack pattern 1
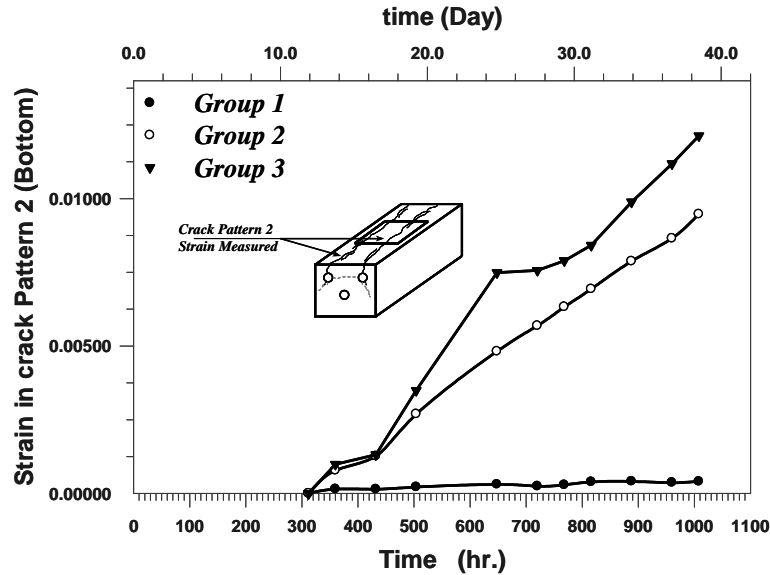
Figure 4-20 : Maximum strains in the corrosion test along the crack path for crack pattern 2

As both Figure 4-19 and Figure 4-20 show, the maximum strain at the sides for the Group 1 specimens are almost 10 times smaller compared to the maximum strain at the bottom of the Group 2 and 3 specimens. This indicates that corrosion can be reduced significantly by using the FRP overlay. The crack widths ranged from 0.2 mm on specimens with FRP overlay (Group 1) to 1.5 mm for specimens without the overlay (Group 2). Thus the FRP overlay also reduces crack widths. The results of the strain gage reading compare well with the FE analysis regarding the prediction of the crack pattern in corrosion specimens as explained in below.

Crack pattern: FRP specimens and non FRP specimens showed very different crack patterns and measured strains under the accelerated corrosion test. 3-D FE analysis of these specimens was conducted to understand why the FRP overlay changes the crack pattern and reduces crack widths. As done when selecting the FRP overlay, the expansive behavior due to rebar corrosion of the reinforcement was modeled using a uniform expansion of the 17500 µε on the rebar cross section.

In order to understand the overall effect of the FRP overlay on the stress distribution and crack pattern in the concrete substrate and patch material, the TCI was calculated in the cross section of the model along the two most probable crack paths that were obtained in the experiment. Figure 4-21 and Figure 4-22 show the calculated TCI in the concrete and patch material along the crack paths observed in the experiment and confirm that Pattern 1 cracks will

90

occur for Group 1 specimens but not for Group 2 specimens, while Pattern 2 cracks will occur for Group 2 specimens but not for Group 1 specimens. The FE analysis indicated that when 14% of the corrosion expansion strain is applied on the Group 2 specimens (without FRP) the first crack opens in the patch material as in Pattern 2, and when the first crack is fully opened the concrete substrate is not yet cracked.
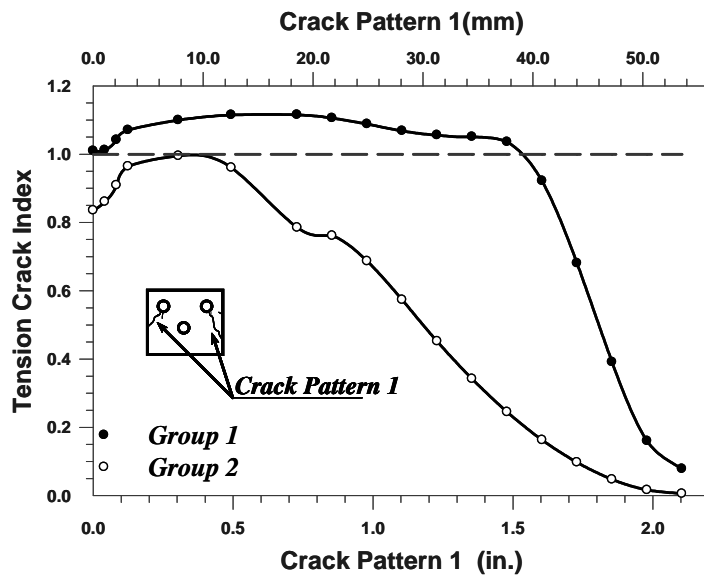
Figure 4-21: TCI along different crack pattern 1
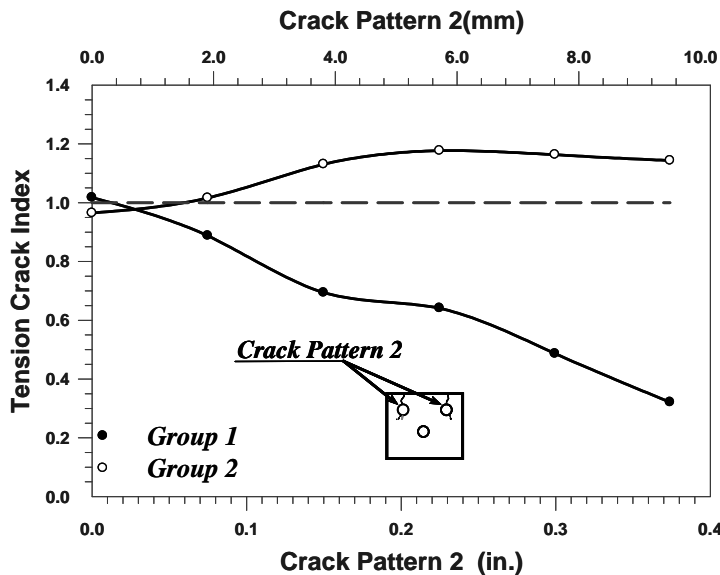
Figure 4-22: TCI along different crack pattern 2

91

On the other hand, the first crack opens as in Pattern 1 after applying 58% of the expansion strain on the Group 1 specimens (with FRP overlay). The numerical results match the crack patterns observed in the experiment, and cracking is delayed when the FRP overlay is used. The match between experimental and numerical results show that the FE analysis with the rebar corrosion modeled as an initial expansion strain applied uniformly across the entire cross section of the bar gives reasonable results. The FE analysis also is able to explain the mechanical effect of the FRP overlay on the crack pattern and how it delays the onset of cracking.

It is apparent that the cracking of the concrete is a direct consequence of the radial expansion of the corroded reinforcement bar. Internal cracking always starts at the location of the maximum expansion and extends in the direction of the weakest region, which in most cases is the cover region when the patch material is not reinforced by an FRP overlay. However, when an overlay is used, the overall stress distribution changes and the crack propagate sideways away from the region influenced by the overlay. In this case, the crack initiates in the concrete substrate instead of the patch, and since the concrete is stronger than the patch the cracking is delayed as predicted by the FE model. The strain at the surface of the specimens also was calculated in the FE analysis.

Mass loss: As mentioned earlier, the mass loss due to the corrosion was calculated using Faraday Law (equation 4-1) and also measured using the ASTM G1-90 procedure. In the ASTM procedure the bars were cleaned and weighed according to ASTM G1-90 "Preparing, Cleaning, and Evaluating Corrosion Test Specimens" before casting, each bar was named with a unique identifier, and after 6 weeks of accelerated corrosion, the bars were cleaned again according to ASTM G1-90. The bars were initially cleaned with a wire brush to remove all the loose rust products and concrete from the steel bars, and then they were immersed into 35% hydrochloric acid for 25 minutes at room temperature for deep cleaning inside the corrosion pits. More time was needed in some cases to remove heavy rust. The steel bars were washed, hot dried, and weighed. This procedure was continued until the weight of the bars reached a steady state.

Table 4-7 shows the measured mass loss for both batches of specimens as a percentage of the initial weight of the steel bar.

Table 4-7: Average Mass Loss for Each Group in the Corrosion Test

	Group 1	Group 2	Group 3
First Batch	4.90%	12.20%	10.06%
Second Batch	5.67%	17.31%	16.93%

The First batch had 3 specimens and, the second batch had 6 specimens. For the second batch, the applies voltage was 12.83 V, while fir the first batch it was 12 V. this is likely to be the cause for the increased mass loss for the second batch compared to the first batch for all groups.
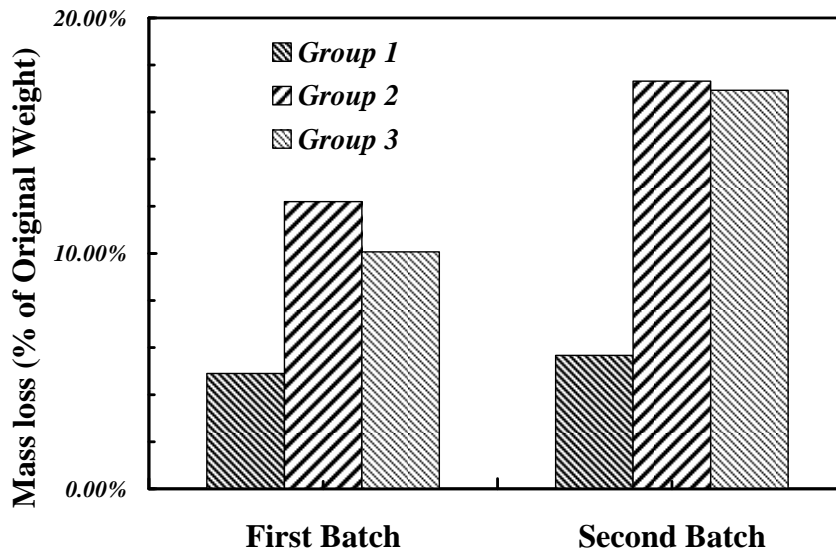
Figure 4-23: Corrosion mass loss for each group

Figure 4-23 indicate that the corrosion level is similar for Groups 2 and 3. However the mass loss for Group 2 (patched specimens) was slightly more than that for Group 3, since the porosity of the patch material is more than that of concrete and allows oxygen and chloride to diffuse more easily toward the steel bars thereby increasing the corrosion level. Also, as mentioned in the literature review, the anode ring effect and difference in potential between old concrete and fresh the patch mortar could increase the corrosion of the reinforcement bars.

<center>(a)   (b)</center>

Figure 4-24: Bars after six weeks of accelerated corrosion testing (a) Group 1 (b) Group 2 & 3

Table 4-7 and Figure 4-23 also indicate that the corrosion level was significantly reduced when the FRP overlay was used. This confirms the inference made earlier from strain gage reading for Group 1 and Groups 2 and 3 specimens.

The most likely reason for the overlay reducing corrosion is the reduction of diffusion of chloride ions, moisture and air through the concrete and patch due to overlay acting as a barrier. Figure 4-24 shows the corroded bars before cleaning for both Group 1 and Groups 2 & 3. It is clear that the corrosion level in Group 1 specimens (with FRP overlay) was considerably lower compared to the other two groups. Reduction in the corrosion is the main reason for the decrease in the measured strain and the reduction in the crack width for Group 1 specimens.

Table 4-8 shows the mass loss that was measured an estimated through value Faraday's Law agrees with the measured mass loss when only for a few specimens. Specimen H1C8-2 shows the maximum difference of almost 800%. This unusually large difference could be due to an error in the instrumentation of the concrete specimens and circuit assembly or malfunction of the data logging system.

Table 4-8: Mass Loss Measurements: (1) Measured Mass Loss, (2) Mass Loss Estimated through Faraday's Law

Specimen Name	Bar Name	weight1 (gr)	weight2 (gr)	ΔW	Faraday's Law	Percentage Error
H1C5-1*	15S5A	312.3	302.5	9.8	31.68	116.98
	17S5A	310.6	291.2	19.4	31.68	
H1C8-2	27S8A	313.2	303.6	9.6	60.63	804.87
	28S8A	313.3	309.5	3.8	60.63	
H1C9-2	31SA	313.3	287.9	25.4	60.69	132.10
	32SA	310.1	283.2	26.9	60.69	
H2C4-1*	12S4A	305.9	275.7	30.2	31.65	10.66
	13S4A	301.7	274.7	27	31.65	
H2C6-2	20SA	310.4	266.6	43.8	61.13	36.00
	21SA	312.8	266.7	46.1	61.13	
H2C7-2	23S7A	306.7	264.6	42.1	60.69	30.79
	24S7A	308.3	257.6	50.7	60.69	
H3C1-2	1S1A	310.8	268.3	42.5	61.23	34.56
	2S1A	311.8	263.3	48.5	61.23	
H3C2-2	4S2A	311.3	270.4	40.9	61.79	39.63
	5S2A	305.9	258.3	47.6	61.79	
H3C3-1*	8S3A	310.7	282.8	27.9	31.84	11.33
	10S3A	314.9	285.6	29.3	31.84	

* Specimens in the first batch

The difference between the measured mass loss and the estimated through Faraday's Law is generally small for the specimens in the first batch. It is possible that because the applied voltage for the specimens in the second batch was larger (12.83 volts compared to 12 volts for the first batch), some of the applied current caused more secondary reactions in addition to oxidation of the anode. For example, it is possible that the difference between the measured and estimated mass loss is due to the secondary reaction in which water is split in to hydrogen and oxygen. At the larger voltage this secondary reaction could have been stronger, thereby leading to greater differences between the measured and estimated mass loss.

4.3.2.3 Freeze-Thaw Test

In the freeze-thaw exposure study, specimens with dimensions of 4" × 3" × 16" with one #3 reinforcing bar, half in the patch and half in the concrete, with a cavity size of 3" × 4" × 0.625", were used with both patch materials. A total of 25 specimens (10 specimens

with patch material 1 and 10 specimens with patch material 2, and 5 control specimens) were subjected to 300 cycles of freeze-thaw. The ASTM C666 Procedure A was used in which each freeze–thaw cycle consisted of a one-hour and fifty minutes freezing period at $0^{o}F$ and a one-hour and ten minutes thawing period at $40^{o}F$ in a freeze-thaw machine. The freeze-thaw cycles started on February 24, 2006 and 300 cycles was completed on April 4, 2006. The specimens were inspected after each 100 cycles to monitor whether any significant deterioration occurred on the unwrapped specimens, but no significant damage was observed after 300 cycles for wrapped or unwrapped specimens.

The only problem that could be detected on the specimens after 300 cycles of freeze-thaw was peeling of the layer of the curing component in Group 2 specimens, especially in patch Material 2.

4.3.2.4 Wet- Dry Test

For the wet- dry exposure study, specimens with dimensions 4" × 3" × 16" with one #3 reinforcing bar, half in the patch and half in the concrete, with a cavity size of 3" × 4" × 0.625" were used with only patch Material 1. The specimens were subjected to 300 wet-dry cycles. A 3.5 percent (by weight) sodium chloride solution was used to wet the specimens for one hour in each 12-hour period. Figure 4-25 shows the wet–dry set up. The wet-dry test was started on March 2, 2006, and 300 cycles was completed on July 2, 2006. At the end of each 100 cycles the specimens were inspected to detect any debonding, cracking of the patch material, or damage on the FRP.

Figure 4-25 : Wet–dry tank

After 300 cycles wet-dry, no damage was observed on any of the specimens with or without FRP. There was some change in color due to the corrosion of the steel bar on the concrete substrate and patch material, but no edge spalling, debonding or cracking was detected in the specimens.

4.3.2.5 Cyclic Loading

After specimens were exposed to the freeze-thaw and wet-dry environments they were to be subjected to a fatigue test under 4-point loading. The maximum fatigue load was initially limited to that which caused a peak strain of $0.2\varepsilon_y$ in the steel reinforcement to simulate real field conditions in bridges. A dummy specimen with a strain gage on the reinforcement bar was tested under flexure, and loaded to failure to determine the required load and moment to obtain the target strain and also to determine the load capacity of the specimens. Figure 4-26 shows the test set up for the flexural test, and Figure 4-27 shows the moment–strain results for the dummy specimens. The beam failed in shear at a load of 4.945 kips. The maximum frequency for applying the load was 2 Hz for the MTS machine at the MSU laboratory.
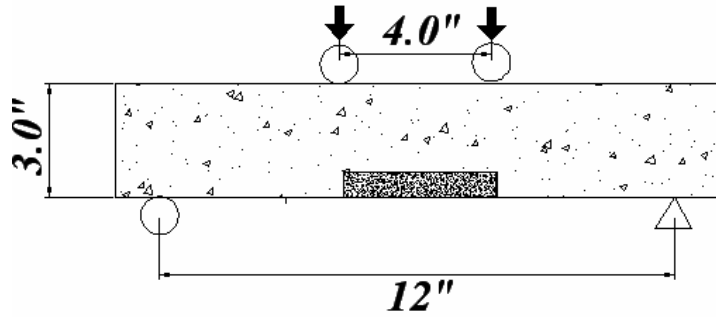
Figure 4-26 : Flexural test set up
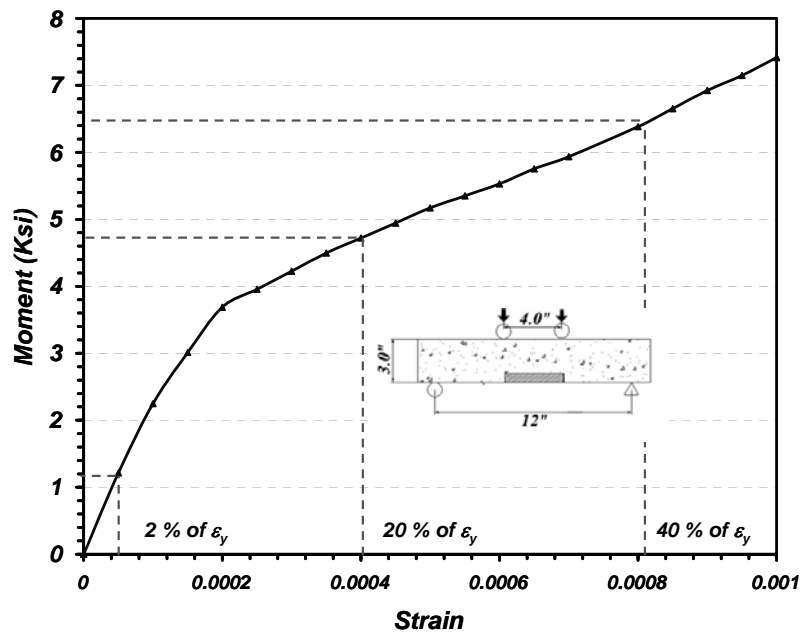
Figure 4-27: Moment- strain relation for dummy specimen

Problems Encountered and Test Results

Initially an R2F3 specimen (freeze-thaw specimen with patch Material 2 and without FRP overlay) was subjected to the fatigue test for almost two million cycles. A photograph of the specimen after this load application is shown in Figure 4-28. The maximum damage on the specimens was limited to debonding on the sides of the patch directly under the applied loads. In order to induce more damage the maximum bending moment was increased by increasing the applied load to 2.7 kips. This increased the strain level in the steel to $0.4\varepsilon_y$. Since the capacity of the specimen was limited by its shear strenght the maximum load could not be increased beyond

some point. The same specimen was tested again with the new loading, and the test was continued for more than 25,000 cycles. However, no more additional damage was observed on the specimen. To further increase the maximum moment and strain in the steel, the specimen was then tested under three point loading as shown in Figure 4-29. The maximum moment, and consequently the maximum induced strain, was increased by increasing the span from 4 in. to 7 in. The specimen failed by slip of the rebar after less than fifty cycles when the strain in the steel bar was close to the yield stain. Some additional approaches like welding plates at the end of the specimens were also tried but none of were successful. The specimens always failed in an attempt to further increase the strain in the steel before any significant damage occurred to patch.
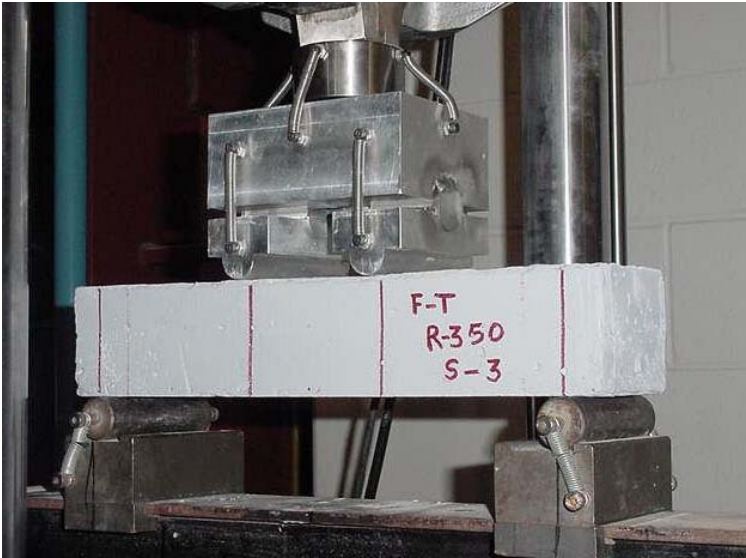
Figure 4-28: Freeze-thaw specimen after almost two million cycles of fatigue testing
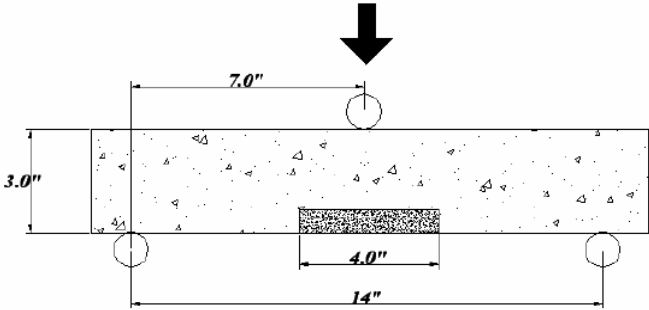
Figure 4-29: New fatigue test set up

It was originally expected that the patches would show significant damage either during freeze-thaw cycles or during the fatigue test. However, even the weaker patch material performed well. In retrospect the specimens should probably have been preloaded to induce cracking before being subjected to the environmental exposure. This would be more representative of the real field conditions and might have resulted in greater damage as moisture entered the cracks. Based on this hypothesis it was proposed that the specimens be subjected to about 1000 cycles of fatigue loading to induce cracking and then be exposed to an additional 100 cycles of freeze-thaw or wet-dry cycling.
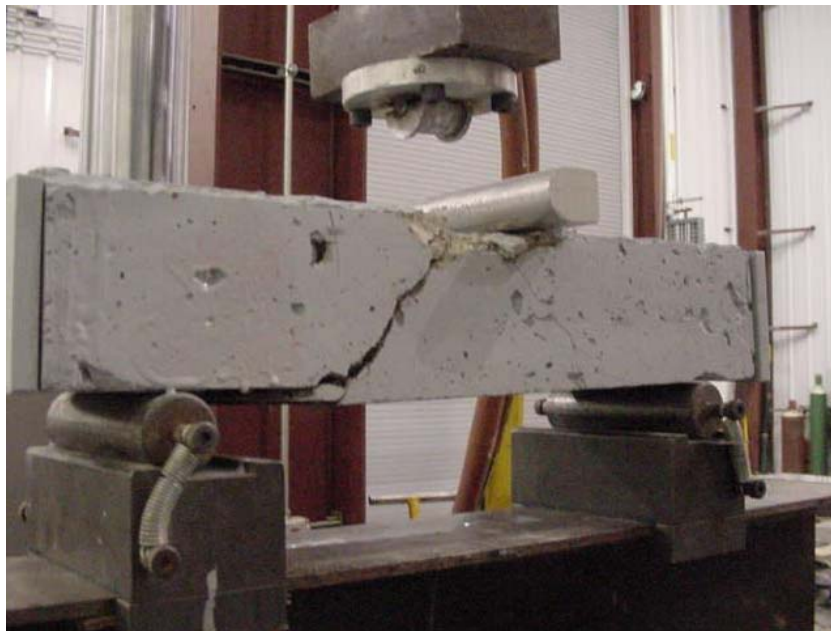
Figure 4-30: failed specimens due to slipping of the bar

4.3.2.6 Pre-Loading

With agreement from the Research Advisory Panel, the specimens were subjected to 1000 cycles of fatigue loading, after which they were exposed to 300 more cycle of freeze-thaw and wet-dry cycling. For pre-loading the initial test set up of 4-point loading was used with a span of 12 in., but the load was increased such that that the strain introduced in the steel bar did not exceed $0.4\varepsilon_y$ to avoid shear failure of the specimen or slip of the reinforcing bar. The loading was limited to 2.7 kips as an upper limit and 0.22 kips as the lower limit. The pre-loading was started at August 21, 2006. Table 4-9 shows the extension of the damage on each specimen after 1000 cycles of loading.

Table 4-9: Damage on Each Specimen after Pre Loading

Specimen Name	Explanation of Damage Type	Damage Type (Bottom View)
H2W1	Two sides debonded at both ends of the patch, and the crack opened up to 0.5"into the concrete surface. Both crack had the same opening size. No cracking in the patch material.	
H2W2	Two sides debonded at both ends of the patch, and the crack opened up to 0.5"into the concrete surface. Both crack had the same opening size. No cracking in the patch material.	
H2W3	Two sides debonded at both ends of the patch, and the crack opened up to the top concrete surface. Both crack had the same opening size. No cracking in the patch material.	
H2W4	Two sides debonded at both ends of the patch, and the crack opened up to the top concrete surface. The right crack opened more then the other crack. Debonding on the other side but it did not extend more then half an inch. No cracking in the patch material	
H2W5	Two sides debonded at both ends of the patch, and the crack opened up to the top concrete surface. The right crack opened more then the other crack. Debonding on the other side but it did not extend more then 1.5 in. No cracking in the patch material	
H1W1	No damage detected.	
H1W2	No damage detected.	
H1W3	No damage detected.	
H1W4	Some debonding of the FRP from the patch at the interface of patch/concrete	
H1W5	No damage detected.	
N3W1	Two cracks under both loads separated by of 4 inches. Neither crack extended to the top surface.	

N3W2	Two cracks one under the load and the other one in the middle of the specimen. Neither crack extended to the top surface.	
N3W3	Two cracks under both loads separated by of 4 inches. Neither crack extended to the top surface.	
N3W4	Two cracks under both loads separated by of 4 inches. Neither crack extended to the top surface.	
N3W5	No damage detected (perhaps because the steel bar was placed very low in the specimen).	
N3F1	One crack at the middle of the specimen (possibly caused by asymmetry in the loading and imperfection of the specimen).	
N3F2	No damage detected.	
N3F3	One crack at the middle specimen	
N3F4	Two cracks under both loads separated by of 4 inches. One appeared after 500 cycles loading	
N3F5	Two cracks one under the load and the other in the middle of the specimen. The middle crack did not open across the specimen.	--- *Crack Path*
H2F1	Two sides debonded at both ends of the patch. Both crack had same opening size. No cracking in the patch material.	
H2F2	Two sides debonded at both ends of the patch. Both crack had same opening size. No cracking in the patch material.	
H2F3	Broke during the first test due to slip of the steel bar.	
H2F4	Two sides debonded at both ends of the patch. Both crack had same opening size. No cracking in the patch material.	
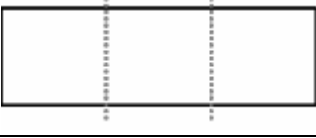
H2F5	Two sides debonded at both ends of the patch. Both crack had same opening size. No cracking in the patch material.	
H1F1	No damage detected.	
H1F2	No damage detected.	
H1F3	No damage detected.	
H1F4	No damage detected.	
H1F5	No damage detected.	
R2F1	Had more damage than other specimens. Full debonding on both sides and partial debonding along other bonded surfaces. One crack propagated to the patch but did not continue to the other sides.	
R2F2	Three main cracks. The side cracks opened more then the middle crack.	
R2F3	Broke during the first test due to shear failure and slip of the steel bar.	
R2F4	Two sides debonded, but one of the cracks was diagonal to the patch. Some debonding almost 1 inch on the other bonded surface.	
R2F5	Two sides debonded at both ends of the patch. Both crack had same opening size. No cracking in the patch material.	
R1F1	Broke during the test due to accidental loading up to 5.6 kips.	
R1F2	No damage detected.	
R1F3	Some debonding of FRP from patch at the interface of patch and concrete.	
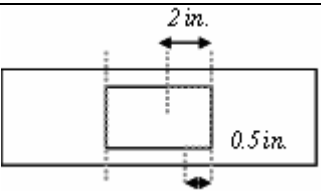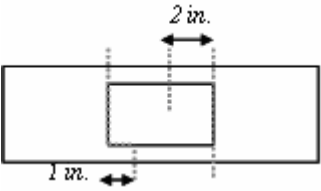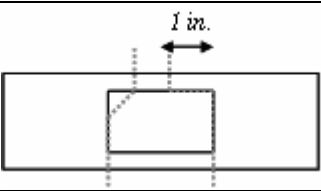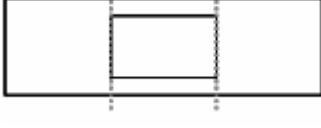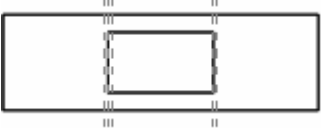
R1F4	Some debonding of FRP from patch at the interface of patch and concrete.	
R1F5	No damage detected.	
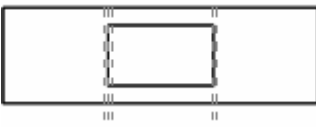
┄┄┄┄┄┄┄   *Crack Path*

≡ ≡ ≡ ≡   *FRP debonding*

The results of the pre-loading show that the FRP overlay reduces the damage on the patch material under the mechanical loading. The pre-loading results also indicate that material 1 had better bonding behavior to the FRP overlay and also to the concrete substrate.

After pre-loading the specimens were exposed again to the environmental exposure for 100 more cycles. A wet-dry cycle was started on August 22, 2006, and the freeze thaw exposure was started at September 22, 2006. The specimens were inspected after each 100 cycles inspect them for damage. Since there was no visible damage, the freeze-thaw and wet-dry cycles were continued for a total of 300 cycles, until October 31, 2006. There was no major cracking, spalling, or extension in debonding between the patch mortar and concrete substrate or FRP overlay after all 600 cycles of the freeze-thaw on the specimen. The weakest specimen on pre-loading (R2F3) was the first specimen that was subjected to the fatigue test after the second exposure. The test set up and loading and frequency was chosen to be same as for the pre-loading. After 4 days of fatigue testing and more than one million cycles, no more damage than what was observed after pre-loading could be detected in the repair mortar.

4.4 Second Test Set-up

The lack of any deterioration of the patch after 600 freeze-thaw cycles and a million cycles of fatigue loading led the research team to believe that the geometry of the patch was too small and that the patch was effectively bonded to the concrete. The test was therefore inconclusive in comparing durability of the repair mortar with and without an FRP overlay. It was consequently decided that a second test would be conducted with larger patch geometry. The patched region was extended as large was possible compared to the geometry of the concrete substrate. Since a 2 in. extension beyond the patch was required for the FRP overlay, the

104

geometry of the maximum patch dimensions was 4" × 9". The thickness of the patch was not changed.

4.4.1 Revised Freeze-Thaw and Fatigue Testing

The following procedure was adopted for the revised test:

1. The cavity size was increased from 3" × 4" × 0.625" to 4" × 9" × 0.625".

2. The specimens were preloaded with 1000 cycles of fatigue loading and then exposed to 300 freeze-thaw cycles. After environmental exposure, the specimens were tested under cyclic fatigue loading for 500,000 cycles.

3. All the specimens were subjected to a pull out test after cyclic loading in which the patch was pulled out from the concrete substrate to determine the bond strength.

4. Ten more specimens were added. These specimens were patched with both Material 1 and Material 2 but were not exposed to any environmental condition or fatigue loading, and were used as control samples to compare the initial bond strength with that after exposure.

5. In order not to delay the project by casting new specimens, 15 old specimens that had been subjected to wet-dry cycling were used. The size of the cavity was increased by cutting with a saw as shown for the dummy specimen. These specimens were supplemented by extra specimens that were cast with the originals.

The old specimens that had already been subjected to 600 freeze-thaw cycles were discarded. The specimens subjected to wet-dry cycling were used to conduct additional freeze-thaw tests as described above. Freeze-thaw cycling was significantly more aggressive than wet-dry cycling, and therefore not performing fatigue tests on the specimens subjected to wet-dry cycling should not negatively impact the evaluation of the patches.

4.4.1.1 Demolition

To reduce the bonding of the patch to the concrete along vertical surfaces, and to provide more area along which the patch can crack, it was proposed to increase the size of the cavity at the bottom of the test specimens to 4" × 9" × 0.625" as shown in Figure 4-2. The patch now extended across the entire width of the specimens. To prepare the new specimens from the old ones that had a 3" × 4" × 0.625" cavity, the size of the cavity in the old specimen was increased by removing the concrete for the bottom surface using a concrete saw, chisel and hammer. The specimens the saw depth was adjusted so the steel bars were not damaged to the extend possible.

Saw cuts were separated by roughly half an inch from each other and the concrete was removed with a hammer and chisel. Figure 4-31 shows the procedure used to prepare the new specimens. Figure 4-32 shows a typical specimen with the enlarged cavity.

Figure 4-31: Expanding cavity size

Figure 4-32: Specimen with expanded cavity

4.4.1.2 Repair of Specimens

A total of 30 specimens were prepared for the new test set-up. All cavities were enlarged by saw cutting and removing concrete with a chisel and hammer. After preparing the specimens the surfaces were washed and dried with air pressure. The specimens were sand-blasted on all sides and then blown. Individual wooden forms were used to form two edges for patching the

concrete specimens. Pine boards having one inch thickness were selected for this purpose. The wooden boards were attached to the concrete substrate temporarily with tape. No release agent was applied to the wood forms. Specimens were placed in an overhead position when applying the repair mortar and left in that position for one day, after which they were turned upside down. Figure 4-33 shows the specimens curing in the overhead position.

Figure 4-33: curing specimens in overhead position

Fifteen specimens were patched with Material 1 and 15 specimens were patched with Material 2. All specimens were repaired on January 18, 2006. From each batch of 15 specimens, 10 were exposed to freeze-thaw cycles (5 with patch only and 5 with patch and FRP), and the other 5 were not subjected any exposure and used as control specimens. The same naming procedure as in the first test was used to name the specimens.

Since in the new specimens the repaired part had a free edge, the FRP overlay could not be applied on the same day. The patch was to cure for almost 24 hours before the FRP overlay

was applied, and these specimens were cured for 10 days at room temperature. The specimens were inspected to identify any damage on the patch after 10 days of curing. The best specimens where chosen as control specimens ("No exposure"). Figure 4-34 shows a typical specimen after applying the repair mortar.

Figure 4-34: New specimen after patching

4.4.1.3 Trial Test

After 10 days of curing a dummy specimen patched with Material 2 was tested under cyclic loading for more than a million cycles. Figure 4-35 shows the condition of the specimen and patch during the fatigue test. The patch cracked and partially debonded from all the bond surfaces. However, while the cracks seemed to have penetrated through the entire bond surfaces, the patch did not actually break apart and could not even be pulled apart by hand.

(a)   (b)

Figure 4-35: Specimen after 1000 cycles of fatigue test

4.4.1.4 Grouping of Specimens

The specimens were inspected after 24 hours of initial curing, and the specimens were divided into three groups: (1) specimens with patch and FRP overlay (Group 1), (2) specimens with patch only (Group 2), and unexposed specimens (Group 3). The best specimens were chosen as control specimens (Group 3) and reminders were divided into Groups 1 and 2. The specimens in Group 1 and 2 were balanced to the extent possible by placing the specimens with similar damage into each group.

4.4.2 Experimental Results and Observation

This section presents the results and observation of the experimental study for the second test. In addition to analysis of the numerical data, this chapter also documents the durability of the patch material under the applied load.

4.4.2.1 Initial Inspection

Figure 4-36 shows some of the specimens after 1 day of curing.

Table **4-10** documents the damage observed at the initial inspection after 24 hours of curing. The FRP overlay was applied to Group 1 specimens after the initial inspection.

Table 4-10: Visual Damage in Specimens after 1 Day of Curing

Specimen Name	Explanation of Damage Type
H3N1	No debonding or cracking.
H3N2	No debonding or cracking.
H3N3	No debonding or cracking.
H3N4	No debonding or cracking.
H3N5	No debonding or cracking.
H1F1	Some debonding (visible gap) at the top surface, and debonding at sides.
H1F2	Significant debonding at the top surface and significant sagging of the patch on one side caused a gap of about 1cm between the concrete substrate and patch. No debonding observed at the side surfaces.

H1F3	Slight debonding at the top surface and slight sagging of the patch on one side caused a gap of about 2 mm between the concrete substrate and patch. No debonding was observed at the side surface.
H1F4	No debonding or cracking.
H1F5	No debonding or cracking.
H2F	No debonding or cracking.
H2F2	No debonding or cracking.
H2F3	No debonding or cracking.
H2F4	Significant debonding at the top surface and significant sagging of the patch on one side caused a gap of about 5mm between the concrete substrate and patch. No debonding observed at the side surfaces. (See Figure 4-36: Sample specimens after 1 day of curing (a) and (b)).
H2F5	No debonding or cracking.
R3N1	Slight debonding (visible gap) at the top surface, and debonding at sides.
R3N2	No debonding or cracking.
R3N3	No debonding or cracking.
R3N4	No debonding or cracking.
R3N5	No debonding or cracking.
R1F1	Slight debonding (visible gap) at the top surface and debonding at sides.
R1F2	No debonding or cracking.
R1F3	No debonding on the top surface and debonding on both sides.
R1F4	No debonding or cracking
R1F5	Slight debonding at the top surface and slight sagging of the patch on one side caused a gap of about 1 mm between the concrete substrate and patch. No debonding was observed at the side surface. (See Figure 4-36: Sample specimens after 1 day of curing (c) and (d)).
R2F1	Slight debonding (visible gap) at the top surface, and debonding at sides.
R2F2	No debonding or cracking
R2F3	No debonding or cracking
R2F4	Slight debonding at the top surface and slight sagging of the patch on one side caused a gap of about 2 mm between the concrete substrate and patch. No debonding was observed at the side surface.
R2F5	No debonding on the top surface, and debonding on both sides

4.4.2.2 Pre-Loading

Specimens in Group 1 and 2 were first subjected to the flexural cycling loading for 1000 cycles, after which they exposed to 300 cycles of freeze-thaw. In the revised test 3-point loading was used as shown in Figure 4-29: New fatigue test set up The span was increased to 14″ and the load was also increased to induce a strain of $0.6\varepsilon_y$ at the steel bar. Table 4-11 describes the extent of damage in each specimen. The pre-loading was begun on February 14, 2007.

(a) Bottom view of H2F4 specimen

(b) Side Elevation H2F4 specimen

(c) Bottom view of R1F5 specimen

(d) Bottom view of R1F5 specimen

Figure 4-36: Sample specimens after 1 day of curing Pre-Loading

Table 4-11: Extent of Damage after Pre-Loading

Specimen Name	Explanation of Damage Type	Damage Type (Bottom View)
H1F1	No damage detected.	
H1F2	No damage detected.	
H1F3	No damage detected.	
H1F4	No damage detected.	
H1F5	No damage detected.	
H2F1	One crack at the side of the patch, close to the bonded area. Slight debonding of patch.	
H2F2	One crack in the middle of the patch.	
H2F3	Two cracks in the middle of the patch. slight debonding at top surface around one of the cracks.	
H2F4	One crack at the side of the patch close to the bonded area. Debonding on one side of the patch over entire length and sides.	
H2F5	One crack in the middle of the patch. And slight debonding at top surface	
R1F1	No damage detected.	
R1F2	No damage detected.	
R1F3	Two small cracks in the patch surface observed because of FRP debonding around the crack	
R1F4	No damage detected.	
R1F5	No damage detected.	
R2F1	Debonding on the top surface, and some on debonding on sides.	
R2F2	Initial shrinkage crack existed before pre- loading and. After pre-loading debonding extended around the crack.	
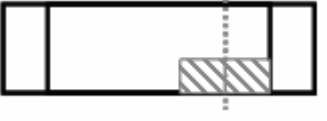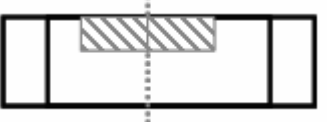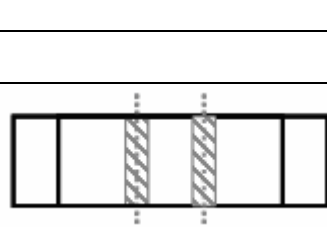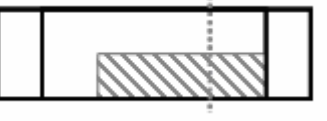
R2F3	One crack in the middle of the patch, and some debonding at the top surface	
R2F4	Almost complete debonding on the top surface and some debonding on sides.	
R2F5	Complete debonding on sides.	
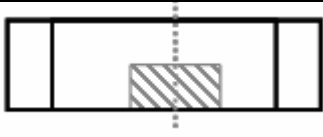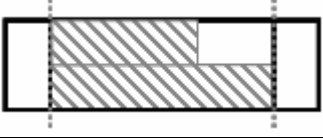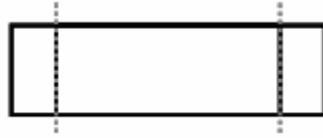
  Debonding

  Crack Path

4.4.2.3 Freeze-Thaw

The 20 specimens in Groups 1 and 2 were taken to M-DOT for freeze thaw exposure on March 15, 2007. The specimens were brought back to MSU after completing 296 freeze-thaw cycles on April 13, 2007. ASTM C-666 Procedure B (freezing in air, thawing in water) was used with each cycle consisting of a one-hour and fifty minute freezing period at 0°F and a one-hour and ten minutes thawing period at 40°F.

4.4.2.4 Cyclic Flexural Loading

All specimens were subjected to cyclic flexural loading for 500,000 cycles from April 2007 and it was continued up to August 2007. The specimens did not show any noticeable further damage than what they had after pre-loading. Only in one specimen (R2F4) did the patch fall off after about 4000 cycles of loading. Figure 4-37 shows specimen R2F4 and debonded patch. The patch broke in to two pieces after falling from the concrete during the test.

4.4.2.5 Pull-Out Test

The pull-out test was performed on all exposed and unexposed patches specimens except R2F4 in which the patch fell off. This test was intended to measure the bond strength of the patch.

113

Figure 4-37: Specimen R2F4 after about 400 cycles

Test Set-up

A 1.5 inch thick steel was glued to the patch surface using the Huntsman TDR 1100-11 two-component epoxy adhesive. The steel plate had the handle at the middle as shown in Figure 4-38. The concrete specimen was secured with two steel grips to the support of the MTS machine, and a tensile force was applied to the handle to pull out the patch. Figure 4-38 and Figure 4-39 show details of the pull-out test set-up.
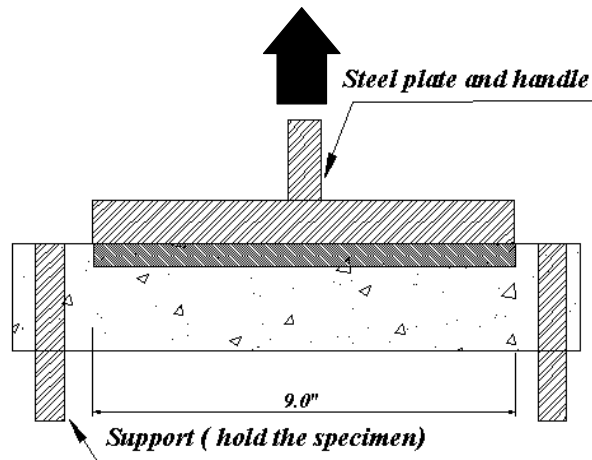
Figure 4-38: Schematic of pull-out test set-up

Figure 4-39: Photograph of pull-out test

<u>*Surface Preparation*</u>

The surfaces of the steel and patch mortar was rubbed with a wire brush, blow, and cleaned with alcohol. The steel plate was then glued to the patch. The adhesive used was a two component epoxy and the curing time was 24 hours. The optimum thickness for the adhesive was about 0.1 mm.

<u>*Failure Modes*</u>

The test load was applied by MTS machine and the maximum value for each test was recorded. Since there is no standard test for such an experiment, the rate of loading was kept the same as for a regular flexure test at 0.01 mm per second. Four different failure modes for Group 2 and 3 specimens, and five different failure modes for Group1 specimens were observed. The modes are:

Mode 1: Failure in the adhesive the steel plate separating from the path or FRP overlay, when this occurred, the steel plate was re-glued and pull-out test was repeated.

Mode 2: Failure in the patch material

Mode 3: Bond failure between the patch and concrete substrate. This was a desired failure mode for measuring the bond strength between the patch and the concrete substrate.

Mode 4: Partial failure of the bond combined with failure in the patch material.

115

Mode 5: Separation of the FRP overlay from the patch material. When this occurred, the FRP removed and the steel plate was glued directly to the patch and pull-out test was repeated again (Group 1 specimens only).

Each failure mode is illustrated in Figure 4-40. Only one of the specimens failed due to shear failure of the concrete substrate. This specimen had a shear crack from the pre-loading and since the bond between the patch and the concrete was the specimen failed in shear.
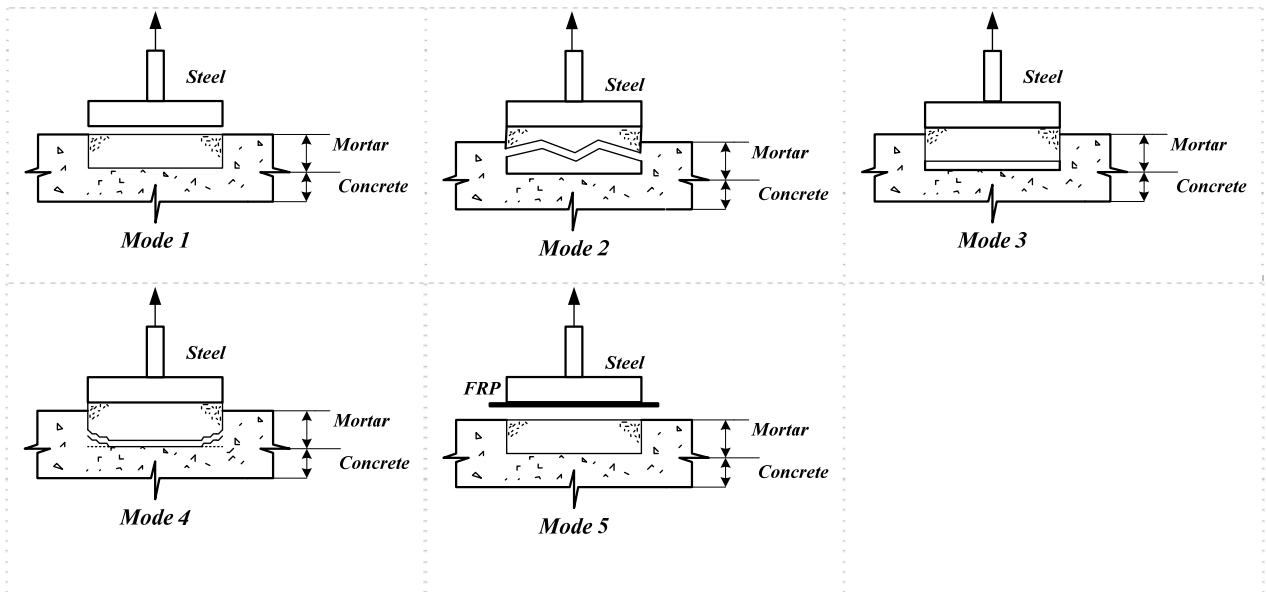
Figure 4-40: Failure modes in pull-out test

(a)   (b)

Figure 4-41: Pull-out test: (a) failure mode 3, and (b) failure mode 4

When it was difficult to distinguish clearly between mode 3 and 4 failure the failure was categorized as 3 & 4 failure mode. For Group 1 specimens that failed in mode 1, if the FRP overlay mostly peeled off from the mortar, the FRP was completely removed, the steel plate was re-glued again directly to the patch and the pull-out test was repeated.

FRP Extension

The length of extension of the FRP overlay over the concrete substrate was not always the same in all specimens due to variation in fabrication but the differences in extension were at most 0.25 in. Since this extension of the FRP overlay is directly related to the bond strength in Group 1 specimens, the FRP overlay was cut exactly at an extension of 2 in. in the top and 0.625 in. on the sides using saw. This was done so that the results could be compared with each other. Figure 4-42 shows the extension of the FRP overlay over the concrete substrate after cutting.
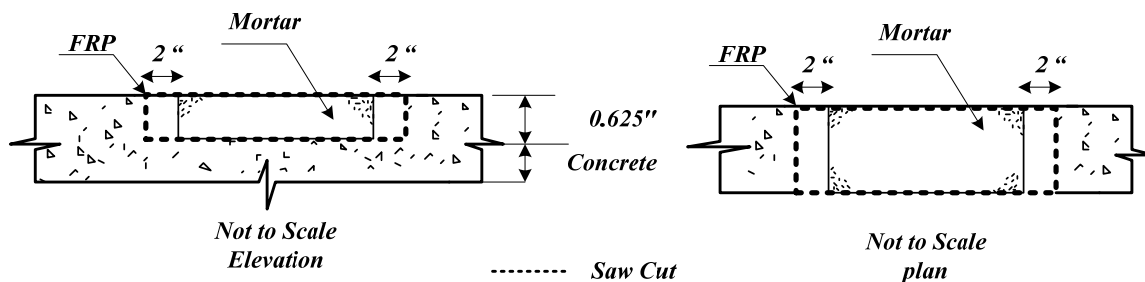
Figure 4-42: Dimension of FRP overlay for pull-out test

Bond Strength

Detailed observations from the pull-out test for each specimen are described in Table 4-12. For Group 1 specimens when failure occurred in mode 1 or 5 the FRP was removed, the steel plate was re-glued, and the pull-out test was repeated. Both loads are reported in the Table 4-12.

For the four specimens in which the pull-out test was repeated because either the FRP peeled or the adhesive failed during the first test, the pull-out load in the second test was smaller than the failure load in the first test. The higher strength during the first test is most likely due to the extension of the FRP over the concrete.

Table 4-13 and Table 4-14 show the statistics for the final bond strength of each group and patch material separately. For the five specimens in which the FRP peeled or the adhesive

failed and the pull-out test was repeated, the second load at which the patch debonded from the concrete substrate is used.

Table 4-12: Pull Out Test Results

Specimen Name	Failure Mode	Force (kips)	Comments
H3N1	Mode 3 & 4	1.026	
H3N2	Mode 3 & 4	0.694	
H3N3	Mode 3 & 4	0.857	
H3N4	Mode 3 & 4	0.727	
H3N5	Mode 3 & 4	1.061	
H1F1	Mode 1	3.822	
	Mode 3 & 4	3.082	
H1F2	Mode1	1.386	The adhesive failed after partially pulling out the FRP overlay. The FRP was removed and the steel plate was re-glued back to the patch and the test was repeated. This was one of the weakest specimens.
	Mode 3 & 4	2.165	
H1F3	Mode3&4	1.028	
H1F4	Mode 2	3.005	
H1F5	Mode 1	4.115	The adhesive failed after partially pulling out the FRP overlay. The FRP was removed and the steel plate was re-glued back to the patch and the test was repeated. This was one of the weakest specimens.
	Mode 3 & 4	2.469	
H2F1	Mode 3 & 4	0.661	
H2F2	Mode 3 & 4	0.484	
H2F3	Mode 3 & 4	0.754	
H2F4	Mode 3 & 4	0.735	This was the second weakest specimen. One side of the patch was already sagging and debonded from the concrete after 10 days of the curing.
H2F5	Mode 3 & 4	0.250	
R3N1	Mode 3 & 4	0.652	
R3N2	Mode 3 & 4	0.600	
R3N3	Mod e3 & 4	0.718	
R3N4	Mode 3 & 4	0.818	
R3N5	Mode2	1.196	

R2F1	Mode2	0.575	
R2F2	Mode3&4	0.542	
R2F3	Mode3&4	0.299	
R2F4	Mode3&4	0.000	The patch mortar had already fallen off during the fatigue test.
R2F5	Mode2	0.565	
R1F1	Mode3&4	2.795	
R1F2	Mode3&4	3.194	
R1F3	Mode2	2.660	
R1F4	Mode5	3.123	The FRP overlay totally peeled off from the concrete and patch. The steel plate re-glued to the patch the pull-out test was repeated.
	Mode3&4	2.272	
R1F5	Mode1	2.911	The adhesive failed after partially pulling out the FRP overlay. The FRP was removed and the steel plate was re-glued back to the patch and the test was repeated. This was one of the weakest specimens.
	Mode3&4	1.463	

Table 4-13: Statistics of Pull-out Force for Patch Material 1

	Group 1		Group 2		Group 3	
	Specimen	*Force (kips)*	*Specimen*	*Force (kips)*	*Specimen*	*Force (kips)*
	H1F1	3.09	**H2F1**	0.76	**H3N1**	1.03
	H1F2	2.17	**H2F2**	0.74	**H3N2**	0.70
	H1F3	1.03	**H2F3**	0.25	**H3N3**	0.86
	H1F4	3.02	**H2F4**	0.58	**H3N4**	0.73
	H1F5	2.48	**H2F5**	0.21	**H3N5**	1.07
Mean	2.36		0.51		0.88	
St. Deviation	0.83		0.26		0.17	
95% Confidence	0.73		0.23		0.15	

Table 4-14: Statistics of Pull-out Force for Patch Material 2

	Group 1		Group 2		Group 3	
	Specimen	*Force (kips)*	*Specimen*	*Force (kips)*	*Specimen*	*Force (kips)*
	R1F1	2.80	**R2F1**	0.58	**R3N1**	0.65
	R1F2	3.21	**R2F2**	0.54	**R3N2**	0.60
	R1F3	2.67	**R2F3**	0.30	**R3N3**	0.72
	R1F4	2.28	**R2F4**	0.00*	**R3N4**	0.82
	R1F5	1.47	**R2F5**	0.57	**R3N5**	1.20
Mean	2.49		0.40		0.80	
St. Deviation	0.66		0.25		0.24	
95% Confidence	0.58		0.22		0.21	

*Patch fell off prior to pull-out test and the pull-out force was assumed to be zero
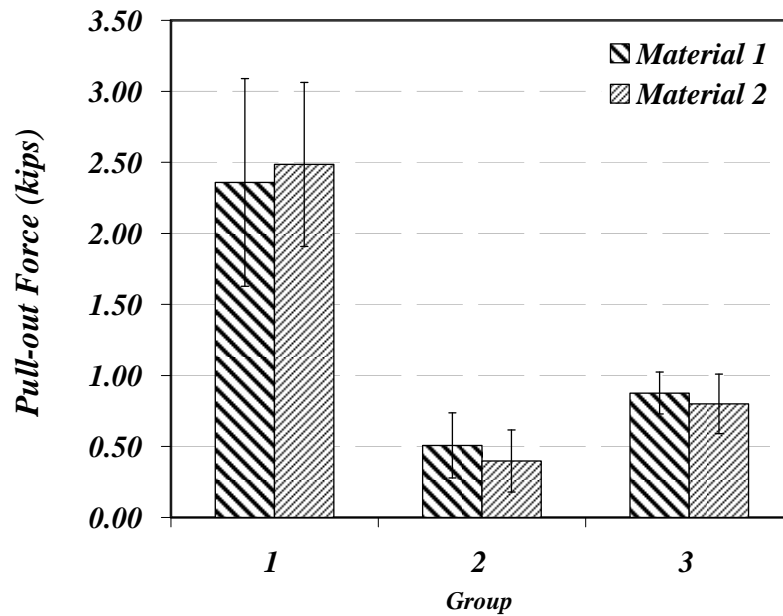
Figure 4-43: Comparison of mean bond strength

Hypothesis Test of Two Means

Since some of the differences in mean bond strength for patch materials 1 and 2 and also between groups are sometimes small, more detailed analysis is needed to ascertain whether the difference are statistically significant. Hypothesis testing can be used to compare the differences in two means using the *t*-statistic

$$t = \frac{m1 - m2}{s_p \sqrt{\dfrac{1}{n_1} - \dfrac{1}{n_2}}} \qquad (4\text{-}2)$$

where m_1 and m_2 = means of samples 1 and 2, respectively, n_1 and n_2 = number of specimens in samples 1 and 2, respectively, and, s_p^2 = pooled variance given by

$$s_p^2 = \frac{(n_1 - 1)s_1^2 + (n_2 - 1)s_2^2}{n_1 + n_2 - 2} \qquad (4\text{-}3)$$

where s_1 and s_2 = standard deviations of samples 1 and 2, respectively.

The null hypothesis

H_o: $m_1 = m_2$

was tested against the alternative hypothesis

H_a: $m_1 > m_2$

If $t > t_{\alpha,n1+n2\text{-}2}$ then H_a is accepted, where $t_{\alpha,n1+n2\text{-}2}$ = value from the t table for the α significance level with $n_1 + n_2 - 2$ degrees of freedom. α was chosen to be 0.05 and $t_{\alpha,n1+n2\text{-}2} = 2.015$ when $n_1 = n_2 = 5$. When both patch materials were compared for each group so that $n_1 = n_2 = 10$, then $t_{\alpha,n1+n2\text{-}2} = 1.812$. All pairs were tested against each other for each patch material respectively, and then for both patch materials together.

Table 4-15: Pairwise Hypothesis Tests

	Pairs		m_1	m_2	s_1	s_2	s_p	t	Accept H_a
Material 1	Group 1	Group 2	2.359	0.507	0.834	0.261	0.618	4.738	Yes
	Group 3	Group 2	0.876	0.507	0.168	0.261	0.220	2.655	Yes
	Group 1	Group 3	2.359	0.876	0.834	0.168	0.601	3.897	Yes
Material 2	Group 1	Group 2	2.486	0.398	0.658	0.250	0.498	6.633	Yes
	Group 3	Group 2	0.800	0.398	0.239	0.250	0.244	2.602	Yes
	Group 1	Group 3	2.486	0.800	0.658	0.239	0.495	5.386	Yes
Both Material	Group 1	Group 2	2.422	0.453	0.711	0.248	0.533	5.847	Yes
	Group 3	Group 2	0.838	0.453	0.199	0.248	0.225	2.714	Yes
	Group 1	Group 3	2.422	0.838	0.711	0.199	0.522	4.797	Yes
Group 1	Material 2	Material 1	2.486	2.359	0.658	0.834	0.751	0.268	No
Group 2	Material 1	Material 2	0.507	0.398	0.261	0.250	0.256	0.679	No
Group 3	Material 1	Material 1	0.876	0.800	0.168	0.239	0.206	0.588	No

Table 4-15 indicates that at the 0.05 significance level the mean bond strength between the patch and the concrete is:

- Stronger for Group 1 specimens (with FRP overlay), and
- Weakest for Group 2 specimens

The difference in the mean bond strength for patch material 1 and 2 are not statistically significant within each group.

The mean bond strength and 95% confidence interval for each mean strength are shown in Figure 4-43. It is apparent that the mean bond strength for Group 1 is significantly higher than that for Groups 2 and 3.

It is some what surprising that use of FRP overlay produced a stronger bond between that patch and the concrete substrate, even compared to the controll specimens that were not exposed to freeze-thaw and load cycles. The following reasons might contribute to this improved bond:

- The FRP overlay support the patch during curing
- The FRP overlay seals the moisture within the patch thereby reducing shrinkage and interfacial shear stresses between the patch and the concrete substrate.
- The FRP overlay serves as a physical barrier to moisture diffusion during freeze-thaw cycles, and thereby reduces freeze-thaw damage to the patch/concrete interface.
- The epoxy resin used to bond the FRP to the concrete substrate might also partially bond the interfaces between the patch and the concrete substrate.

4.5 Conclusions

The experimental test results that were conducted reveal many of the advantages of using an FRP overlay over the patch.

- The FRP overlay changes the crack patterns in concrete under the expansion caused by corrosion of the reinfocing steel by preventing cracking toward the surface on which the FRP is applied. It also reduces crack widths. The FRP overlay most likely reduces the diffusion of moisture and chloride to the reinforcing bars and therefore ongoing corrosion is reduced.
- The patch pull-out tests that were conducted indicate that the bond strength between the patch and the concrete substrate is significantly enhanced when an FRP overlay is used.

Even after subjecting specimens to cyclic preloading (to induce cracking), followed by 300 freeze-thaw cycles, and 500,000 cycles of fatigue loading, the bond strength between the patch and the concrete substrate was significantly stronger when the FRP overlay was used even compared to patches specimens without an overlay that were not exposed to cyclic loading or freeze-thaw cycles.

Although the finite element analysis indicated that patch material 1 should have better performance than patch material 2 due to its lower shrinkage properties, the experimental results indicate that the differences in the pull-out loads for the two patch materials is not statistically significant at the 0.05 significance level.

Chapter 5
Cost-Benefit Analysis

5.1 Introduction

This chapter focuses on the life-cycle cost estimation of the traditional patching repair and the proposed dual patch and FRP overlay. The lifetime of the different patching techniques is estimated using the results of the pull-out tests and the reported life of conventional patches.

5.2 Definitions

5.2.1 Life- Cycle Cost Analysis

Life-cycle cost analysis (LCCA) is a methodology that provides the means to include the total cost to both agency's and the users in an investment decision (FHWA 1994). The definition for LCCA as modified by TEA-21 is a process for evaluating the total economic worth of the project segment by analyzing initial costs and discounted future cost, such as maintenance, user, reconstruction, rehabilitation, restoring, and resurfacing costs, over the life of the project segment.

LCCA is a valuable cost-centered engineering economic analysis whose objective is to evaluate the economical effectiveness of different mutually exclusive investment alternatives over a certain time period and to identify the most cost-effective alternative. LCCA provides a significantly better assessment of the long-term cost effectiveness of a project than alternative economic methods that focus only on the first costs or on the operating related cost in the short run (Walls and Smith, 1998).

5.2.1.1 Analysis Period

The LCCA period, or the time horizon over which the alternative are evaluated, should be sufficient to reflect long-term cost and performance differences between the alternatives (Fuller and Peterson, 1995). Competing alternative may each have a different service life, which is the time period that an asset will remain open for public use. LCCA, however, uses a common

period of time to assess cost differences between these alternatives so that the results can be fairly compared.

5.2.1.2 User Benefits and Agency Costs

The aim of benefit-cost analysis is to maximize the equivalent value of all benefits less that of all costs (expressed either in present values or annual values). In general, the benefits of public projects are difficult to measure, whereas the costs are easier to determine.

Since here the objective is the rehabilitation cost, we limit ourselves to this definition. The rehabilitation costs are larger future periodic cost associated with keeping the project in a usable condition. The objective of the rehabilitation treatment is to raise the condition of the facility and increase its level of service (Walls and Smith, 1998; Material Manual, 2002).

5.2.1.3 Comparison

One of the key components that is important in understanding LCCA is the concept of the time value of the money. A given amount of money received today has higher value than the same amount received at a later date. For LCCA, costs associated at different times must be converted to their value at a common point in time (US Department of Transportation, 2002). A number of techniques based on the concept of discounting are available for converting future costs to the present. The most common include Benefit/Cost (*B/C*) Ratio, Internal Rate of Return (IRR), and Net Present Value (NPV). An alternative way of expressing the worthiness of a public project is to compare the user benefits (*B*) to the agency costs (*C*) by taking the ration *B/C*.

Benefit-Cost Ratio

The *B* and *C* for a give problem can be calculated using the following equations.

$$B = \sum_{n=0}^{N} b_n (1+i)^{-n} \tag{5-1}$$

$$C = \sum_{n=0}^{N} c_n (1+i)^{-n} \tag{5-2}$$

where b_n = benefit at the end of period n, $b_n \geq 0$; c_n = cost at the end of period n, $c_n \geq 0$; N = project life; and i = sponsor interest rate (discount rate).

For this patch repair problem the user benefit is assumed to be the same for both patching approaches, and therefore only the *C* value is compared for both patching approaches.

5.3 Cost Analysis

5.3.1 Repair Durability

Since no State Highway Agency has experience with the patching approach using an FRP overlay, some assumptions must be made to conduct a cost-benefit analysis. To estimate the life of the dual patching system, the life of each patching approach was estimated based on the known life of regular patching and the bond strength from the pull-out test results. According to MDOT experience, traditional patches last for a maximum of about 5 years. We associate the 5-year life with bond strength of Group 3 specimens for both materials (these specimens were repaired using the traditional patching technique, and were not exposed to freeze-thaw and cyclic loading). The life of Group 1 (with FRP overlay) and Group 2 (traditional patch) specimens are estimated through:

$$T_1 = \frac{\text{Bond Strength of Group 3}}{\text{Bond Strength of Group 1}} * 5 \text{ years} \qquad (5\text{-}3)$$

$$T_2 = \frac{\text{Bond Strength of Group 3}}{\text{Bond Strength of Group 2}} * 5 \text{ years} \qquad (5\text{-}4)$$

Table 5-1 shows the estimates for both patch materials.

Table 5-1: Life of Each Group

	Life (Years)	
	Group 1	**Group 2**
Material 1	14.0	3.0
Material 2	15.0	2.5
Both	14.4	2.7

Since patch materials 1 and 2 did not show any significant difference in bond strength for both Groups 1 and 2 in the experimental investigation, and Material 2 is cheaper than Material 1, Material 2 is chosen for the LCCA. It should be noted, however, that due to higher shrinkage strain, Material 2 is expected to display more cracking.

Table 5-2: Cost Comparison between Material 1 and Material 2

	Yield per Bag (ft³)	Number of Bags Required for 385 Cubic Yards*	Price
Material 1	0.50	20789.5	$ 395,000
Material 2	0.61	17041.0	$ 289,700

* The costs reported by MDOT (see Table 5-3) are for 385 cubic yards.

Table 5-3 shows the details of the costs for both patching approaches. Most costs were obtained from MDOT's cost analysis for activity 15100 (Bridge Maintenance), and 16600 (Non-Routine Traffic Control).

Table 5-3: Detailed Cost for Bridge Maintenance (Dollars)

	Reg-Sal/hours	Ovr tm/hours	Material 2	FRP & Coating	Eqp Pur	Trv/EqUsg	Units Accomplshd	Equalizd Unit Cost
Maintenance without FRP	253595/13588	23446/758	289692			23091	385 cu. yd	**1532.01**
Maintenance with FRP	311024/16668	28766/930	289692	549173		23091	385 cu. yd	**3061.44**
Non- Routine Traffic Control	43177/2269	51444/1772			100	969	4041 hrs	**28.79**

It should be noted that in activity 15100, the cost of the material did not match the cost of either of the chosen patch materials and hence the cost was changed to the value shown in Table 5-2. Further the following assumptions were used to calculate the cost of the patch repairs with the FRP overlay:

- For each 8 hours of the regular patching process, 2 hours was added for the application of the FRP overlay.

- An average thickness of 1 inch was assumed for the shallow depth patches to estimate the surface area of the patched area from the volume of repair shown in Table 5-3.

- It is assumed that on average twice the surface area that is patched will be covered with the FRP overlay. This is done to compensate for:
    1. The patch thickness being less shallow than one inch (which would increase the surface area patched).
    2. The extra extension of the FRP over the concrete substrate
    3. Waste (in case of poor bonding of the FRP after application)

If it assumed that traffic control is needed during the entire repair process, and that from the crew size of 5 recommended by MDOT, one is needed as a traffic regulator. The total cost of the bridge maintenance is:

Table 5-4: Total Cost

	Cost per Cubic Yard
With FRP	$ 3391
Without FRP	$ 1800.

Figure 5-2, Table 5-5 and Table 5-6 show the cost analysis for the bridge maintenance for 15 years using both patching approaches. The interest rate was assumed to be 2.9% for each year based on a 15-year evaluation period (OMB 2007).

Table 5-5: Total Maintenance Cost per Cubic Yard for 15 Years with FRP

Year	0
At the beginning of period, c_n	$3391
Present Value, $c_n(1+i)^{-n}$	$3391
Total Present Value	**$3391**

Patch Material 2 with FRP

Patch Material 2 without FRP
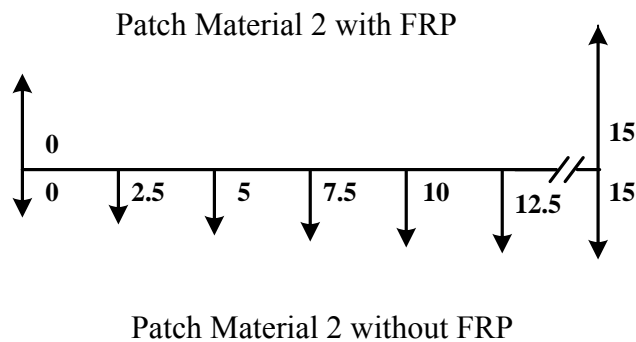
Figure 5-1: Cost timeline

Table 5-6: Total Maintenance Cost per Cubic Yard for 15 Years without FRP

Year	0	2.5	5.0	7.5	10.0	12.5
At the beginning of period, c_n	$1800	$1914	$2036	$2164	$2302	$2448
Present Value, $c_n(1+i)^{-n}$	$1800	$1800	$1800.	$1800	$1800	$1800
Total Present Value	**$10800**					
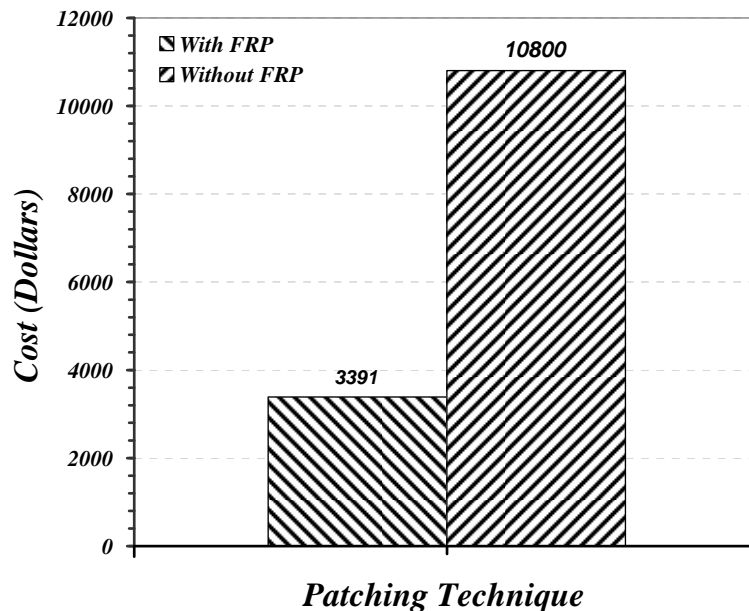
Figure 5-2: Present value of the cost of repair per cubic yard over 15 years

5.4 Conclusion

Based on the various assumptions made, the application of the FRP overlay is expected to increase the cost of the repair by about $1600 per cubic yard (including materials, labor, and traffic control costs) at today's costs. However, the patch/FRP overlay repair is expected to last about 15 years, while the patch repair by itself is expected to last only about 2.5 years. As a result, the present value of the cost of traditional shallow depth patch repairs using Material 2 alone is estimated to be about $7400 more per cubic yard than the repair using the patch and FRP overlay over a 15 year period. It is therefore recommended that the dual patch/FRP overlay system be adopted for all future shallow depth bridge repairs.

Chapter 6

Conclusions and Recommendations

6.1 Conclusions

The research conducted in this project evaluates the proposal to use a dual polymer mortar patch with an FRP overlay to improve shallow depth patching of concrete bridges.

6.1.1 Numerical Studies

The performance of four different patch materials (HB2, Emoco R350 CI, ChemPatch VO1 and Sonopatch 200) were assessed under shrinkage, mechanical and corrosion loads using 2-D finite element (FE) models. The models represented rectangular beam specimens with a cavity at the bottom that was patched. The specimen and cavity dimensions were 16" × 4" × 3" and 4" × 3" × 0.625" for assessing the effects of mechanical and shrinkage loads, and 12" × 6" × 6" and 4" × 5" × 0.625" for assessing the effects of corrosion, respectively. Cracking of the patch and debonding of the patch from the concrete substrate were studied. The analyses indicated that the HB2 (Material 1) patch performed the best, and the R350 CI (Material 2) performed the worst.

The performance of patch materials 1 and 2 were then studied in more detail using 3-D FE models. The 3-D models also were used to evaluate the performance of five different fiber reinforced polymer (FRP) overlays (uni- and bi-directional glass and carbon, and a chopped glass). In addition to cracking and debonding of the patch material, rupture and debonding of the FRP also were studied when the overlay was used. These analyses indicated that uni-directional and chopped glass FRPs were inadequate, and that a bi-directional glass or carbon FRP overlay would be sufficient to resist all loading effects with either of the two patching materials. Since glass FRP is more economical than carbon FRP, one layer of bi-directional glass FRP should be an effective solution for use as an overlay for improving the performance and durability of shallow depth patches in concrete structures.

6.1.2 Experimental Studies

Experimental investigations were performed to verify the finite element results, and also to consider the effects of freeze-thaw and wet-dry cycles on the durability of the patches which are difficult to assess using numerical techniques. Beam specimens were constructed using patch materials 1 and 2, and some had a bi-directional glass FRP overlay. Initial exploration indicated that the FRP could be applied to the specimens after about one hour of applying the patch. Initially specimens having the geometries used in the numerical studies were constructed and exposed to 300 freeze-thaw and wet-dry cycles, and then subjected to four-point flexural fatigue loading. The patches were expected to show deterioration. However, other than for minor cracking or debonding, the patches did not deteriorate significantly.

A second test set-up was then devised to induce damage to the patches. The cavity in the specimens were enlarged to 9" × 4" × 0.625", the specimens were patched and subjected to 1000 cycles of flexural fatigue loading to induce cracking, exposed to 300 freeze-thaw cycles, and finally subjected to 500,000 cycles of three-point flexural fatigue loading. While the patches showed more degradation under this more aggressive test protocol, they still did not completely fall off (except in one specimen). To assess the effectiveness of patch materials 1 and 2, and the improvement obtained with the FRP overlay, pull-out tests were conducted in which a steel plate was bonded to the patch and the force required to pull the patch out was measured. This force indicates the bond strength between the patch and the concrete substrate.

The results of the second test indicated that the FRP overlay significantly increased the bond strength between the patch and the concrete substrate. Surprisingly, the bond strength of specimens with the FRP overlay that had been subjected to freeze-thaw exposure and cyclic loading was even higher than that of specimens without the FRP overlay that were not subjected to freeze-thaw and cyclic loading. The difference in bond strengths for patch materials 1 and 2, were not statistically significant at the 0.05 significance level.

An accelerated corrosion test also was conducted to verify the FE results. This test indicated that the FRP overlay changes the crack patterns induced by corrosion, reduces crack widths, and reduces the corrosion in the steel bars. The change of the crack pattern and the reduction of crack widths was confirmed using FE analysis.

6.1.3 Cost-Benefit Analysis

Many assumptions are needed to perform a cost-benefit analysis of using the FRP overlay for shallow depth repairs. No State Highway Agency has experience with the patching approach using an FRP overlay. Assumptions were made regarding the time required to apply the overlay, the average thickness of patches, the area covered by the overlay, and the life of the patch with the overlay.

The life of the patch with the FRP overlay was estimated by scaling the known life of traditional patches by the proportional increase in bond strength between the patch and the concrete substrate when the overlay is used. Using this approach, and assuming that the bond strength of patches not exposed to freeze-thaw or load cycles is 5 years, the life of patches exposed to freeze-thaw and load cycles was estimated to be 2.5 years when the FRP overlay is not used, and 15 years when the overlay is used.

Using MDOT's bridge maintenance cost data and an interest rate of 3%, the present value of 15 years of patch repair is estimated at $10,800 per cubic yard for a repair using patch material 2 alone, and $3,390 per cubic yard for a repair using patch material 2 with one layer of bi-directional glass FRP. These estimates include material, labor, and lane closure costs, but not user delay costs. The cost savings realized by using the FRP overlay is therefore expected to be sizable.

6.2 Recommendation

Based on all aspects of performance and cost, it is highly recommended that MDOT use a bi-directional glass FRP overlay on all shallow depth patch repairs performed on bridges. The HB2 patch material has the best performance amongst the four materials considered. However, the difference in performance between the HB2 material and the weakest Emoco R350 CI material was not statistically significant, and even the weakest material should perform adequately with the FRP overlay.

References

1. Abaqus, 6.4 , *Abaqus Inc.*, Providence, Rhode Island,USA, 2004.

2. ACI . "ACI 116R-90 - Cement and Concrete Terminology," *American Concrete Institute*, Farmington Hills, Michigan. ACI (1990b).

3. ACI 224R-90, "Control of Cracking in Concrete Structures," *American Concrete Institute*, Farmington Hills, Michigan, 1990

4. Ahlborn, T.M, Aktan, H., Kasper, J.M., and Ovanesova, A.V. "Interim Report: Causes and Cures for Prestressed Concrete I-beam End Deterioration," Michigan Technological University, Houghton, Michigan. 2002.

5. Al-Qadi, I.L., Prowell, B.D., Weyers, R.E., Dutta, T., Gouru, H., and Berke, N. "Concrete Bridge Protection and Rehabilitation: Chemical and Physical Techniques, Corrosion Inhibitors and Polymers.," *SHRP-S-666, National Research Council*, Washington, D.C. 1993.

6. Al-Qadi, I.L., Weyers, R.E., and Cady, P.D., "Field evaluation of preformed membranes," *Journal of Transportation Engineering*, v 119, n 2, Mar-Apr, 284-300, 1993.

7. Baiyasi, M.I. "Repair of Corrosion-Damaged Columns using FRP Wraps." *Ph.D. Thesis*, Michigan State University, East Lansing, Michigan, 2000

8. Baiyasi, I.M., and Harichandran, R.S. "Corrosion and Wrap Strains in Concrete Bridge Columns Repaired with FRP Wraps," *Proceedings (CD-ROM), 80th Annual Meeting of the Transportation Research Board*, Washington, D.C., Paper No. 01-2609, 2001.

9. Baluch, M.H., Rahman, M.K., and Al-Gadhib, A.H., "Risks of Cracking and Delamination in Patch Repair," *Journal of Materials in Civil Engineering*, July/August, pp 294-302, 2002.

10. Batis, G., Routoulas, T., "Steel Rebars Corrosion Investigation with Strain Gages," *Cement and Concrete Composites*, Vol. 21, no. 3, pp. 163-171, 1999.

11. Baskar, K., Shanmugam, N.E., and Thevendran, V., "Finite-Element Analysis of Steel-Concrete Composite Plate Girder," *Journal of Structural Engineering*, v 128, 2002.

12. Beaudette, M.R, "Investigation of Patch Accelerated Corrosion with Galvashield Xp," Interim Report, January, 2001.

13. Blaga, A., and Beaudoin, J.J., "Polymer Concrete," *Division of Building Research, National Research Council Canada, Canadian Building Digest 242*, Ottawa, 1983.

14. Du, Y.G., Chan, A.H.C., and Clark, L.A., "Finite Element Analysis of the Effects of Radial Expansion of Corroded Reinforcement," *Computers and Structures*, 84(13-14), pp 917-929, 2006.

15. El Maaddawy, T. A., Soudki, K.A., and Khaled, A., "Effectiveness of Impressed Current Technique to Simulate Corrosion of Steel Reinforcement in Concrete," *Journal of Materials in Civil Engineering*, vol. 15, no. 1, pp. 41-47, 2003.

16. Emberson, N.K., and Mays, G.C., "Significance of Property Mismatch in the Patch Repair of Structural Concrete, Part 3: Reinforced Concrete Members in Flexure," *Magazine of Concrete Research*, v 48, n 174, p 45-57,1996.

17. Emmons, P.H., "Concrete Repair and Maintenance Illustrated," *Construction Publisher and Consultants*, MA, pp 100-136, 1993.

18. Fowler, D.W., "Polymers in Concrete: A Vision for the 21st Century ," *Cement and Concrete Composites,* v 21, n 5-6, p 449-452,1999.

19. Fuller, S.K., and Peterson, S.R., "Life-Cycle Costing Manual for the Federal Energy Management Program," *NIST Handbook*, 1995.

20. Hibbit, K., and Sorensen Inc., "Abaqus Theory Manual and Users' Manual," version 6.3, 2002.

21. Kelley, P.L., Brainerd, M.L., Liepins, A.A., and Bergstrom, T., "Understanding Cracking in Concrete Repairs, *Construction Specifier*, v 49, n 12, p 32-36, 1996.

22. Mehta, P., and Monteiro, J., *Concrete, Structure, Properties, and Materials*, Second Edition, Prentice-Hall, Englewood Cliffs, pp 160-164, 1993.

23. Mangat, P.S., and O'Flaherty, F.J., "Factors Affecting the Efficiency of Repair to Propped and Unpropped Bridge Beams," *Magazine of Concrete Research*, v 52, n 4, p 303-319, 2000.

24. Parameswaran, S., "Investigation of the Role of Material Properties and Their Variability in the Selection of Repair Material.," *M.S. Thesis*, Purdue University, Indiana, 2004.

25. Rizzo, E.M., and Sobelman, M.B, "Selection Criteria for Concrete repair Material," *Concrete international*, 45-49, 1989.

26. Staton, J. "Re: Approval process for vertical and overhead concrete repair materials," E-mail to James Kasper, November 27, 2001.

27. Vaysburd, A.M., Carino, N.J., and Bissonette, B., "Prediction the Performance of Concrete Repair Materials," *Summary of Workshop Report*, 1999.

28. Weyers, R.E., "Concrete bridge protection repair & rehabilitation," *Pacific Rim TransTech Conference*, p 353-356, 1993.

29. Weyers, R.E., Prowell, B.D., Sprinkel, M.M., and Vorster, M., "Concrete Bridge Protection, Repair, and Rehabilitation relative to Reinforcement Corrosion: A Methods Application Manual," *SHRP-S-360, National Research Council*, Washington, D.C. 1993.

30. Yuan, Y., Li, G., and Cai, Y.. "Modeling for Prediction of Restrained Shrinkage Effect in Concrete Repair." *Cement and Concrete Research*, Vol. 33, No. 3, pp 347-352, 2003.

31. Xanthakos, P.P. *Bridge Strengthening and Rehabilitation*, Prentice-Hall, New Jersey, 1996.

Appendix A

Patch Materials from MDOT Qualified List
and Other States

Table A-1: Patch Materials from MDOT and some other states

			Material	Approved by	Horizontal application	Vertical application	Company	Description	Other explanation
MDOT		Structural repair (mostly)	Durapatch highway	MDOT,UDOT,MiDOT,WV DOT,DOTD,ODOT, NeDOT,ADOT				DURAPATCH HIWAY is a one-component, fiber-reinforced; instant strength cement based patching system. This non-shrink, high strength cement patch contains the necessary ingredients to assure instant strength, sulfate resistance, elevated temperature stability, superior bond ability and increased flexural and tensile strengths.	
			Five star highway patch	MDOT,MiDOT,KDOT,GDOT,FIDOT, NHDOT,ODOT,NDOT,MaDT,NeDOT, ADOT	Mostly for pavement patching		US high way product	Five Star Highway Patch is a patented, cementitious mixture. It is a rapid setting, high-strength product, which is, salt, oil, and gas resistant.	
			MBR P&R Set45-Dot	MODT,MiDOT,MoDOT.ODOT,MaDOT		Formed	Chem Rex	Set@ 45 is a one-component magnesium phosphate-based patching and repair mortar. This concrete repair and anchoring material sets in approximately 15 minutes and takes rubber-tire traffic in 45 minutes.	Pump
			MBR P&R thorocl 10-60,61	MDOT,UDOT,MiDOT,ODOT,FLDOT, NHDOT,NDOT,MaDOT	Traffic repair	(10-61)	Chem Rex	10-60,61 Mortar is a one -component shrinkage-component very rapid-setting cement-based mortar. It is designed for horizontal concrete surfaces where high early strength gain is required.	
	Polymer modified		Fast patch 928	MDOT,UDOT,NDOT,KeDOT,DOTD,ODOT			The hurke company	Basics Uses: Fast Patch 928 is a one component, cement-based system containing polymers and fibers formulated for making fast repairs to £-t concrete. Fast Patch 928 is designed for structural repairs to damaged concrete highways, bridge decks, airport runways, and industrial floors.	
			chern speed 65	MDOT,KeDOT			The hurke company	Chem Speed 65 is a high strength, very rapid setting, and structural concrete repair mortar. It is a Portland cement based material modified with an EVA copolymer and requires only water for mixing.	
			HD-Dot patch	MDOT,MiDOT,MaDOT,OhDOT,NeDOT,ADOT	Mostly for pavement patching		Symon Corp	D.O.T. PATCH is a rapid setting, fiber-reinforced and polymer modified material for concrete repair. It is easily mixed with water to provide a flow able material that exhibits greater compressive, flexural and shear bond strengths than most other repair materials	Pump

140

			HD-50 heavy Duty concrete patch	MDOT,MiDOT,KDOT,GDOT,FLDOT,WVDOT,NDOT,KeDOT,DODT,ODOT,MaDOT,NeDOT		Can be used	Dayton Superior Inc	A latex-modified, fiber reinforced, fast setting concrete repair designed for horizontal areas where high strength and fast setting are required to minimize downtime.	Pump
OTHER STATES	*Polymer modified*	*Cosmetic repair (mostly)*	Chem patch VO1	WVDOT,KeDOT			chem master	ChemPatch VOl represents a breakthrough in cementitious repair technology. It is a one component, polymer modified, fast setting, Non-shank repair mortar. ChemPatch VOl is a proprietary structural repair compound unique for its light concrete color and finishing characteristics. With its high ultimate strength, density and durability	.
			Day-chem perma patch	WVDOT,KeDOT.DOTD			Dayton superior Inc	An excellent holding agent consisting of acrylic latex emulsion used primarily for bonding hew to new or new to old concrete in interior or exterior applications. Ad Bond is also extremely effective when used as an admixture with cementitious products such as patching compounds, coatings, or grouts.	
			Thorute	MoDOT	Non traffic (formed)		thoro System	Thorite 400 is cement based, polymer modified, patching mortar available in a range of factory made, batch blended, standard and custom colors. It contains inorgarric, alkali-resistant pigments with good resistance to weathering and fading	Hand applied
			Deco-Rez tem 722	MoDOT				Deco-Rez TPM 722 is a specially formulated co-polymer mortar designed for co-polymer mortar designed for repair and patching of horizontal and vertical concrete and masonry surfaces.	Not for less than 1/8"
			Silikatop 122	UDOT,MoDIT,ODOT,MaDOT,NeDOT	Formed	Formed	silika corporation	Polymer-modified, plus migrating inhibitor, cementitious, 2 components, fast setting, high strength.	Hand applied, thickness can be less than 1/4"
			Silikatop 123	UDOT,MoDIT,ODOT,MaDOT	Formed	Formed	silika corporation	Polymer-modified, plus migrating inhibitor, cementitious, 2 components, fast setting, high strength.	Hand applied, thickness can be less than 1/4"
			Silikatop 126	UDOT			silika corporation	Polymer-modified, plus migrating inhibitor, cementitious, 2 components, fast setting, high strength.	Hand applied

			Sono patch 200	UDOT,NeDOT		█	Sonneborn	Sonopatch 200 is a two-component, polymer-modified. Portland-cement-based repair mortar. Its rapid strength gain reduces downtime	
			Burke V/O patch	UDOT,NeDOT	Can be used	█	Educe	Single-component. Polymer modified patching and repair material. Repairing of interior and/or exterior horizontal. Vertical or overhead surfaces.	Pump. Spray
			Euco-verticoat	UDOT		█	Euchdchemi cal company	VERTICOA T is a polymer modified cementitious mortar for vertical and overhead concrete and masonry repairs. It sets rapidly to allow quick. Easy repaid of concrete surfaces both inside and outside.	Hand applied
			SD-1048	UDOT	█		Border	SD-1048 is a polymer resin that has been tested by Universities. Engineer and hundreds of contractor. Since I 994. It is user-friendly and does not require expensive equipment to apply	
			Quick set 20	UDOT	█	█	US mix product company	Quick Set 20 is a blend of Portland cements. Aggregate and proprietary admixtures.	
			Euco-speed-MP	UDOT,MiDOT,KDOT,FLDOT,WVDOT,NDOT,KeDOT,DOTD,MaDOT,NeDOT	█	Formed	Euchdchemi cal company	EUCO-SPEED is a rapid setting. rapid harde1l1lng cementitious material for patching and repair of concrete surfaces. Requiring only the addition of water.	
			Silika Repair SHB	UDOT			silika corporation	Product is a one component. Cementitous ready to use repair mortar for vertical and over head application	
		Structural repair (mostly)	Emoci S77 CI	UDOT			Master builder	Emaco@ S77 CI is a rhea plastic. Flow able. Shrinkage-compensated. Designed for replaced aggregate applications. Emaco@ S77 CI repair mortar provides high pump ability for structural repaid of columns and beams.	Formed-and-pump repair
			Speed crete 2028	KDOT,GDOT,FLDOT,MoDT,KeDOT,DOTD	█		Tamms Inc	SPEED CRETE 2028 is cement based. Ready to use. Patching and repair tuortar, which sets fast. And achieves rapid strength gain.	
			Transpatch	UDOT	█		US SPEC	Trans patch is a rapid setting. Rapid hardening concrete patching material that exhibits excellent flexural properties. Shear bond strength and compressive strength, This product is a blend of Portland cement, selected aggregates and proprietary admixtures.	

Table A-1(continued): Patch Materials from MDOT and some other states

	Pavement patching (mostly)	Rapid set concrete mix	UDOT,DOTD,ADOT			cts cement	When mixed with water Concrete Mix produces a workable. High quality concrete material that is ideal where fast strength gain, high durability and low shrinkage are desired. Apply Concrete Mix in thickness from 2in to 24-in.	Hand applied-not less than 2"
		Geo Bond	KDOT			GeoBond International Inc	GeoCement is a cementious-based product with a unique catalyst. It is very rapid hardening, early strength gaining.	
		Pave patch-3000	KDOT,GDOT,MoDT,DOTD,NHDOT			Conspect Marketing & Mfg	Especially formulated patching material for concrete pavement repairs, Pave patch-3000 sets fast, develops high early strength and expand slightly	
		Dot patch	GDOT,FLDOT,NDOT,KeDOT			Symon Corp	Dot patch and Dot patch HD are fast setting cement-based repair materials designed to meet many state Department of Transportation repair specification	
Polymer modified		Transpo T-17	GODOT,DODT			transpo international, Inc	T-17 methyl methacrylate polymer concrete is a 100% reactive pre-paksged two component system	

Appendix B

Field Installation of Fiber Reinforced Plastic (FRP) Overlay for Shallow Depth Patches

B1. Patch Materials

The following two patch materials are commonly used by MDOT and are included in MDOT's Qualified Product List.

1. HB2: polymer-modified high build repair mortar
   Vendor   BASF – The Chemical Company
             889 Valley Park Drive
             Shakopee, MN 55379
             Tel: 952-496-6000
             Fax: 952-496-6062

   Local Rep.: Chris Jensen
             BASF Building Systems
             2155 Airwest Blvd
             Plainfield, IN 46168
             Tel: 800-433-9517

2. Emaco R350 CI: polymer-modified light weight repair mortar
   Vendor   BASF – The Chemical Company
             889 Valley Park Drive
             Shakopee, MN 55379
             Tel: 952-496-6000
             Fax: 952-496-6062

   Local Rep.: Chris Jensen
             BASF Building Systems
             2155 Airwest Blvd
             Plainfield, IN 46168
             Tel: 800-433-9517

The mechanical properties of the two repair materials are given in Table B-1.

Table B-1: Mechanical Properties of the Two Selected MDOT Repair Materials

Material	ASTM C109 Compressive Strength (psi)	ASTM C348 Flexural Strength (psi)	ASTM C496 Tensile Strength (psi)	ASTM C469 Elastic Modulus (psi)	Drying Shrinkage (με)	ASTM C882 Slant Shear Bond Strength (psi)
Emoco R350 CI	5000	900	600	2×10^6	1410	1500
Hb2	5800	1000	590	2×10^6	350	2700

B1.1 Construction Methods

Do not mix partial bag.
Do not apply when the ambient temperature is lower than 7°C
Do not over mix for more than 5 minutes.
Make certain the most current versions of product bulletin and MSDS are being used; call Customer Service (1-800-433-9517) to verify the most current versions. Proper application is the responsibility of the user. Field visits by manufacturer personnel are for the purpose of making technical recommendations only and not for supervising or providing quality control at the jobsite.

B1.2 Repair using HB2 Polymer-Modified Mortar

A. Concrete substrate must be structurally sound. Loose or unsound concrete should be removed.

B. Saw cut the edges of the repair locations to a depth of at least 3/8" (10 mm) to avoid featheredging and to provide a square edge. Break out the complete repair area to a minimum depth of 3/8" (10 mm) up to the sawn edge.

C. Clean the surface by removing any dust, unsound or contaminated material, oil, paint, greases, and corrosion deposits.

D. Where breaking out is not required, roughen the surface and remove any laitance by mechanical means or high-pressure water wash. Remove oil and grease deposits by steam cleaning, detergent scrubbing, or degreasing.

E. To ensure optimum repair results, assess the effectiveness of decontamination by a pull-off test.

F. Remove all oxidation and scale from the exposed reinforcing steel.

G. For additional protection from future corrosion, coat the prepared reinforcing steel.

H.   Ensure that the HB2 Repair Mortar is thoroughly mixed; a forced action mixer is essential. Do not use free-fall mixers.

I.   For the occasional 1 bag mix, use a suitably sized container, an appropriate paddle, and a variable-speed (400-500 rpm) heavy-duty drill. Do not mix partial bags. Always mix the material in a clean container.

J.   For normal applications, place 3 quarts (2.8 L) of ThoRoc® Polymer Liquid into the clean mixer for each complete 45 lb (20.5 kg) bag of HB2 Repair Mortar. The powder should always be added to the liquid.

K.   Depending on the ambient temperature and the desired consistency, additional ThoRoc® Polymer Liquid may be added, but the maximum liquid content should not exceed 1 gallon (3.8 L) per 45 lb (20.5 kg) bag of HB2 Repair Mortar.

L.   The concrete substrate should be saturated surface-dry (SSD) with no standing water.

M.   Using a stiff brush, scrub a thin coat of the mixed material thoroughly into the surface to ensure sufficient bonding.

N.   HB2 Repair Mortar can be applied in single lifts up to 3" (76 mm) in thickness on vertical surfaces and up to 1-1/2" (38 mm) in thickness on overhead surfaces (without the use of form work).

O.   If the material sags during application, completely remove the HB2 Repair Mortar. Properly reprime the substrate and reapply the mortar at a reduced thickness.

P.   Finish the HB2 Repair Mortar by striking off with a straight edge and smooth with a steel trowel. Wooden or plastic floats or sponges may also be used to achieve the desired surface texture. Do not overwork the completed surface.

Q.   Proper curing is extremely important. For peak performance of the repair, cure immediately after finishing in accordance with good concrete practices (refer to ACI 308).

R.   Remove the HB2 Repair Mortar from tools, equipment, and mixers with clean water immediately after use. Cured material can only be removed mechanically. Clean hands and skin immediately with soap and water or industrial hand cleaner.

B1.3 Repair using Emaco R350 CI Polymer-Modified Mortar

A.   Perform surface preparation in compliance with ICRI Technical Guideline No. 03730.

B.   Square cut or undercut the perimeter of the area being patched to a minimum depth of 1/8" (3 mm) to prevent featheredges. Do not cut reinforcement.

C.   Chip and remove unsound and delaminated concrete to a depth of 1/8" (3 mm) or to whatever additional depth is necessary to reach sound concrete. Limit the size of chipping hammers to 15 lbs (6.8 kg) to reduce micro fractures. Hydrodemolition may be used. Do not use a method of surface preparation that will fracture the concrete. Verify the absence of microcracking or bruising in accordance with ICRI Guideline No. 03732.

D.   After concrete removal, thoroughly abrade the roughened surface and exposed reinforcement to remove all bond-inhibiting materials such as rust, dirt, loose chips, dust, oil, and grease.

E.   Saturate the area thoroughly with water for several hours before placing Emaco® R350 CI.

F.   Remove 3/4" (19 mm) of concrete behind the corroded reinforcing steel to provide adequate space for preparation and material placement.

G.   Sandblast or shotblast corroded reinforcing steel after chipping to remove oxidation and scale in compliance with ICRI Technical Guideline No. 03730 "Guide for Surface Preparation for Repair of Deteriorated Concrete Resulting from Reinforcing Steel Corrosion." For additional protection from future corrosion, coat the prepared reinforcing steel with Emaco® P22 or Emaco® P24 rebar coatings.

H.   Use a slow-speed drill (400-600 rpm) with a Jiffy-type paddle or an appropriately sized mortar mixer.

I.   Add 0.95-1.1 gallons (3.6-4.1 L) of clean potable water per 55 lb (25 kg) bag of Emaco® R350 CI. Pour approximately 90% of the mix water into the mixing container, then charge the mixer with the bagged material. Add remaining mix water as required for vertical or overhead applications.

J.   Mix to a uniform consistency. Typical mixing time is 3-5 minutes. Do not mix longer than 5 minutes.

K.   Remove excess water from the saturated surface-dry (SSD) substrate.

L.   Scrub a bond coat of Emaco® R350 CI repair mortar into the prepared surface with a stiffbristled broom or brush. Emaco® R350 CI repair mortar must be placed before the bond coat dries. Do not dilute the bond coat with water.

M.   Apply material while taking proper consideration for compaction around reinforcing steel.

N. When applying in multiple lifts, scratch the preliminary lift before initial set. Apply the next lift after the preliminary lift has reached final set. If the next lift will not be placed immediately, keep the surface continually moist.

O. Cut off or level as required to match the original concrete elevation. Maximum application thickness is 2-3/4" (70 mm).

P. Where rapid drying conditions exist (e.g., hot, dry, windy conditions) use Confilm® evaporation reducer. Refer to the Confilm® product data sheet for more information.

Q. Finish the final surface as required.

R. Proper curing is extremely important and should be conducted in accordance with ACI 308, "Standard Practice for Curing Concrete."

B2. FRP Materials

The following is a list of FRP overlay material

1. SikaWrap Hex 106G: Composite System (glass)
    Vendor: Sika Co.
                   201 Polito Ave.
                   Lyndhurst, NJ 07071
                   Tel: 201-933-8800
                   Fax: 201-804-1076

    Local Rep.:   Bill Bergeron
                   1891 E. Whitefeather Road
                   Pinconning, MI 48650-8416
                   Tel: 248-207-2122
                   Fax: 734-464-1588

    Fabric: SikaWrap Hex 106G
    Epoxy: Sikadur 300/306
    Top Coat: Sikagard 670W, Color:
                   Concrete gray

The mechanical properties of the glass FRP composite is given in Table B-2.

Table B-2: General Properties of FRP Composite used

Product Name	Type	Fiber Orientation	Elastic Modulus E_{11} (psi)	Ultimate Tensile Strength (psi)	Thickness (in.)
Hex 106 G	Glass	Bidirectional	2.47×10^6	4.40×10^4	0.013

B2.1 Construction Methods

Do not apply when ambient temperatures are lower than 4°C.
Do not apply to wet surface or when rainfall is anticipated.
Do not apply when humidity is 90% or higher.
Manufacturer's representative shall be on site for initial placement.
Directions of the manufacturer's representative shall be followed.

B2.2 Overlay using SikaWrap Hex 106G Composite System

A. Remove loose concrete from the column surface and fill all voids to a smooth surface using one of the polymer modified mortars referenced above using the procedures described above.

B. Remove dust, laitance, grease, curing compounds, impregnations, waxes, foreign particles, disintegrated materials, and other bond inhibiting materials from the surface area of the concrete around the area to be patched where the FRP overlay will be extended.

C. Round or bevel corners by grinding to a radius of at least 25 mm.

D. Pre-cut one layer of fabric to dimensions exceeding the patched area by at least 2.5 in. on each side. Use off-site labor where possible.

E. Concrete may be dry or damp, but should be free of standing water and frost.

F. Pre-mix each component of the epoxy. Mix entire unit, do not batch. Pour contents of part 'B' to part 'A'. Mix thoroughly for 5 minutes using a paddle style mixer attached to a low speed (400-600 rpm) drill until uniformly blended.

G. For vertical and horizontal applications, use Sikadur Hex 300. For overhead applications use Sikadur Hex 306. Resins may be applied to fabric by either manual or mechanical means. For further information, consult installation guidelines.

H. SikaWrap Hex 106G can be applied using wet or dry lay-up methods as outlined below.

Dry Lay-Up

- Apply the mixed Sikadur 330 epoxy resin directly onto the substrate at a rate of 40-50 ft^2/gal. (32-40 mils), depending on the surface profile.
- Carefully place the fabric into the resin with gloved hands and smooth out any irregularities or air pockets using a plastic laminating roller.
- Allow the resin to squeeze out between the rovings of the fabric. If more than one layer of fabric is required apply additional Sikadur 330 at a rate of 100 ft^2/gal. (16 mils) and repeat as above.

- Apply a final coat of Sikadur 330 to the exposed surface at a rate of 160 ft^2/gal. (10 mils).

Wet Lay-Up

- Seal the prepared concrete surface using Sikadur 300, Sikadur Hex 300 or Sikadur Hex 306.
- Material may be applied by spray, brush or roller. SikaWrap Hex 106G can be impregnated using either Sikadur 300, Sikadur Hex 300 or Sikadur Hex 306 epoxy.
- For best results, the impregnation process should be accomplished using an automated fabric saturating device.
- Once saturated, apply fabric to the sealed concrete surface and smooth out any irregularities or air pockets using a plastic laminating roller.
- Coat the exposed surface of the fabric layer using Sikagard 670W or Sikagard 62.